applied sciences

MDPI

Review

A Review of Wind Turbine Reliability and Long-Term Performance: Failure Mechanisms, Monitoring Strategies, and AI-Enabled Predictive Maintenance

Sajid Ali [1], Muhammad Waleed [2] and Daeyong Lee [2,*]

[1] Energy Innovation Research Center for Wind Turbine Support Structures, Kunsan National University, 558 Daehak-ro, Gunsan-si 54150, Jeonbuk-do, Republic of Korea; sajid_ali@kunsan.ac.kr
[2] Department of Wind Energy, The Graduate School of Kunsan National University, 558 Daehak-ro, Gunsan-si 54150, Jeonbuk-do, Republic of Korea; waleedmuhammad6555@gmail.com
* Correspondence: daeyong.lee@kunsan.ac.kr; Tel.: +82-10-4490-0980

Abstract

Wind turbines are increasingly deployed at larger scales and in harsher operating environments, leading to greater structural complexity, stronger load variability, and higher maintenance demands across both drivetrain and structural components. Reported field data indicate that gearboxes and bearings account for approximately 30–40% of total turbine downtime, while blade-related failures contribute roughly 20–25% of reported failure events, primarily through fatigue, delamination, leading-edge erosion, and lightning-induced defects. In parallel, large-scale and offshore turbines show increasing susceptibility to tower fatigue cracking, corrosion-assisted degradation, and flange joint bolt-preload loss under cyclic and environmental loading. This review provides a comprehensive applied-engineering synthesis of failure mechanisms, reliability challenges, and monitoring strategies for major wind turbine components, including gearboxes, bearings, blades, towers, and flange joints. A wide range of condition monitoring, structural health monitoring (SHM), and prognostics and health management (PHM) approaches is critically examined, including vibration analysis, acoustic emission, ultrasonic inspection, infrared thermography, impedance-based sensing, electromagnetic methods, machine vision, SCADA-based diagnostics, and artificial-intelligence-assisted fault classification. The review compares these techniques in terms of detectable damage types, spatial coverage, sensitivity, deployment practicality, and limitations under real operating conditions. In addition, statistical reliability methods and data-driven models are discussed to interpret failure trends and uncertainty. Recent AI-based studies have reported fault classification accuracies exceeding 90% under controlled or semi-controlled conditions; however, their field reliability remains constrained by data imbalance, domain shift, limited labeled failure datasets, model interpretability, and insufficient validation under realistic turbine operating environments. The main contribution of this review is an integrated applied synthesis that connects drivetrain and structural failure mechanisms with measurable monitoring indicators, diagnostic technologies, AI-enabled PHM limitations, and predictive-maintenance decision needs. The paper provides practical guidance for monitoring design, early fault detection, predictive maintenance, and long-term reliability improvement in next-generation wind turbine systems.

Keywords: wind turbine reliability; failure mechanisms; structural health monitoring; predictive maintenance; condition monitoring; AI-based diagnostics

Check for updates

Academic Editor: Guang Li

Received: 1 May 2026
Revised: 3 June 2026
Accepted: 18 June 2026
Published: 23 June 2026

Copyright: © 2026 by the authors. Licensee MDPI, Basel, Switzerland. This article is an open access article distributed under the terms and conditions of the Creative Commons Attribution (CC BY) license.

1. Introduction

(R2) Wind energy is one of the most promising renewable energy sources because of its wide availability, long-term sustainability, and low operational emissions. Global installed wind power capacity has therefore increased rapidly over recent decades. At the same time, many existing wind turbines are approaching or exceeding their nominal 20-year design life, which increases the need for inspection, maintenance, retrofitting, and lifetime-extension assessment. In parallel, new wind turbine technology is moving toward larger rotor diameters, higher hub heights, increased rated capacity, and offshore deployment in remote and harsh environments. These trends create additional reliability, accessibility, and maintenance challenges. Consequently, operation and maintenance (O&M) costs have become a major concern for both onshore and offshore wind farms and must be reduced to maintain the long-term economic viability of wind energy [1–3].

Maintenance access is constrained by turbine size, safety requirements, weather windows, humidity, temperature, and allowable wind-speed limits. These constraints become more severe for offshore wind farms, where marine exposure, vessel availability, distance from shore, wave conditions, and limited weather windows increase downtime and repair cost [4–6]. Reduced component reliability and unplanned turbine shutdowns therefore increase O&M expenditure and reduce energy availability [7–9]. At present, O&M costs represent approximately 10–30% of the overall energy-generation cost of an operational offshore wind farm [10]. In some offshore projects, maintenance and operation costs can increase to 25–50% of total power-generation costs, despite the higher energy yield associated with stronger offshore wind resources [11].

Figure 1 illustrates the wind turbine energy-conversion process, in which aerodynamic energy from the rotor is converted into mechanical shaft power and then into electrical power through the generator. The mechanical shaft transfers torque from the rotor, with or without a gearbox depending on drivetrain configuration. The generator output is then conditioned using power-electronic converters, filters, and a step-up transformer before being delivered to the grid at the required voltage and frequency. Table 1 summarizes the technological development of wind turbines over different generations, while Table 2 presents the main components of a typical large-scale horizontal-axis wind turbine.

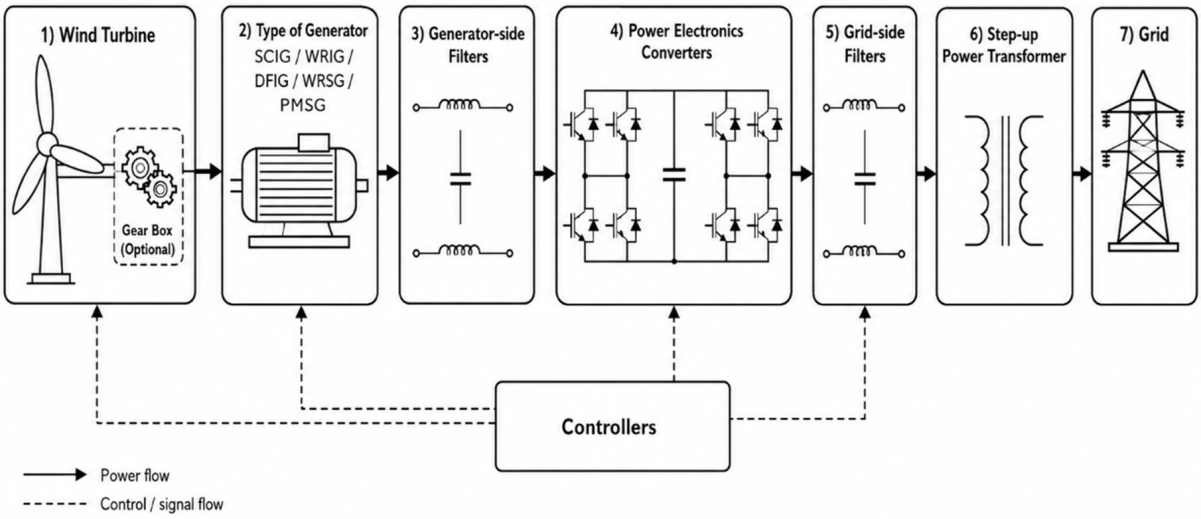

Figure 1. Wind turbine energy conversion system (recreated from [12]).

Table 1. Wind turbines over the years.

Generation	Year Introduced	Typical Capacity	Features	Technological Advancements
First	1980 s	Up to 50 kW	Fewer blades, fixed pitch	Steel tube towers, asynchronous generators
Second	1990 s	50 kW to 500 kW	More blades, variable pitch	Tubular steel towers, induction generators with variable speed
Third	2000 s	500 kW to 2 MW	Improved aerodynamics	Full-scale converter systems, increased reliability
Fourth	2010 s	2 MW to 8 MW	Smart turbines, offshore designs	Direct drive systems, permanent magnet generators, advanced materials
Fifth	2020 s	8 MW and above	Large rotor diameters, high altitude	Enhanced grid integration, machine learning for predictive maintenance

Table 2. Wind turbine components.

Component	Function	Material	Specifications	Technological Advancements
Rotor Blades	Capture wind and transfer force to the rotor	Fiberglass, Carbon fiber, Wood-epoxy	Length, airfoil shape, pitch control	Aerodynamic design, pitch control mechanisms
Gearbox	Increase rotational speed from rotor to generator	Steel alloys	Gear ratios, power rating, efficiency	Planetary stages, load distribution technologies
Generator	Convert mechanical energy into electrical energy	Various metals, Advanced composites	Power rating, type (asynchronous/synchronous)	Direct drive technology, permanent magnet materials
Tower	Support the structure of the turbine	Steel, Concrete	Height, base diameter, weight	Tubular steel, lattice designs, modular construction
Nacelle	House the generator and gearbox	Composite materials, Steel	Weight, aerodynamic profile	Modular designs, improved thermal regulation

(R2) Wind turbine failures can be broadly categorized into gearbox faults, bearing faults, blade faults, generator faults, pitch-control system faults, and mechanical braking system faults. Among these, gearbox fault diagnosis remains a major reliability challenge because gearboxes operate for long periods under variable torque, fluctuating rotor speed, transient wind loading, and harsh environmental conditions. The gearbox is also a capital-intensive drivetrain component, accounting for approximately 18% of turbine cost, and has historically been associated with high failure rates and long repair durations. The failure rate and downtime characteristics of major turbine subsystems are shown in Figure 2 [13].

As shown in Figure 2, minor and major gearbox failures can lead to substantial annual maintenance downtime, which directly reduces turbine availability and energy production. Gearbox repair requires approximately 18.38 days per failure, ranking among the longest repair durations because the gearbox is large, heavy, and mechanically integrated with other drivetrain components [14]. This makes access, removal, replacement, and restoration particularly difficult, especially in offshore wind farms where vessel logistics and weather windows further constrain repair operations. Although gearbox design life is often specified as approximately 20 years, field observations show that actual service life can be considerably shorter, typically around six to eight years in some operating fleets [13]. This gap between design life and field performance increases maintenance cost and reduces energy availability, confirming the need for reliable gearbox fault diagnosis and early-warning technologies [15–23].

Although Figure 2 is based on earlier reliability statistics, it is retained as a historical baseline because it clearly illustrates the classical distinction between high-frequency failures and long-downtime failures across wind turbine subsystems. However, the figure should not be interpreted as a complete representation of current 2025 turbine reliability. Modern turbines require additional consideration of offshore accessibility, larger blade and drivetrain components, power-electronics complexity, generator replacement logistics, and fleet-scale digital monitoring. For this reason, the historical statistics are supplemented in this review with recent RAM literature, standardized reliability-data recommendations, and current examples of large-component reliability challenges.

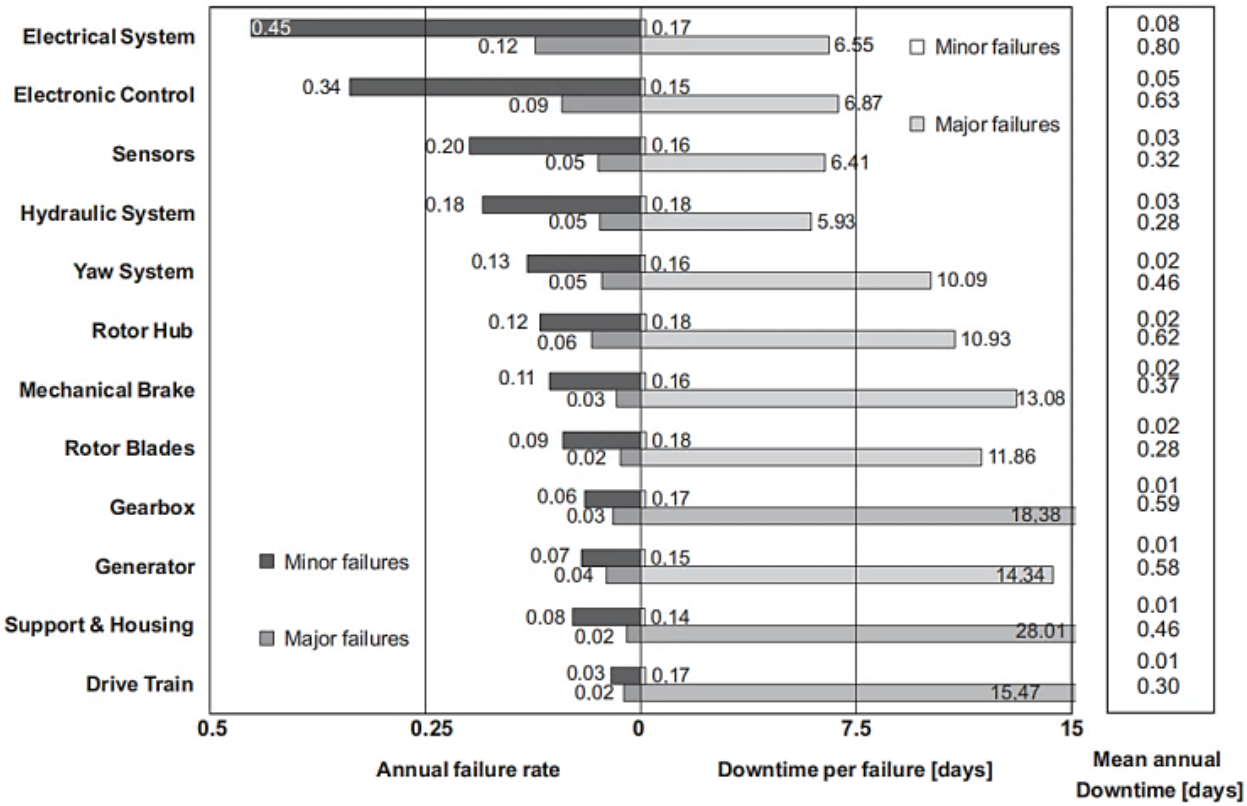

Figure 2. Statistical failure data for different components of wind turbine [13].

Historical wind turbine failure statistics remain useful because they provide a baseline for understanding which subsystems have traditionally caused high failure frequency and long downtime. However, the reliability profile of modern wind turbines has changed because turbine capacity, rotor diameter, hub height, drivetrain architecture, offshore deployment, control complexity, and digital monitoring capability have all increased substantially. Therefore, older failure statistics should be interpreted as historical context rather than as the sole basis for assessing current large-scale or offshore turbine reliability.

More recent reliability literature confirms that component reliability remains a central barrier to reducing O&M cost, but it also shows that the reliability challenge has become more system-level and data-driven. Recent RAM reviews for offshore wind turbines emphasize the need for improved reliability, availability, and maintainability of data collection, and highlight that offshore environmental conditions negatively affect reliability and maintainability figs. IEA Wind Task 33 also emphasizes that standardized wind-farm data collection is essential for reliability assessment and O&M optimization, because inconsistent event definitions and maintenance records make cross-farm comparison difficult. In addition, recent industrial reliability reports and public failure events show that generator, drivetrain, bearing, blade, and power-electronics issues remain relevant in modern turbine fleets, while blade quality problems and large-component replacement can cause major downtime and safety concerns. Therefore, this review retains historical statistics for comparison but supplements them with recent evidence and discusses their limitations for modern wind turbine reliability assessment.

Table 3 shows that historical reliability statistics should be used carefully in a modern review. Earlier datasets remain valuable because they identify recurring critical subsystems such as gearboxes, generators, bearings, blades, and electrical/control systems. However, modern turbines are larger, more highly controlled, and increasingly installed offshore, where accessibility, weather windows, logistics, and replacement operations strongly influ-

ence downtime. Recent literature and operational evidence therefore shift the reliability discussion from simple failure-rate ranking toward integrated RAM analysis, standardized data collection, fleet-scale monitoring, and predictive maintenance. This broader interpretation is important because a component with moderate failure frequency may still dominate maintenance cost if repair requires cranes, vessels, blade replacement, nacelle access, or long shutdown periods.

Table 3. Historical and recent evidence on wind turbine reliability and downtime.

Evidence Source/Period	Turbine Context	Component or Subsystem Emphasis	Main Reliability Observation	Relevance to the Present Review
Historical failure statistics used in earlier wind turbine reliability studies	Mainly earlier-generation onshore turbines	Gearboxes, blades, generators, electrical/control systems	Gearboxes and drivetrain components often produced long downtime, while electrical/control systems often produced frequent but shorter events	Useful as historical baseline, but not sufficient alone for modern large-scale and offshore turbines
NREL subsystem reliability report	Operational turbine fleet data, mostly turbines installed since 2008	Gearboxes and generators	Average gearbox annual failure rate was estimated around 5% over 10 years, while generator annual failure rate was typically lower; serial failures can distort component-level reliability estimates	Shows that drivetrain and generator reliability remain important, but also that fleet statistics require careful interpretation
Offshore wind RAM review by Cevasco and other authors	Onshore and offshore reliability, availability, maintainability literature	Critical offshore turbine subsystems and maintenance categories	Offshore environmental conditions negatively affect reliability and maintainability; improved reliability data are needed for future offshore project performance prediction	Supports the need to discuss offshore-specific accessibility, downtime, and maintainability challenges
IEA Wind Task 33 recommended practice	Wind farm reliability data collection and O&M optimization	Failure, maintenance, inspection, operating, and equipment data categories	Standardized data collection is required because inconsistent definitions limit reliability comparison across wind farms and studies	Supports the need for transparent reliability databases and harmonized reporting
NREL generator reliability analysis	Wind turbine generator reliability, turbines installed since 2008	Generator full replacement and up-tower replacement	Generator annual failure rate is typically about 1–4%, but replacement-related downtime can be long	Shows that generator failures remain relevant even when gearbox failures receive more attention
Industrial monitoring database evidence	Large monitored turbine populations	Major components monitored across modern fleets	Large monitoring databases track thousands of major component failures annually and are used to estimate future turbine reliability risks	Indicates the growing importance of fleet-scale monitoring, but public access to detailed component statistics is limited
Recent public offshore blade-failure case	Modern offshore wind project	Blades and manufacturing quality	Blade failure required inspection, quality checks, and replacement/strengthening of some blades before full operational recovery	Demonstrates that blade reliability and inspection remain critical for modern offshore wind deployment
Recent bearing/blade reliability incidents reported in operating fleets	Modern utility-scale turbines	Bearings, blades, large replaceable components	Large-component failures can require extensive repair logistics and long turbine outages	Reinforces the need for early fault detection, PHM, and maintenance planning

Similarly, large-scale bearings in wind turbines, in particular, are essential parts that support enormous loads and handle large stresses. Unlike universal industrial bearings, these large-scale wind turbine bearings are exposed to harsh conditions and are positioned at high elevations, resulting in increased rate of failure and repair costs [24]. Condition monitoring and fault diagnosis (CMFD) of these bearings is essential for maintaining dependability in wind turbine operation in order to increase wind turbine output and reduce maintenance and operation costs. In terms of the rotation speeds, wind turbines have a total of three kinds of large-scale bearings: (I) very slow-speed bearings (yaw bearings and pitch bearings), (II) slow-speed bearings (main bearings and gearbox low-speed bearings), and (III) high-speed bearings (gearbox high-speed bearings, gearbox intermediate speed bearings, and generator bearings) [25]. Their varying speeds of rotation and unique operating mechanisms result in an array of failure scenarios. In contrast, due to the short history of wind turbine studies, the vast majority of CMFD techniques of wind

turbine bearings concentrate mainly on identifying the problematic parts of the bearing (inner race, outer race, and balls) while including the mechanism of failure evaluation. As a consequence, more effort is required to improve the maturity of the developed CMFD methods. Existing methods, while readily applicable in idealized lab environments, may not be appropriate for in situ CMFD of turbine bearings due to complicated failure scenarios and specific bearing working mechanisms. As a consequence, it is critical to classify the failure types and then develop comprehensive CMFD procedures. Figure 3 shows different bearings installed in a typical large-scale horizontal axis wind turbine.

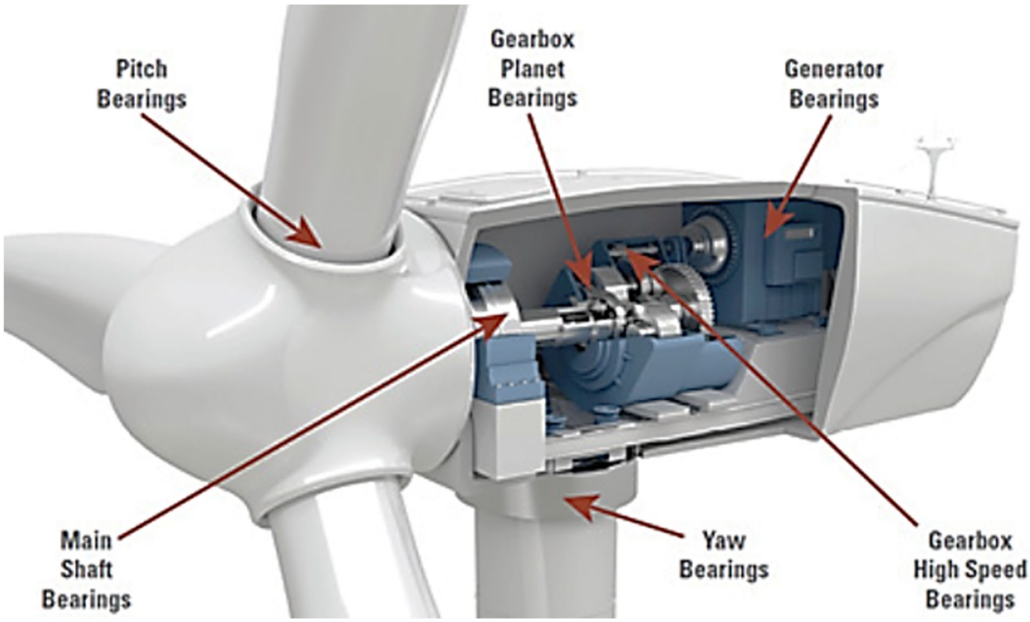

Figure 3. Different bearings in a large-scale horizontal axis wind turbine [26].

This review was conducted using a structured literature-screening strategy to reduce selection bias and improve transparency in the identification, classification, and synthesis of relevant studies. Although the present work is not a statistical meta-analysis, the search and screening process was organized using a PRISMA-informed approach, where the main objective was to identify peer-reviewed studies on wind turbine reliability, failure mechanisms, condition monitoring, structural health monitoring, prognostics and health management, and AI-enabled predictive maintenance. PRISMA 2020 provides updated reporting guidance for systematic reviews, including transparent reporting of identification, screening, eligibility, and inclusion steps; therefore, it was used as a methodological reference for structuring the literature search and reporting process [27].

The literature search was carried out using major scientific databases, including Scopus, Web of Science, ScienceDirect, IEEE Xplore, SpringerLink, MDPI, Taylor & Francis, Wiley Online Library, and Google Scholar. The search covered studies published mainly between 2000 and 2025, with stronger emphasis on works published after 2015 because of the rapid growth of large-scale and offshore wind turbines, digital condition monitoring, and AI-based PHM methods. Older studies were retained only when they provided foundational failure statistics, benchmark gearbox and bearing datasets, classical signal-processing methods, or widely used reliability formulations.

The search keywords were organized into five groups. The first group addressed component reliability and failure modes using terms such as “wind turbine reliability,” “wind turbine failure mechanisms,” “gearbox fault diagnosis,” “bearing fault detection,” “blade damage,” “tower fatigue,” and “flange bolt loosening.” The second group addressed monitoring technologies using terms such as “condition monitoring,” “structural health

monitoring," "vibration analysis," "acoustic emission," "ultrasonic testing," "infrared thermography," "oil debris monitoring," "SCADA diagnostics," and "impedance-based SHM." The third group addressed PHM and maintenance using terms such as "prognostics and health management," "remaining useful life," "predictive maintenance," "reliability modeling," and "maintenance optimization." The fourth group addressed AI methods using terms such as "machine learning," "deep learning," "CNN," "SVM," "DBN," "autoencoder," "transfer learning," and "domain adaptation." The fifth group addressed operating environment and field deployment using terms such as "offshore wind turbine," "large-scale wind turbine," "field validation," "non-stationary operating conditions," "data imbalance," and "domain shift."

The inclusion criteria were as follows: studies focused on wind turbine components or systems; studies addressing mechanical, structural, electrical, or data-driven reliability; studies presenting monitoring, diagnosis, prognosis, or maintenance methods; review papers that summarized major component-level failure mechanisms; and experimental, numerical, or field studies with clear relevance to wind turbine reliability. The exclusion criteria were as follows: papers unrelated to wind turbines; studies focused only on power-grid integration without component reliability; publications without sufficient methodological detail; duplicated records; nontechnical web articles; and studies where the component, monitoring method, or failure mechanism could not be clearly identified. When several studies reported similar methods, priority was given to papers with field data, long-term operational datasets, clear performance metrics, or explicit discussion of limitations.

After screening, the selected studies were classified into five major categories: drivetrain components, blade systems, tower and support structures, monitoring and sensing technologies, and AI-enabled PHM methods. This classification was used to organize the review and to connect physical failure mechanisms with measurable monitoring indicators, diagnostic methods, and maintenance implications. The purpose of the screening strategy was not only to collect a large number of publications, but also to compare the applicability, limitations, maturity, and field-deployment challenges of different reliability and monitoring approaches.

Table 4 summarizes the structured literature-search and screening strategy adopted in this review. The table defines the review type, databases, search period, keyword groups, inclusion and exclusion criteria, and final classification categories used to organize the selected studies. By separating component-related, monitoring-related, PHM-related, AI-related, and field-deployment keywords, the screening process ensured that the review covered both drivetrain and structural reliability topics while also capturing recent developments in data-driven predictive maintenance. This structured procedure improves transparency, reduces selection bias, and provides a clear basis for the subsequent critical comparison of wind turbine failure mechanisms, monitoring technologies, and PHM methods.

The article deals with developments in fault detection and Prognostics and Health Management (PHM) of gearboxes and bearings in horizontal axis wind turbines (HAWTs) in detail. It covers a wide range of testing methods, from classic methods to cutting-edge options based on statistical analysis and artificial intelligence. The scope is defined by the vital requirement to increase HAWT reliability as well as effectiveness through improved preventative maintenance and the implementation of PHM systems, considering both physical and electrical systems.

Although wind turbine reliability, condition monitoring, structural health monitoring, and AI-based PHM have each been reviewed in previous studies, most existing reviews focus on either a single component group or a single diagnostic category. For example, gearbox and bearing reviews commonly emphasize drivetrain vibration, oil-debris analysis, and signal-processing methods, whereas blade SHM reviews focus on delamination,

leading-edge erosion, acoustic emission, ultrasonic testing, thermography, and vision-based inspection. Similarly, tower and support-structure studies often emphasize fatigue cracking, corrosion, bolted connections, and strain-based monitoring, while AI-oriented PHM reviews mainly focus on data-driven classification and remaining useful life prediction. As a result, the physical connection among drivetrain failures, structural degradation, monitoring indicators, AI model limitations, and maintenance decision-making is often fragmented.

Table 4. Literature search and screening strategy used in this review.

Item	Description
Review type	Structured engineering review with PRISMA-informed screening [27]; not a statistical meta-analysis
Main databases	Scopus, Web of Science, ScienceDirect, IEEE Xplore, SpringerLink, MDPI, Taylor & Francis, Wiley Online Library, Google Scholar
Search period	Mainly 2000–2025, with emphasis on studies after 2015
Older studies retained when	They provide foundational failure statistics, benchmark datasets, classical diagnostic methods, or reliability formulations
Component keywords	Wind turbine reliability, gearbox fault diagnosis, bearing fault detection, blade damage, tower fatigue, flange bolt loosening
Monitoring keywords	Condition monitoring, SHM, vibration analysis, acoustic emission, ultrasonic testing, infrared thermography, oil debris monitoring, SCADA diagnostics, impedance-based SHM
PHM keywords	Prognostics and health management, remaining useful life, predictive maintenance, reliability modeling, maintenance optimization
AI keywords	Machine learning, deep learning, CNN, SVM, DBN, autoencoder, transfer learning, domain adaptation
Field-deployment keywords	Offshore wind turbine, large-scale wind turbine, field validation, non-stationary operation, data imbalance, domain shift
Inclusion criteria	Wind turbine component/system reliability; failure mechanisms; monitoring, diagnosis, prognosis, maintenance, SHM, PHM, AI diagnostics; experimental, numerical, field, and review studies relevant to reliability
Exclusion criteria	Non-wind-turbine studies; grid-only studies without component reliability; duplicated records; nontechnical web articles; insufficient methodological detail
Final classification	Drivetrain, blades, towers/support structures, sensing/monitoring technologies, AI-enabled PHM

To clarify the specific contribution of this review, Table 5 compares the present work with the main categories of existing review studies. The novelty of this paper is not the isolated discussion of gearbox faults, bearing defects, blade damage, tower cracking, flange loosening, or AI models individually. Instead, the contribution is the integrated applied synthesis of drivetrain and structural reliability within a single monitoring and predictive-maintenance context. This review connects physical failure mechanisms with measurable indicators, compares monitoring technologies in terms of field applicability and limitations, evaluates AI-based PHM models under practical data constraints, and identifies the remaining barriers to reliable deployment in large-scale and offshore wind turbines.

Table 5 clarifies how the present review differs from earlier component-specific or method-specific surveys. Previous reviews provide valuable detailed knowledge on individual subsystems, but their separation makes it difficult to understand how drivetrain failures, blade degradation, tower cracking, flange loosening, sensing technologies, and AI-based prediction interact within one reliability-management process. The present review addresses this gap by organizing the literature around four connected questions: what fails, how the failure physically develops, which measurable indicators can detect it, and how monitoring data can support diagnosis, prognosis, and maintenance decisions. This positioning also defines the scope of the paper as an integrated applied review rather than a new mathematical diagnostic algorithm or a statistical meta-analysis.

The key goals are to incorporate the current understanding of fault identification and PHM, assess the performance of different diagnostic and prognostic approaches, and emphasize difficulties and potential study paths in this area of study. In addition, the evaluation aims to examine the impact of PHM systems on wind turbine maintenance and operation plans, with particular emphasis on the transition to proactive upkeep. In doing so, the study aims to serve as a complete resource for wind power stakeholders such as scientists, researchers, and practitioners, as well as encourage additional advances in the reliability and effectiveness of HAWT systems.

Table 5. Positioning of the present review relative to existing wind turbine reliability and PHM reviews.

Review Category	Typical Focus in Previous Reviews	Commonly Covered Components	Main Strengths	Common Limitations	Added Contribution of the Present Review
Gearbox fault-diagnosis reviews	Gear vibration, gear-mesh frequency, oil contamination, signal processing	Gears, shafts, gearbox bearings, lubrication system	Strong coverage of vibration and oil-based diagnostics	Often limited to drivetrain; less connection to structural reliability and maintenance planning	Links gearbox failure mechanisms to PHM, AI limitations, and cross-component reliability decisions
Bearing diagnostic reviews	Bearing spalling, raceway defects, envelope analysis, acoustic emission, current-based monitoring	Main bearings, generator bearings, gearbox bearings, pitch/yaw bearings	Detailed fault-frequency and signal-processing discussion	Often based on laboratory/test-rig datasets and component-level diagnostics	Compares bearing diagnostics with field constraints such as non-stationary speed, data imbalance, and limited labels
Blade SHM reviews	Delamination, cracks, erosion, lightning damage, inspection and sensing	Blades, spar caps, leading edge, trailing edge, adhesive joints	Strong focus on structural damage and inspection methods	Often separated from drivetrain PHM and whole-turbine maintenance strategy	Connects blade damage mechanisms with sensing indicators, AI vision methods, and predictive maintenance needs
Tower and support-structure reviews	Fatigue cracking, corrosion, weld damage, vibration and strain monitoring	Towers, foundations, welded joints, support structures	Strong structural-mechanics emphasis	Often weak integration with drivetrain monitoring and AI-based PHM	Includes towers and flange joints together with drivetrain components in a unified reliability discussion
AI/ML-based PHM reviews	Fault classification, remaining useful life, neural networks, transfer learning	Usually drivetrain, SCADA systems, bearings, gearboxes	Strong coverage of algorithms and data-driven models	Often overemphasize accuracy without sufficient discussion of data imbalance, domain shift, and field validation	Critically discusses AI limitations, evaluation metrics, interpretability, and deployment barriers
Digital twin and maintenance reviews	Data fusion, virtual models, predictive maintenance, decision support	Whole turbine or selected subsystems	Useful for system-level maintenance planning	Often conceptual, with limited physical failure-mechanism detail	Connects digital twin concepts with component-level failure mechanisms and measurable monitoring features
Present review	Integrated reliability, monitoring, PHM, and AI-enabled predictive maintenance	Gearboxes, bearings, blades, towers, flange joints, sensing systems, AI/PHM models	Cross-component synthesis of failure mechanisms, indicators, methods, limitations, and maintenance implications	Does not perform statistical meta-analysis or introduce a new diagnostic algorithm	Provides an applied-engineering framework linking drivetrain and structural degradation to monitoring strategy and predictive maintenance

2. Wind Turbine Gearbox and Bearings: An Overview

2.1. Design and Function

The transfer theory regarding the wind turbine shows that the speed of turbine blades is different from the nominal speed of the generator. To achieve the desired input velocity, wind power is sent to the engine. At present, many commercial wind turbine systems use a fixed transmission ratio gearbox for connecting the rotor of the turbine to the generator. Employing a variable ratio gearbox (VRG) in a wind turbine that has a constant-speed output improves aerodynamic performance by allowing for discrete rotor speed change. Gearboxes frequently are built as solar and planetary gearboxes with similar gear configurations for optimum input speed and transmission ratio. Wind turbine gearboxes usually consist of one or two planetary gearing stages and a few parallel stages [28]. Figure 2 shows the framework of a 1.5 MW wind turbine gearbox [29].

Figure 4 illustrates the wind turbine gearbox's inside framework, which is extremely complicated. Due to a chain reaction, if any one of the components fails, the entire gearbox system may fail. Wind turbines are exposed to severe conditions, including heavy loads, gusts, and dust, that can cause gearbox failure. Wind turbine gearbox defects can be categorized into two kinds: wear-out breakdowns and temporary random faults [20]. Wind turbine gearbox problems include gear damage, bearing damage, broken shaft, leaky oil, high oil temperatures, and inadequate lubrication [30,31].

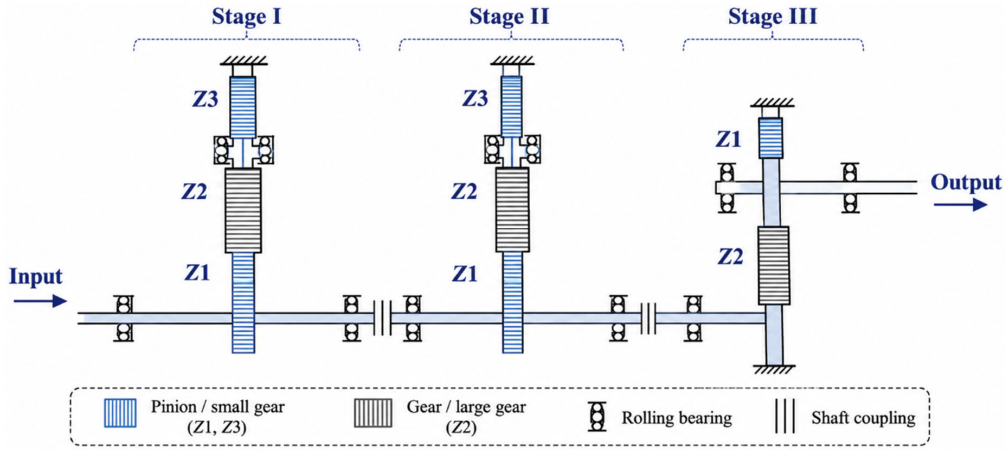

Figure 4. Wind turbine gearbox (1.5 kW) (recreated from [32]).

2.2. Common Faults and Their Implications

Studies on fixed-axis and planetary gearboxes have been substantially released, including many reviews. A preliminary research on gear dynamics utilized nonlinear vibration theory [32]. These works concentrate on creating dynamic models in order for predicting gear system operation. Initial studies neglected key aspects including opposition, transmitting error, TVMS, and gear tooth friction until the mid-1990s. Later, dynamic representations of spur gearing for fixed axes gearbox were developed, taking into consideration friction, flank deviations, wear, and spalling [33]. The development of nonlinearity in gear dynamics, encompassing backlash, vibro-impact, and TVMS, has been addressed [34]. The mathematical representations for planetary and epicyclic gear train systems established TVMS, gyroscopic effects, planet sharing of loads, and teeth surface alterations [35]. The study has looked at how tooth profile shift, mesh stiffness, meshes phase difference, teeth profile error, eccentricity error, and misalignment affect the dynamic of planetary gearboxes [36]. Utilizing lumped mass model (LMM), dynamic simulations, fractured gear systems [37] and gear errors, comprising tooth fractures, corrosion, cutting, wear, manufacturing error, and incorrect alignment, have been described [38].

The monitoring of condition methods, such as signal-processing methods including TSA, WVD, and wavelets, in addition to the fault extraction of feature variables and intelligent algorithms for classification, has been examined to find deficiencies [31,39–42]. Certain presumptions in these methods may not ensure real-world operating circumstances for pure irregular systems [43]. The analyses do not address the effect of non-stationary operating conditions on TVMS and dynamical models, despite documents highlighting their importance. A methodical investigation of a defect diagnosis methods for gearing systems under irregular situations is suggested. Gearboxes are producing irregular signals for vibration with complicated modulations and significant statistical fluctuations [44]. Identifying gear faults can be difficult in these circumstances. This review will address useful ways for detecting gear faults under irregular operating circumstances since they first appeared.

The article covers methods for studying stationary and irregular circumstances, using both modeling and experimental approaches. This review includes an examination of the propagation path of gear vibrations, non-stationary signal-processing methods like entropy, filter-based evaluation, multi-sensor-based approaches, integration techniques, and the application of intelligent categorization algorithms. Table 6 summarizes different failure modes whereas Figure 5 shows the cost occurred due to the failures of different components of wind turbine gearbox whereas Figure 6 shows the gearbox components. Similarly, Figures 7 and 8 show the different types of faults occurring in wind turbine gearbox and bearings, respectively.

Table 6. WT gearbox and bearing failure modes, monitoring indicators, and diagnostic methods.

Component	Failure Mode	Root Cause	Physical Mechanism	Measurable Indicators	Suitable Diagnostic Methods	Typical Consequence
Gear tooth	Pitting/micro pitting	Repeated contact stress, poor lubrication, surface roughness, high torque fluctuation	Local contact fatigue causes small surface cavities and progressive material removal	Gear-mesh frequency sidebands, vibration RMS increase, kurtosis increase, oil-debris particles	Vibration analysis, envelope analysis, oil-debris monitoring, acoustic emission	Increased vibration, noise, loss of gear accuracy, progressive tooth damage
Gear tooth	Bending fatigue crack	Cyclic tooth root stress, overload, misalignment, stress concentration at root	Crack initiates at tooth root and propagates under repeated bending load	Impulsive vibration, modulation sidebands, AE bursts, abnormal torque fluctuation	Vibration analysis, order tracking, acoustic emission, model-based residual analysis	Tooth fracture, sudden gearbox shutdown, severe secondary damage
Gear tooth	Scuffing	Lubricant film breakdown, high sliding velocity, excessive temperature, poor oil quality	Adhesive wear and surface tearing occur due to metal-to-metal contact	Oil temperature rise, high-frequency AE activity, metallic debris, surface roughness increase	Oil-condition monitoring, temperature monitoring, acoustic emission, vibration analysis	Accelerated wear, heat generation, surface damage, reduced gear life
Gear tooth/spline	Fretting corrosion	Small-amplitude oscillatory motion, insufficient clamping, micro-slip at contact surfaces	Repeated micro-slip removes oxide layers and produces oxidized wear debris	Red-brown debris, local wear marks, AE activity, small-amplitude vibration changes	Visual inspection, acoustic emission, vibration analysis, oil-debris analysis	Spline wear, loss of fit, torque-transfer degradation
Gearbox shaft	Shaft misalignment	Assembly error, foundation deformation, bearing wear, thermal distortion	Non-uniform load distribution increases bending and contact stress in gears and bearings	1× and 2× rotational frequency components, increased vibration, temperature rise	Vibration analysis, shaft orbit analysis, alignment inspection, thermal monitoring	Gear wear, bearing overload, coupling damage
Gearbox lubrication system	Lubricant degradation	Oxidation, water ingress, overheating, long oil-change interval	Oil viscosity and chemical properties degrade, reducing film thickness and load-carrying capacity	Viscosity change, moisture content, acidity, particle count, oil temperature	Online/offline oil analysis, dielectric sensors, particle counters, temperature monitoring	Increased friction, gear wear, bearing wear, overheating
Gearbox lubrication system	Particle contamination	Dust, wear debris, sealing failure, poor filtration	Hard particles cause abrasive wear and initiate surface defects	Increased particle count, ferrous debris, oil discoloration, abrasion marks	Oil-debris monitoring, ferrography, particle counting, filter inspection	Abrasion, accelerated pitting, lubricant-system blockage
Bearing outer race	Outer-race spalling	Rolling-contact fatigue, local overload, poor lubrication, contamination	Localized material loss develops on stationary raceway under repeated rolling contact	BPFO frequency, envelope spectrum peaks, AE energy, impact repetition	Vibration envelope analysis, acoustic emission, spectral kurtosis	Progressive raceway damage, vibration growth, bearing replacement
Bearing inner race	Inner-race spalling	Rolling-contact fatigue, rotating load zone, misalignment, high contact stress	Local defect on rotating raceway produces modulated impacts as rolling elements pass over defect	BPFI frequency, sidebands around shaft frequency, amplitude modulation	Order tracking, vibration analysis, envelope analysis, acoustic emission	Increased dynamic load, heat, vibration, possible secondary gearbox damage
Bearing rolling elements	Roller/ball surface damage	Contact fatigue, debris indentation, lubrication starvation	Local surface defects on rolling elements produce repeated impacts and unstable motion	BSF components, broadband vibration, AE bursts, increased temperature	Vibration analysis, AE monitoring, oil-debris monitoring	Rough operation, cage loading, accelerated raceway damage
Bearing cage	Cage wear or fracture	Skidding, poor lubrication, excessive vibration, misalignment, manufacturing defect	Cage pockets wear or crack, disturbing rolling-element spacing and motion	Cage-frequency components, irregular impacts, temperature rise, modulation	Vibration analysis, acoustic emission, temperature monitoring	Bearing instability, roller skewing, catastrophic bearing failure
Bearing/gearbox	Overheating	Lubricant failure, excessive friction, overload, cooling-system failure	Heat generation increases due to friction and reduced lubrication effectiveness	Bearing temperature, gearbox oil temperature, thermal hot spots, viscosity reduction	Temperature monitoring, SCADA diagnostics, thermal imaging, oil analysis	Oil degradation, accelerated wear, shutdown alarm
Bearing/gear interface	White-etching cracks	Hydrogen effects, transient loads, electrical current, material microstructural change	Subsurface crack networks form and propagate rapidly under rolling contact	Early vibration growth, broadband noise, AE activity, abnormal debris	Vibration analysis, AE monitoring, oil-debris monitoring, metallurgical inspection	Premature bearing failure, unexpected replacement
Gearbox housing/support	Structural looseness	Bolt loosening, foundation flexibility, housing deformation, resonance	Loss of stiffness alters load path and amplifies dynamic response	Low-frequency vibration, looseness harmonics, modal frequency shift	Vibration monitoring, modal analysis, bolt-preload inspection	Increased misalignment, gear/bearing overload, fatigue damage

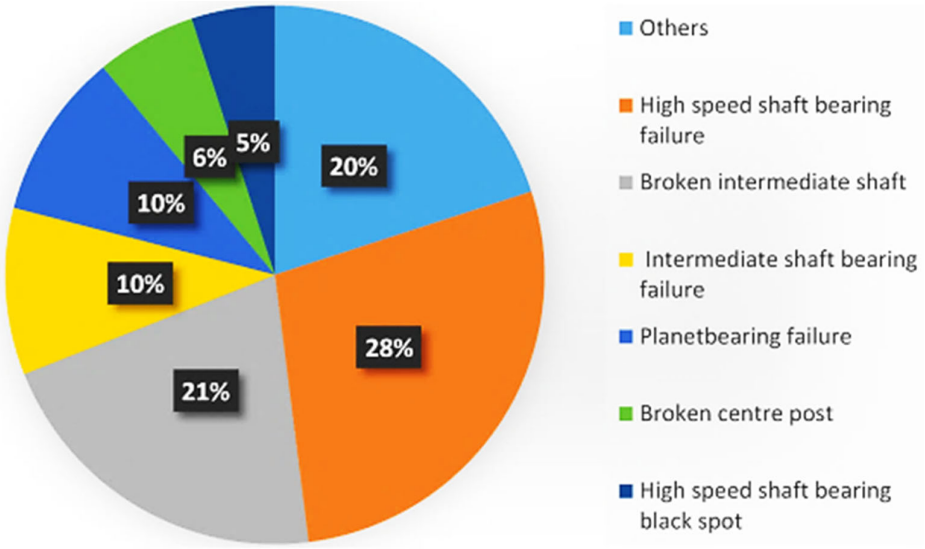

Figure 5. Wind turbine gearbox component failure cost distribution (%) [32].

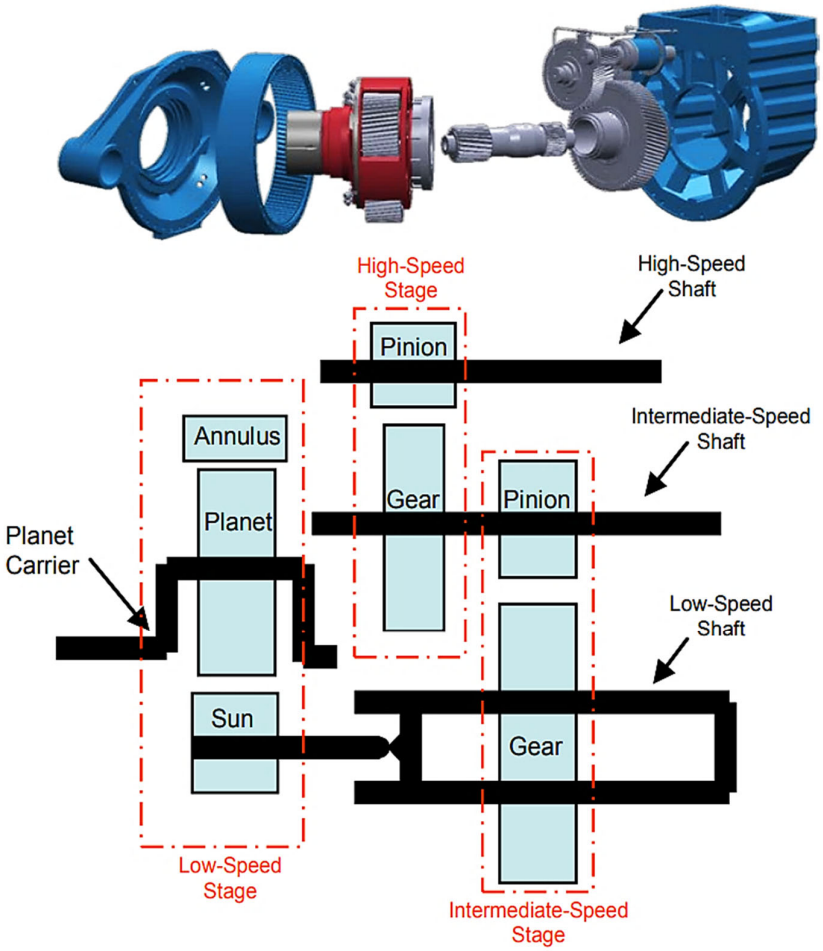

Figure 6. Wind turbine gearbox components [Source: NREL; https://www.nrel.gov/docs/fy12osti/53084.pdf (accessed on 28 December 2025)].

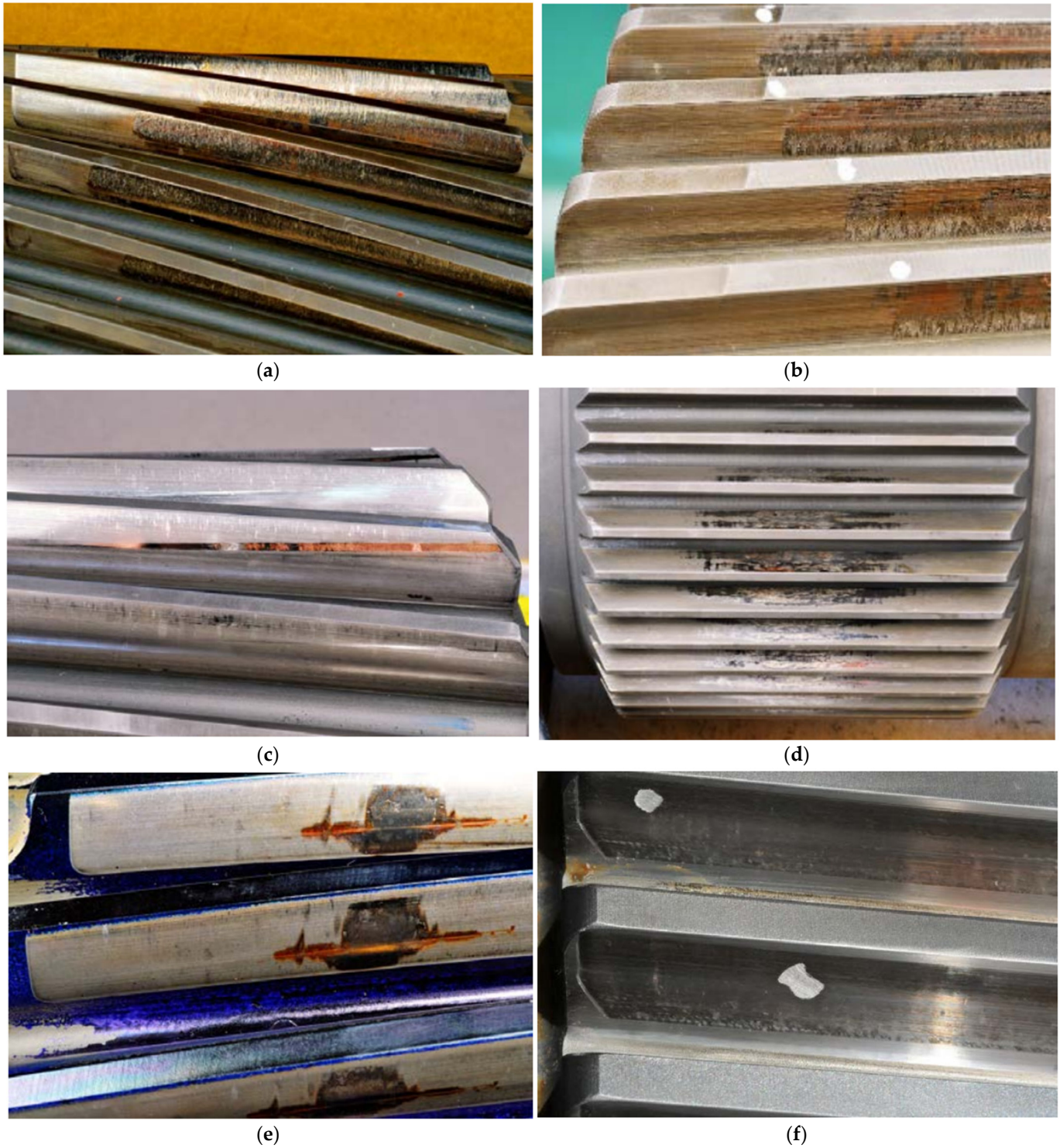

Figure 7. Fault occurrence in wind turbine gearbox components: (**a**) high-speed stage pinion (severe scuffing); (**b**) high-speed stage gear (severe scuffing); (**c**) sun pinion (severe fretting corrosion); (**d**) sun spline (severe fretting corrosion); (**e**) intermediate-speed stage pinion; (**f**) annulus gear [Source: NREL; https://www.nrel.gov/docs/fy12osti/53084.pdf (accessed on 15 December 2025)].

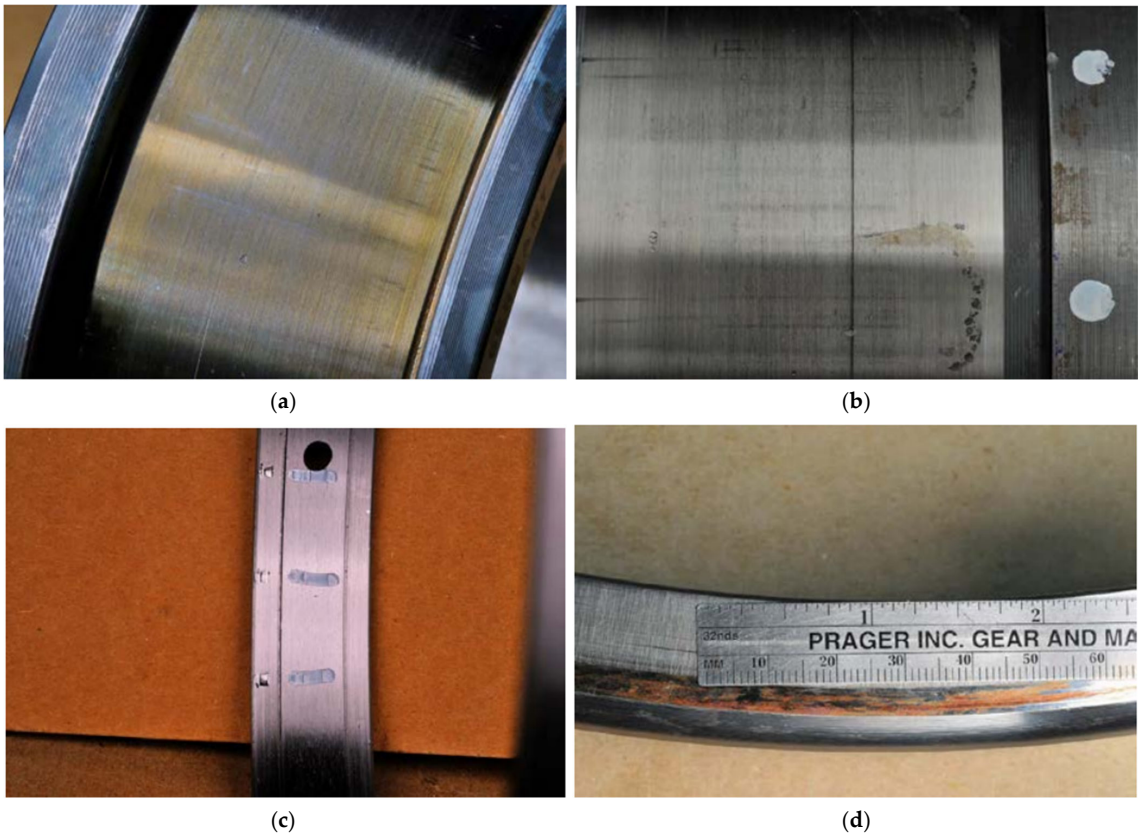

Figure 8. Fault occurrence in wind turbine bearings: (**a**) bearing inner raceway (mild overheating); (**b**) bearing inner raceway (mild contact corrosion); (**c**) bearing outer raceway spacer (severe assembly damage); (**d**) bearing plc-a outer raceway (severe fretting corrosion) [Source: NREL; https://www.nrel.gov/docs/fy12osti/53084.pdf (accessed on 28 December 2025)].

Gearbox and bearing failures are not governed by a single damage mechanism; instead, they arise from interacting mechanical, tribological, thermal, and operational factors. Gear tooth damage is commonly associated with repeated contact stress, root bending fatigue, lubricant breakdown, misalignment, and transient overloads, whereas bearing damage is strongly influenced by rolling-contact fatigue, lubrication quality, contamination, cage instability, and variable-speed operation [13]. Therefore, a more detailed failure-mode classification is required to connect the physical degradation process with measurable monitoring indicators and suitable diagnostic methods. Table 6 expands the gearbox and bearing failure modes by linking root causes, physical mechanisms, monitoring features, and possible operational consequences.

Table 6 shows that gearbox and bearing failures require diagnostic methods matched to the underlying physical degradation process. Gear tooth pitting, bending fatigue, and scuffing are mainly reflected in gear-mesh sidebands, impulsive vibration, acoustic emission activity, oil-debris generation, and temperature rise. Bearing spalling and rolling-element damage are more closely associated with characteristic bearing defect frequencies, envelope spectrum peaks, acoustic emission bursts, and localized temperature increases. Lubricant degradation and contamination are best detected through oil-condition monitoring and particle analysis, while misalignment, looseness, and housing-related problems require vibration, modal, and alignment-based diagnostics [44]. This expanded classification clarifies that gearbox and bearing reliability assessment should combine vibration, acoustic emission, oil monitoring, temperature monitoring, and model-based interpretation rather than relying on a single fault indicator [13].

2.3. Technologies and Techniques in Fault Diagnosis

2.3.1. Gearbox

Signal capture is essential for machine learning-based defect diagnosis [45]. WT gearboxes can be monitored using several signals, including vibration, noise emission, temperature, and lubricating oil parameters. Signal acquisition for WTs now relies on SCADA and CMS [46]. The SCADA system may collect drivetrain status parameters, such as gearbox oil temperature, as well as operating conditions like wind speed and direction. The SCADA system captures low-frequency signals of many forms. The CMS gathers high-frequency signals, such as vibration and acoustic emission [19].

The acquisition of vibration signals involves measuring the displacement, velocity, acceleration, frequency, period, and phase of the vibration body. Vibration signals provide valuable mechanical failure information, particularly for important components like gears and bearings in WT gearboxes. Vibration signals can be detected using vibration sensors. Vibration sensors can be classified as acceleration, speed, or displacement sensors to satisfy certain needs [1]. Accelerometers are the preferred vibration sensors for diagnosing WT gearbox faults due to their wide frequency range. Ren et al. [47] proposed a fault diagnosis method for WT gearboxes using Variational Mode Decomposition (VMD), Multi-scale Permutation Entropy (MPE), and Feature-based Transfer Learning (FTL) to monitor their health under different working conditions. In their study, Elasha et al. [48] used vibration measures to determine the remaining useful life of a WT gearbox using a regression and multilayer artificial neural network. Vibration-based techniques need the installation of sensors and data collecting equipment, leading to increased wiring complexity in TW gearboxes. Vibration sensors may be positioned on a surface or buried in a gearbox, resulting in reduced system reliability.

Cracks are the primary source of acoustic emission in WTs. Acoustic emission sensors fitted in gearboxes can identify structural flaws [49]. Acoustic emission signals from modest structural changes can detect early flaws and track their evolution to failure [50]. Acoustic emission signal waveforms can forecast damage location, timing, and progression to failure [51]. This method is often used to detect flaws in WT gearboxes due to its large frequency range and strong signal-to-noise ratio. It is more successful in diagnosing early defects or faults before they cause damage [52,53]. In a study by Elasha et al. [54], vibration and acoustic emission signals were examined for detecting bearing faults in a WT planetary gearbox. Acoustic emission was found to be more successful in detecting faults sooner. Konig et al. [55] used sonic emission to monitor the wear of sliding bearings in WT planetary gearboxes. This method is useful when transient wear data is not available. The primary downside of employing acoustic emission signals is the high cost of installing numerous sensors. Acoustic emission has another limitation: signal attenuation during transmission. Acoustic emission may not be feasible for some WTs due to the sensor's need to be close to the sound source [56]. Noise reduction methods play a crucial role in noisy surroundings.

Under typical conditions, the temperature of WT gearboxes should not surpass a specific limit. Abnormal temperatures may result from gear degradation, bearing failure, or other factors. Temperature measurement can provide valuable insights into gearbox health [57]. Sensors used for temperature measurement include optical pyrometers, resistive thermometers, and thermocouples. [58] Temperature-based techniques are extensively used for diagnosing gearbox faults. Lu et al. [59] suggested a failure detection system for gearboxes and generators that monitors temperature data from oil, bearings, and windings. Sarma et al. [60] used temperature indications from the gearbox to check its bearings' condition. Temperature-based fault diagnostics is a mature, dependable, and cost-effective technology. However, temperature development is sluggish and insufficient for early and accurate defect diagnosis. Temperature measurements can be impacted by environmental factors. Temperature increases in WT gearboxes can be produced by multiple reasons, mak-

ing it difficult to pinpoint the fundamental cause. Temperature measurement is commonly employed as an additional source of information [61].

Lubricating oil-based condition monitoring is typical in WT gearboxes. Monitoring oil metrics, including viscosity, moisture content, liquid level, particle count, temperature, and pressure, can indicate contamination and degradation processes, as well as the health of the gearbox [62].

Lubricant condition monitoring technologies can be classified as offline or online [62]. Offline oil condition monitoring is widely used in the wind power industry. This method involves analyzing oil samples offline using tools like viscometers and optical emission spectrometers. Lubricants are typically sampled at regular intervals, such as every six months [63], making it difficult to spot defects between sampling operations. Online oil condition monitoring addresses certain shortcomings of offline monitoring [63]. Oil sensors, including viscometers, level sensors, particle counters, and thermometers, provide real-time monitoring of oil conditions [64]. However, adding more sensors raises the overall cost. Additionally, not all oil parameters can be monitored in real-time using sensors. Real-time oil condition monitoring can be challenging to comprehend due to the impact of gearbox operation on oil levels.

Other signals are commonly utilized to diagnose faults in WT gearboxes, in addition to the ones listed above. SCADA systems use low-frequency data like current, voltage, power, speed, and wind speed to expose the operation state of WT gearboxes and provide valuable information about their performance. SCADA signals can be utilized to identify conditions, diagnose faults, and anticipate the life of WT gearboxes using proper algorithms. However, due to the lengthy recording interval of SCADA signals, many dynamic aspects of gearbox breakdowns are lost. Currently, SCADA signals are mostly used in model-based forecasting. Bangalore et al. [65] proposed an ANN-based condition monitoring approach for SCADA data.

Machine learning-based defect diagnosis approaches for WT gearboxes typically use many signals due to their unique advantages and limitations at different degrees of attention. Data mining of multi-source signals fully utilizes machine learning's benefits for efficient data processing and adaptive learning. Alkhadafe et al. [66] introduced a new application for the Automated Sensor and Signal-Processing Approach (ASPS). The researchers collected multi-sensory information from the gearbox test rig, including acoustic emission, vibration, speed, and torque, and used neural network-based classification models to create an effective monitoring system for fault diagnosis. Figures 9 and 10 show the different techniques used for the fault diagnosis and health management of the gearbox of the horizontal axis wind turbine.

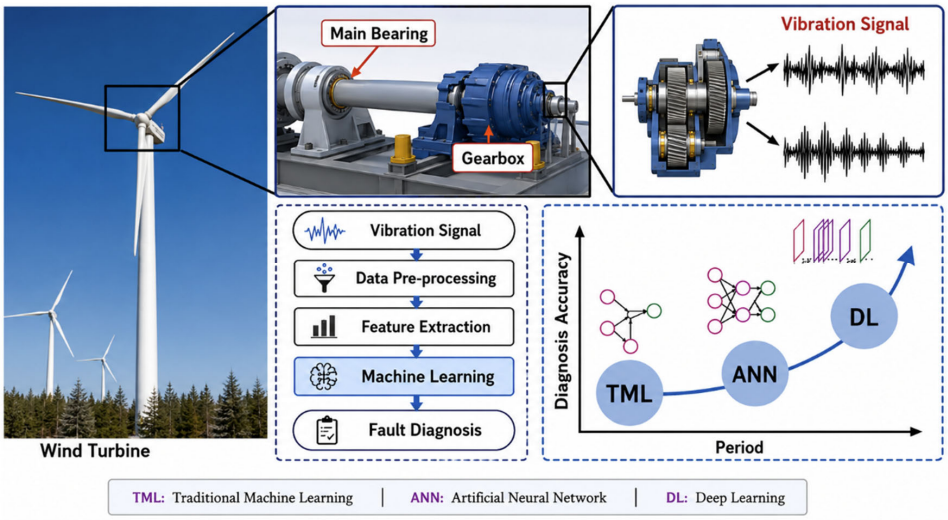

Figure 9. Wind turbine gearbox failure analysis based on vibration signals (recreated from [67]).

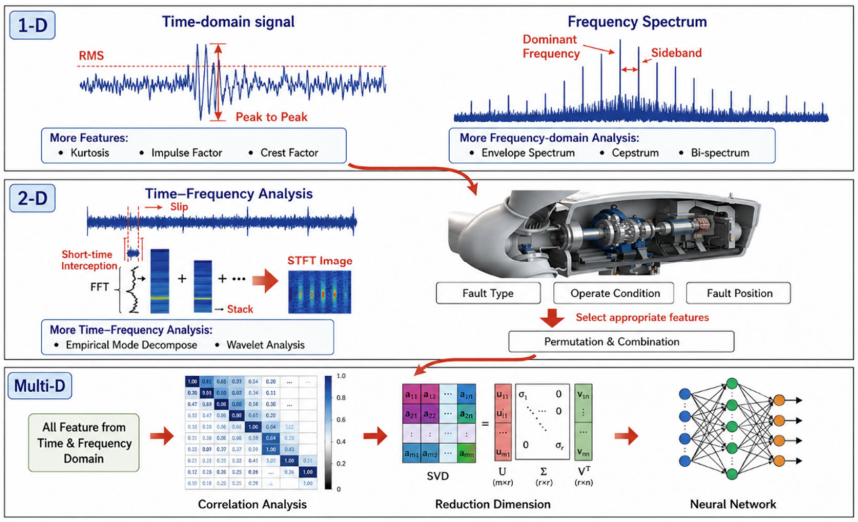

Figure 10. Wind turbine gearbox fault diagnosis using signal-processing techniques (recreated from [67]).

2.3.2. Bearings

Wind turbine main bearings operate in non-stationary operating conditions with dynamic loadings. To extract weak fault vibrating features, inconstant vibration signals are often converted to stationary signals or split into quasi-stationary components. Vibration analysis for main bearings primarily focuses on time–frequency-energy.

An et al. [68] employed the intrinsic time-scale decomposition (ITD) method to break down the vibration signal of a non-stationary direct-drive wind turbine main bearing into correct rotation components. This defines both the immediate amplitude and frequency. Dynamic characteristics for fault diagnosis were retrieved from the appropriate rotation components. A lab-scale experiment was conducted to determine the artificial inner race crack, outer race crack, and roller crack in the bearings.

Xin et al. [69] and Pan et al. [70] performed comparable experiments. They detected vibrations in two main bearings of two 1.5 MW direct-drive wind turbines. One bearing functioned normally, but the other developed a defect. Other works examined the features of normal and problematic bearings using cepstrum analysis [69], narrow-band envelope analysis [69], and spectral correlation analysis [70]. However, the authors were unable to identify the specific bearing problem type.

Zhang et al. [71] introduced the generalized transmissibility damage indicator (GTDI) technique, which relies on transmissibility function analysis. This refers to the spectral ratio between two output measurements. GTDI offers the advantage of eliminating dynamic loadings and noise effects. The authors performed a field test to diagnose wind turbine main bearings using the proposed method. GTDI has the potential for online fault diagnosis due to its ability to detect faults quickly (about 1.5 s) and accurately.

Bodla et al. [72] used Hilbert–Huang transform (HHT), feature extraction, and logistic regression (LR) to assess the health of 18 wind turbines' main bearings with 87% accuracy. Chen et al. [73] suggested a multifractal approach using the wavelet transform modulus maxima (WTMM) to analyze non-stationary vibration data in wind turbine main bearings. The field test was conducted on a real wind farm. Results indicate that incipient fault characteristics can be recovered from a multifractal spectrum.

Purarjomandlangrudi et al. [74] used Anomaly Detection (AD) and Support Vector Machine (SVM) machine learning algorithms to detect wind turbine main bearing faults. The lab-scale experiment demonstrated that the AD approach outperforms SVM in detecting incipient bearing defects. Zhang et al. [75] used this technique to create a new wavelet energy transmissibility function (WETF) that mitigates non-stationary effects and noise.

Han et al. [76] used the Teager energy operator to improve signals and Complementary Ensemble Empirical Mode Decomposition (CEEMD) to reduce noise.

Direct-drive wind turbines may monitor main bearing health through generator stator current signals. This is because the main shaft is directly connected to the generator, and any failures will pollute the signals. Gong et al. [77] used a wavelet filter on stator current signals to improve SNR and detect problems. Gong et al. [78–80] conducted PSD analysis on stator current signals. The approach identifies bearing defects by converting the fluctuating fundamental frequency of the stator current to a constant frequency. Wang et al. [81] presented the multi-scale filtering spectrum (MFS) approach, which uses the Vold–Kalman filter to convert time domain signals into order-domain energy distributions. Wang et al. [82] used a current-aided order tracking approach to determine shaft rotation frequency from stator current signals. The sources [78–82] conducted lab and field scale experiments to assess the effectiveness of proposed approaches for detecting both naturally and intentionally damaged main bearings. The failure modes of bearings include outer ring fracture, inner ring fracture, and cage fracture. Figure 11 shows the wind turbine bearings of health monitoring based on a unique idea of utilizing long-term monitoring data.

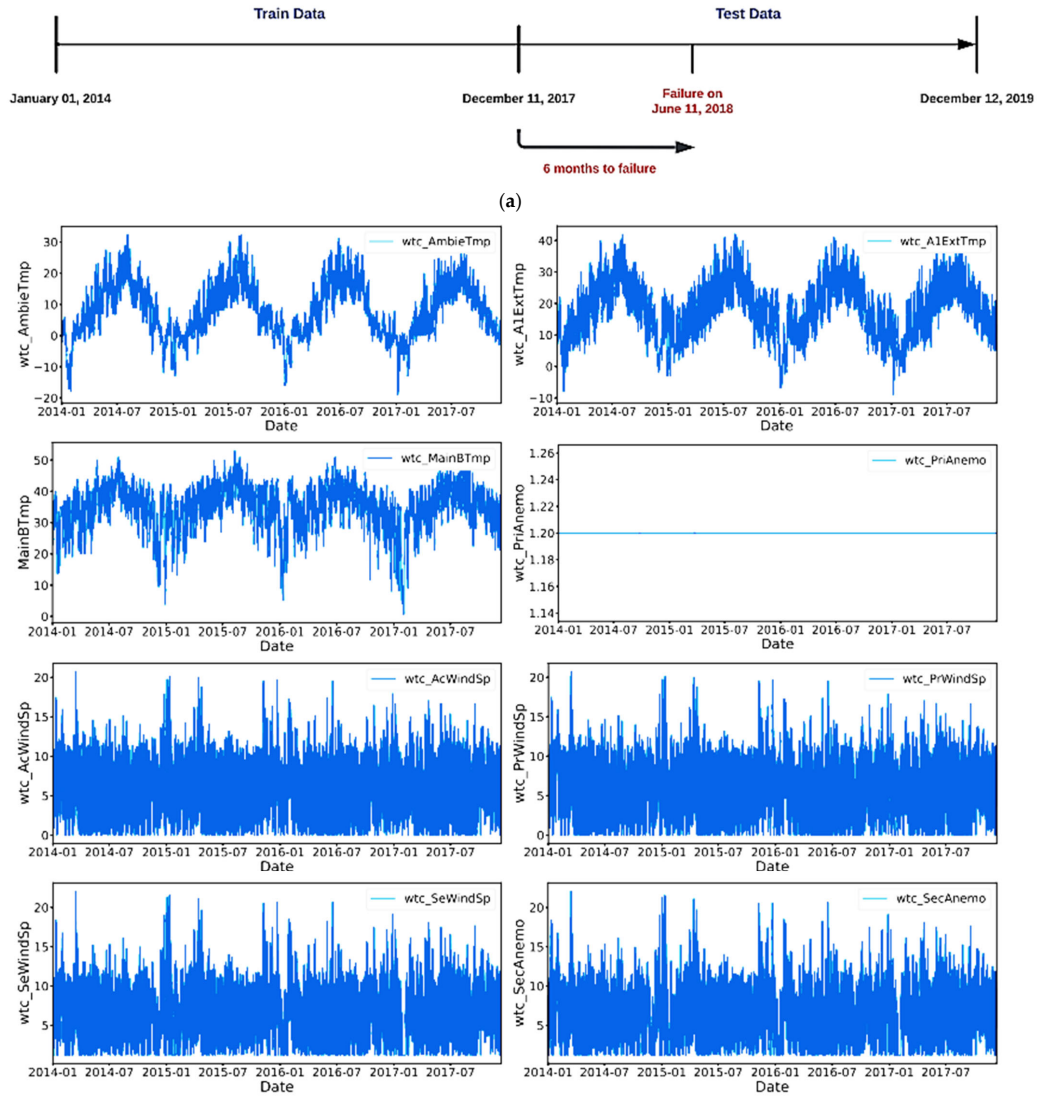

Figure 11. Wind turbine bearing health monitoring based on long-term data, (**a**) time scale, and (**b**) data for selected variables [Source: https://wes.copernicus.org/preprints/wes-2022-111/wes-2022-111-manuscript-version4.pdf (accessed on 28 December 2025)].

3. Advancements in PHM for Wind Turbines

3.1. Mathematical Basis and Assumptions of Representative SHM/PHM Models

Although wind turbine SHM and PHM methods are often described through sensors, algorithms, and diagnostic outputs, their interpretation depends strongly on the mathematical assumptions used to represent structural dynamics, degradation, uncertainty, and classification. For this reason, representative mathematical formulations are summarized here to clarify the physical and data-driven basis of commonly used monitoring models. These equations are not introduced as a new methodology in the present review; rather, they provide a compact mathematical reference for comparing model-based, signal-based, data-driven, and impedance-based SHM/PHM approaches under wind turbine operating conditions.

For structural components such as blades, towers, shafts, bearings, and support structures, the dynamic response can generally be idealized using the following second-order equation of motion:

$$\mathrm{M}\ddot{\mathrm{x}}(t) + \mathrm{C}\dot{\mathrm{x}}(t) + \mathrm{K}\mathrm{x}(t) = \mathrm{f}(t) \tag{1}$$

where $\mathbf{M}$, $\mathbf{C}$, and $\mathbf{K}$ are the mass, damping, and stiffness matrices, respectively, $\mathbf{x}(t)$ is the displacement response vector, and $\mathbf{f}(t)$ is the external load vector. In wind turbines, $\mathbf{f}(t)$ is strongly non-stationary because of turbulent wind, variable rotor speed, pitch-control action, wave loading in offshore turbines, and drivetrain torque fluctuations. Damage can modify the system matrices, particularly $\mathbf{K}$ and $\mathbf{C}$, causing changes in modal frequencies, damping ratios, strain response, vibration amplitude, and impedance signatures.

In residual-based fault detection, a measured signal is compared with the output predicted by a nominal healthy model. The residual can be written as

$$\mathrm{r}(t) = \mathrm{y}(t) - \hat{\mathrm{y}}(t) \tag{2}$$

where $\mathbf{y}(t)$ is the measured output and $\hat{\mathbf{y}}(t)$ is the model-predicted healthy output. A fault is suspected when the residual exceeds a predefined or adaptive threshold:

$$\|\mathbf{r}(t)\| > \eta \tag{3}$$

where η is the decision threshold. Fixed thresholds are simple but may fail under changing wind speed, load, temperature, and rotational speed. Adaptive thresholds or probabilistic residual evaluation are therefore more suitable for non-stationary wind turbine operation.

For degradation and remaining useful life estimation, the health state can be expressed using a discrete state-space degradation model:

$$\mathrm{x}_k = f(\mathrm{x}_{k-1}, \mathrm{u}_k) + \mathrm{w}_k \tag{4}$$

$$\mathrm{y}_k = h(\mathrm{x}_k) + \mathrm{v}_k \tag{5}$$

where $\mathbf{x}_k$ is the hidden degradation state, $\mathbf{u}_k$ is the operating input, $\mathbf{y}_k$ is the measured signal, and $\mathbf{w}_k$ and $\mathbf{v}_k$ represent process and measurement noise, respectively. In many Kalman-filter or Bayesian frameworks, these noise terms are assumed to be zero-mean Gaussian. However, wind turbine data often violate this assumption because of non-Gaussian turbulence, transient faults, missing data, and mixed operating regimes.

For a linear Kalman-filter model, the prediction and update stages can be written as

$$\hat{\mathrm{x}}_{k|k-1} = \mathrm{A}\hat{\mathrm{x}}_{k-1|k-1} + \mathrm{B}\mathrm{u}_k \tag{6}$$

$$\mathrm{P}_{k|k-1} = \mathrm{A}\mathrm{P}_{k-1|k-1}\mathrm{A}^T + \mathrm{Q} \tag{7}$$

$$\mathrm{K}_k = \mathrm{P}_{k|k-1}\mathrm{H}^T \left(\mathrm{H}\mathrm{P}_{k|k-1}\mathrm{H}^T + \mathrm{R}\right)^{-1} \tag{8}$$

$$\widehat{\mathrm{x}}_{k|k} = \widehat{\mathrm{x}}_{k|k-1} + \mathrm{K}_k\left(\mathrm{y}_k - \mathrm{H}\widehat{\mathrm{x}}_{k|k-1}\right) \tag{9}$$

where **A** is the state-transition matrix, **B** is the input matrix, **H** is the observation matrix, **Q** is the processnoise covariance, **R** is the measurement-noise covariance, **P** is the estimation-error covariance, and $\mathbf{K}_k$ is the Kalman gain. These models are efficient for online estimation but are limited when the turbine response is highly nonlinear, non-Gaussian, or affected by abrupt operational transitions.

For support vector machine-based fault classification, the standard soft-margin optimization problem can be expressed as

$$\min_{\mathbf{w},b,\xi_i} \left(\frac{1}{2}\|\mathbf{w}\|^2 + C\sum_{i=1}^{N} \xi_i\right) \tag{10}$$

subject to

$$y_i\left(\mathbf{w}^T\phi(\mathbf{x}_i) + b\right) \geq 1 - \xi_i, \xi_i \geq 0 \tag{11}$$

where $\mathbf{x}_i$ is the feature vector, y_i is the class label, $\phi(\cdot)$ is the kernel mapping, **w** and b define the decision boundary, ξ_i are slack variables, and C controls the penalty for misclassification. SVM models are effective for small-to-medium datasets but depend strongly on feature quality, kernel selection, and the representativeness of training data.

For deep-learning-based diagnosis, the multi-class cross-entropy loss commonly used in CNN, DBN, and other neural diagnostic models is

$$\mathcal{L} = -\frac{1}{N}\sum_{i=1}^{N}\sum_{c=1}^{C} y_{ic}\log(\widehat{y}_{ic}) \tag{12}$$

where N is the number of training samples, C is the number of classes, y_{ic} is the true class label, and $\widehat{y}_{ic}$ is the predicted class probability. Deep models can learn complex nonlinear features from vibration, SCADA, acoustic emission, image, or multi-sensor data, but they require large and representative datasets. Their reliability decreases when field data are imbalanced, labels are uncertain, or the test turbine differs from the training turbine.

For impedance-based SHM, damage is commonly evaluated by comparing the electromechanical impedance signature of a structure in the current condition with that of a healthy baseline. A normalized damage index can be written as

$$DI = \sqrt{\frac{\sum_{i=1}^{n}\left(Z_i^d - Z_i^0\right)^2}{\sum_{i=1}^{n}\left(Z_i^0\right)^2}} \tag{13}$$

where Z_i^0 is the baseline impedance at frequency point i, Z_i^d is the impedance after damage or degradation, and n is the number of frequency points. This approach is highly sensitive to local stiffness changes caused by bolt loosening, cracks, and adhesive degradation, but it also requires environmental compensation because temperature, humidity, bonding condition, and sensor aging can shift impedance signatures even without damage.

Table 7 summarizes the mathematical assumptions behind representative SHM and PHM models used in wind turbine reliability assessment. Physics-based models provide interpretability and direct connection to load transfer, modal behavior, and structural degradation, but they may be limited by uncertain boundary conditions, nonlinear contact, environmental forcing, and model simplification. Data-driven methods such as SVM, CNN, DBN, and autoencoders can identify complex diagnostic patterns from high-dimensional

signals, but their performance depends on data quality, class balance, training diversity, and transferability to new turbines. Impedance-based and residual-based methods provide strong sensitivity to local stiffness change or deviation from healthy behavior, but they require reliable baseline compensation. Therefore, practical wind turbine PHM should combine physical modeling, uncertainty-aware data-driven learning, and field validation instead of relying on any single mathematical model.

Table 7. Mathematical assumptions and limitations of representative SHM/PHM models.

Model/Method	Representative Mathematical Basis	Main Assumption	Handling of Non-Stationarity	Main Strength	Limitation in Wind Turbine Application
Structural dynamic model	$\mathbf{M}\ddot{\mathbf{x}} + \mathbf{C}\dot{\mathbf{x}} + \mathbf{K}\mathbf{x} - \mathbf{f}(t)$	Mass, damping, stiffness, and loading can be represented with sufficient fidelity	Requires time-varying loading or linearization around operating points	Physically interpretable and useful for modal response, load transfer, and damage-sensitive features	May oversimplify nonlinear contact, aeroelastic coupling, drivetrain backlash, and environmental variability
Residual-based FDD	$\mathrm{r}(t) - \mathrm{y}(t) - \hat{\mathrm{y}}(t)$	Healthy model represents normal behavior accurately	Adaptive thresholds needed under variable operation	Simple fault indicator and compatible with SCADA/model-based monitoring	Sensitive to model uncertainty, sensor noise, and changing operating conditions
Kalman filter/Bayesian estimation	State-space prediction and update equations	Noise is often assumed Gaussian and model structure is known	Extended/unscented/particle filters can address nonlinear cases	Suitable for online state estimation and RUL tracking	Performance degrades under non-Gaussian noise, missing data, abrupt faults, or poorly known degradation models
Lumped mass model	Reduced mass–spring–damper representation	Complex structure can be approximated by discrete DOF system	Requires updating with operating speed and load conditions	Computationally efficient for drivetrain and tower dynamic analysis	May miss local damage, distributed flexibility, and complex boundary conditions
SVM classifier	Margin maximization with slack variables	Classes are separable in feature/kemel space	Requires stable feature extraction or order tracking	Effective for small datasets and engineered features	Sensitive to kemel choice, class imbalance, and domain shift
CNN/deep learning classifier	Cross-entropy minimization	Training data represent deployment conditions	Can learn features from raw or transformed signals but needs diverse data	Powerful for vibration, image, SCADA, and multi-sensor classification	Requires large labeled datasets, has limited interpretability, and may overfit laboratory data
DBN/autoencoder	Layer-wise feature learning and reconstruction error	Latent features capture normal/fault behavior	Can be used for anomaly detection when labels are limited	Useful for unsupervised or semi-supervised PHM	Threshold selection and field validation remain difficult
Impedance-based SHM	Baseline-to-current impedance damage index	Impedance change is mainly caused by local damage	Requires temperature and environmental compensation	Highly sensitive to local stiffness change in joints, bolts, and bonded regions	Local sensing range, baseline drift, sensor bonding, and environmental effects limit field deployment
Digital twin/data fusion	Coupling of physical model, sensor data, and updating algorithm	Model and data streams can be synchronized and calibrated	Can update parameters over time using operational data	Supports system-level diagnosis, prognosis, and maintenance decision-making	Requires high-quality data, uncertainty quantification, interoperability, and validation

(R1) The Kalman-filter- and Bayesian-based RUL studies can be interpreted through the state-space degradation and observation formulation introduced in Equations (4) and (5), while the recursive prediction-correction process follows the Kalman update structure summarized in Equations (6)–(9). This connection clarifies that their reliability depends on the validity of the assumed state-transition model, observation model, and process/measurement-noise covariance definitions.

The dynamic-model-based studies reviewed here are related to the generalized equation of motion in Equation (1), where changes in mass, damping, stiffness, or external loading can alter vibration response, modal behavior, and damage-sensitive features. This mathematical connection also explains why simplified lumped mass models may be efficient for system-level interpretation but may miss local nonlinear contact, distributed flexibility, or detailed boundary-condition effects.

CNN-, DBN-, and other deep-learning-based diagnostic studies can be linked to the cross-entropy classification objective in Equation (12). This connection highlights that reported classification performance depends not only on network architecture, but also on

label quality, class balance, training-data diversity, and the similarity between laboratory or historical training data and noisy field SCADA/CMS data.

The mathematical treatment of non-stationarity remains a central challenge in wind turbine fault diagnosis. Algorithms based on fixed spectral features, constant thresholds, or stationary noise assumptions may perform well in laboratory tests but become less reliable under variable-speed, variable-load, and turbulent field operation. For example, bearing characteristic frequencies and gear-mesh sidebands shift with rotational speed, while SCADA relationships between wind speed, power, temperature, and rotor speed vary with control state and environmental conditions. Therefore, order tracking, time–frequency analysis, adaptive thresholds, domain adaptation, and physics-informed feature normalization are often required before applying AI or statistical models to field data. This limitation should be considered when comparing diagnostic algorithms reported under controlled and real operating conditions.

(R1) The equations summarized in this section are used as interpretive references for the following literature analysis. In the subsequent subsections, Kalman-filter and Bayesian prognosis studies are connected with the state-space and recursive update formulations in Equations (4)–(9), residual-based FDD studies are linked with Equations (2) and (3), SVM-based classifiers are interpreted through Equations (10) and (11), deep-learning diagnostic models are related to Equation (12), and impedance-based SHM studies are connected with Equation (13). This cross-referencing helps integrate the mathematical basis with the reviewed literature rather than treating the equations as isolated definitions.

3.2. Mathematical Models

Model-based procedures, unlike signal-based techniques, require "mathematical models" of wind turbines or their primary components. This method does not require high-resolution condition-specific signals like signal-based approaches. Model-based techniques rely on mathematical models of the wind turbine's process and I/O information, which are often available through the control system. Mathematical models are often built as "nominal model" to represent fault-free processes for FDD and "deterioration models" for LTP. Figure 12 illustrates that nominal and deterioration models can be statistically derived by "theoretical/physical model" or "experimental modeling" methodologies.

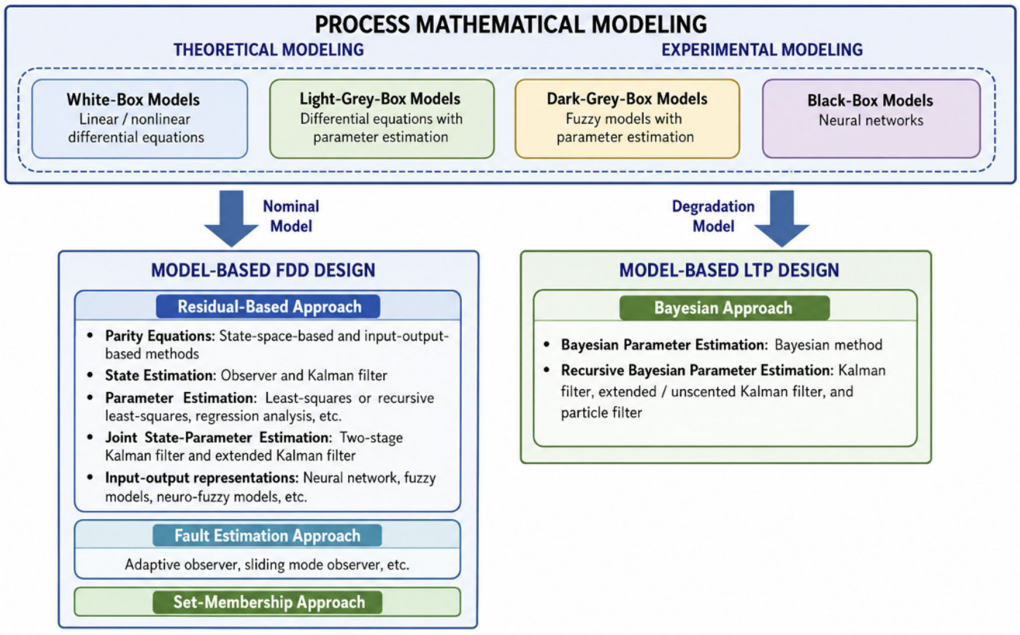

Figure 12. Mathematical models for PHM of wind turbine components (recreated from [83]).

After determining the optimum modeling technique, various design approaches (as shown in Figure 12) can be employed to create a model-based condition monitoring framework. This article provides a quick overview of key model-based design methodologies for FDD and LTP.

Model-based FDD techniques often use residual-based, fault estimation, or set-membership approaches. Residual, also known as symptom signal, is a real-time failure indicator based on the difference between measurements and mathematical model outputs. A model-based FDD approach based on residual generation monitors the trend of the residual signal and acts when it reaches a threshold value [84]. Various methods are used to evaluate residuals, including fixed or adaptive threshold testing, statistical methods, and fuzzy logic approaches. The residual-based approach is simple to implement, but the main challenge is addressing process noise and modeling uncertainty, as well as achieving disturbance decoupling (i.e., ensuring that the residual is not affected by unknown inputs other than faults) [84–86]. Several reference papers, such as [87,88], extensively quote and explain the methods stated above. The residual-based FDD approach in wind turbines has been extensively explored, utilizing the approaches indicated above.

(R1) Residual-based FDD studies are mathematically linked to Equations (2) and (3), where deviations between measured and model-predicted healthy responses are evaluated against a decision threshold. Therefore, the diagnostic performance of such methods depends strongly on the accuracy of the healthy baseline model and the adaptability of the threshold under variable wind speed, load, and environmental conditions.

3.3. Machine Learning and AI in PHM

Signal-processing techniques can detect and diagnose defects in a gear system. An intelligent fault classification method can reliably identify the type of fault in processed vibration signals. SVM-based fault classification was applied to a wind turbine gearbox [89,90]. To improve accuracy, binary tree SVM was used to detect faults in planetary gearboxes with broken, cracked, and pitted teeth in the sun gear [91].

(R1) SVM-based diagnostic studies correspond to the margin-maximization formulation in Equations (10) and (11). This formulation explains why SVM models can perform well with engineered features and small-to-medium datasets, but their reliability depends on kernel selection, feature separability, class balance, and whether the training data represent the operating conditions of the target turbine.

An improved hypersphere SVM method was proposed and tested for fault diagnosis in a wind turbine gearbox [92]. Li et al. [93] statistically and effectively showed least square SVM to complete fault pattern recognition based on entropy-related characteristics. For successful categorization of a misalignment fault, SVM has be used for mixed-domain characteristics recovered after disintegration [94]. Furthermore, a hybrid classifier using SVM and an artificial neural network was designed for the diagnosis of gear defects [95].

Under variable circumstances, an intelligent fault detection method based on the deconstruction algorithm and SVM was proposed by Xing et al. [96] to correctly identify several sorts of gear defects. A study [97,98] proposed employing order cepstrum, the radial basis function, and an artificial neural network to detect gear faults during speedup. Back-propagation neural networks have been used for classification (as described in [99]). A convolutional neural network [100] was used to classify gearbox health issues using a time–frequency image from a wavelet transform [101]. A fault detection approach for a planetary gearbox with difficulties has been proposed, utilizing assignment reduction and a flexible naive Bayesian classifier [102]. A fuzzy predictive framework combining Mamdani models and hierarchical clustering was verified using data from a testbed containing tooth fracture in helical gears [103].

This section concludes with a summary of vibration-based problem diagnosis methodologies for wind turbine gearboxes under non-stationary situations. The next sections will address identified research shortcomings. Figure 13 shows different AI-based techniques being used for the fault diagnosis and health monitoring of wind turbine gearbox and bearings.

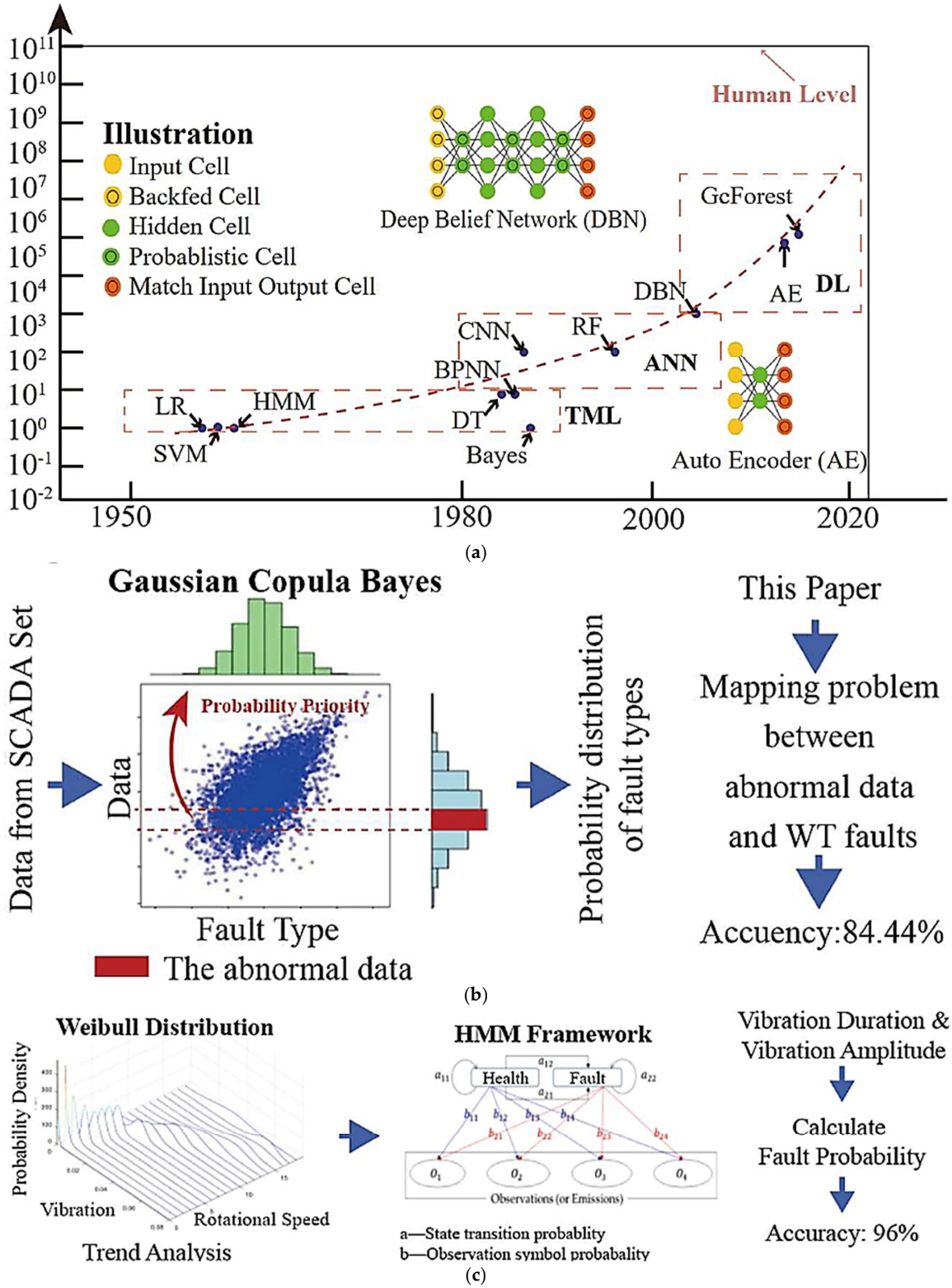

Figure 13. *Cont.*

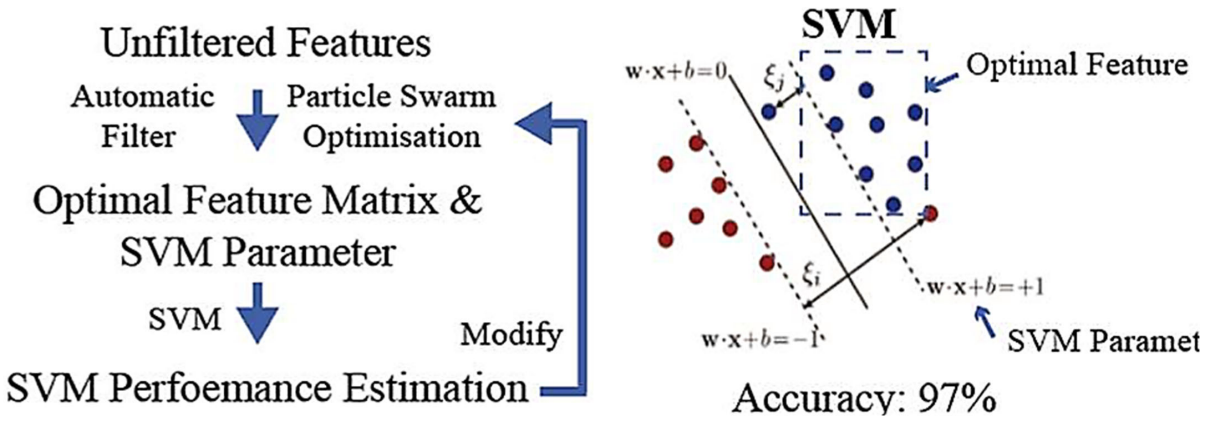

(**d**)

Figure 13. Different AI-based techniques used for fault diagnosis of wind turbine gearbox and bearings; (**a**) historical overview; (**b**) Gaussian method; (**c**) Weibull distribution (**d**) SVM [67].

3.4. Numerical Techniques

Researchers have investigated the dynamic behavior of gearboxes at different speeds. Bartelmus et al. [104] and Chaari et al. [105] created a spur planetary gearbox model with variable motor speed to simulate time-varying loading circumstances. Variations in load cause the simultaneous modulation of the acceleration signal amplitude. Gear pair stimulation during start-up can cause oscillations due to torque variability and nonlinear Hertzian contact force, resulting in variations in meshing rigidity [106]. A multi-body computational simulation of a wind turbine gearbox was developed to investigate the impact of rapid start-up and sudden halt on the motion of the power drive train [107]. Hammami et al. [108] examined the changing behavior of back-to-back planetary gears with varying ring gear loads and run-up conditions. The majority of test cases focused on start-up circumstances to prevent overloads when traversing eigen frequencies [109].

A longitudinal lumped component simulation of a planetary gearbox with time-varying loads showed variations in mesh stiffness and a dominant third harmonic of mesh frequencies in the spectrum [110,111]. Srikanth and Sekhar developed a gear dynamic model with 18 degrees of freedom for a wind turbine drive train under stochastic load based on Danish specification DS 472. Power spectral density was used to analyze the results, emphasizing the impact of aerodynamic loads [112,113]. Nevertheless, an aerodynamic torque is represented as an irregular signal. A question arises regarding the nature of hydrodynamic torque. Mabrouk et al. [114] studied the noise responses of a wind turbine gear train under rapid aerodynamic torque loads. The previously mentioned research focused solely on dynamic analysis under varied loading circumstances. Liu et al. [115] simulated a vibro-impact gear model with blowback. A dynamic mathematical model for a pair of spur gears undergoing random loading was studied, considering several characteristics like backlash, TVMS, damping, and friction [116]. Under stochastic loads, a dynamic LMM of a gear train was evaluated, considering TVMS, transmission error, and backlash [117], as well as tooth root fracture and transfer error [118], to explore the dynamic characteristics and failure processes of a gear transmission system. Rotational load and backlash have a significant impact on torsional vibrations. Liu et al. [119] used a dynamic model of a plane gear to study the impact of centrifugal force on variable-speed operations.

Wei et al. [120] studied the dynamic model of a zigzag planetary gear system with an imbalanced load, in addition to motivating gears. To accurately depict a gear transmission system, an 18DOF, two-stage helical gear LMM design was presented, considering the speed-torque properties of both driving and loading motors [121]. The model has been verified experimentally, considering sinusoidal and step increment stresses. Additionally,

gearbox simulation has been done to identify transmission pathways [122,123]. A study was conducted using power flow FEM to analyze the transmission route of a wind turbine for detecting gearbox faults under irregular conditions [124]. Bearings' impact on transmission route and vibration levels was studied utilizing multi-body modeling and transmission path analysis [125].

In Figure 14, Bakri et al. [126] utilized DBN to identify nonlinear characteristics and invariant framework in input signals to diagnose WT faults under different circumstances. This method avoids interference from outside sources, which is a benefit. Improving the DBN algorithm is a popular research direction. Researchers have developed approaches to optimize DBN algorithms, leading to enhanced diagnostic accuracy.

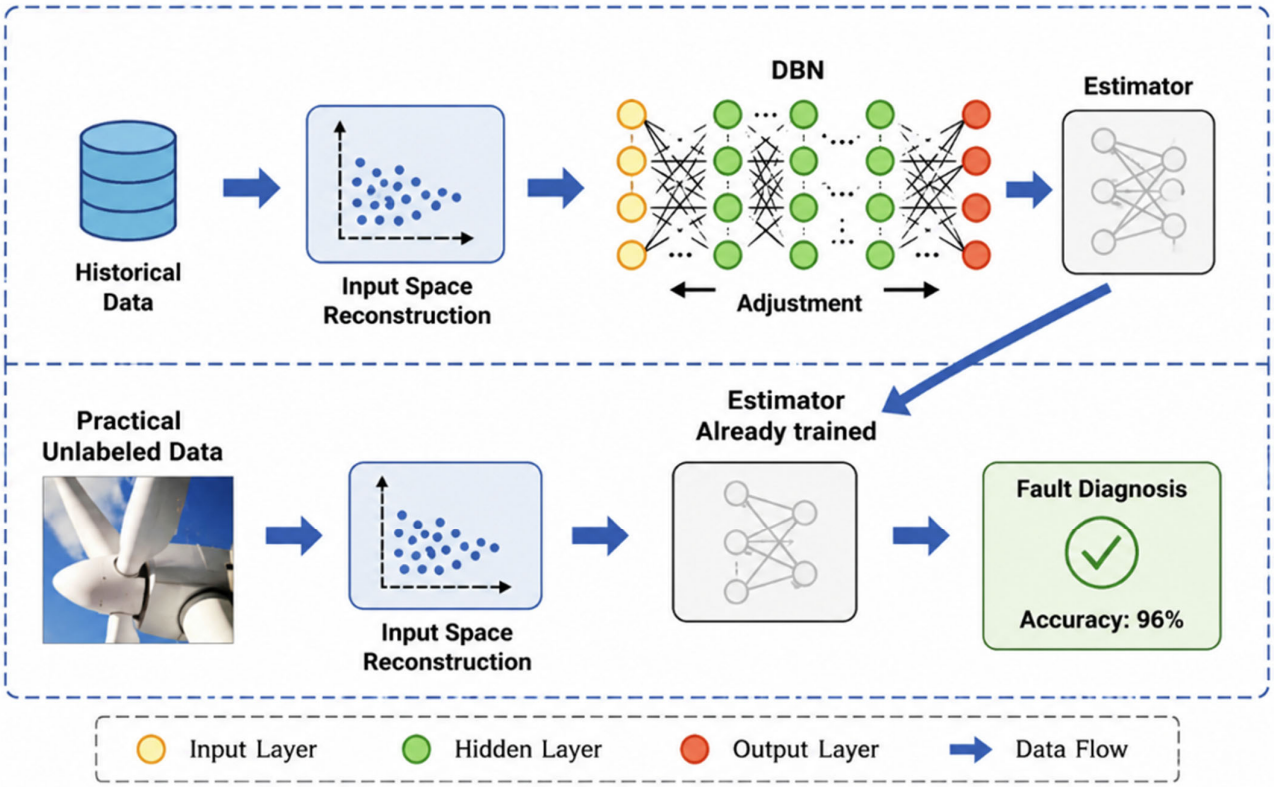

Figure 14. DBN algorithm applied by Bakri et al. for wind turbine fault diagnosis (recreated from [126]).

3.5. PHM of WT Using Digital Twin

Digital twin technology offers a novel approach for detecting and diagnosing equipment faults. Zhang et al. [127] suggested a method to diagnose rolling-bearing faults by gathering fault data ahead of time. As a result, bearings can operate safely while incurring lower maintenance costs. Nevertheless, this method is currently in the offline information processing and diagnostic stage and does not support real-time digital diagnosis. Xiong et al. [128] introduced a real-time field-programmable gate array-digital twin (FPGA-DT) technology. Using identifiable vectors of features and digital twin techniques to diagnose and categorize system faults allows for real-time monitoring of transformers, leading to increased effectiveness and precision. Technique was built around a digital twin. Using a dynamic digital model and an incomplete adaptive method, the twin model reliably diagnoses the health of bearings that roll in unknown fault scenarios.

Nevertheless, the hardware system specifications are high and cannot be met uniformly. Guo et al. [129] suggested an improved random forest (IRF) technique using a digital twin. The use of a digital twin's fault identification method increases accuracy and allows

for speedy discovery and the placement of the defect. Shangguan et al. [130] proposed a digital twin-based fault diagnosis approach for complex satellite networks, addressing the limitations of previous methods that rely on previous and static data. Combining simulation with real-time data allows for real-time diagnostics and the repair of in-orbit satellites. This ensures dependable operation and reduces operator workload. Figures 15–19 show schematics of a typical digital twin-based fault diagnosis methodology for wind turbine gearbox [131].

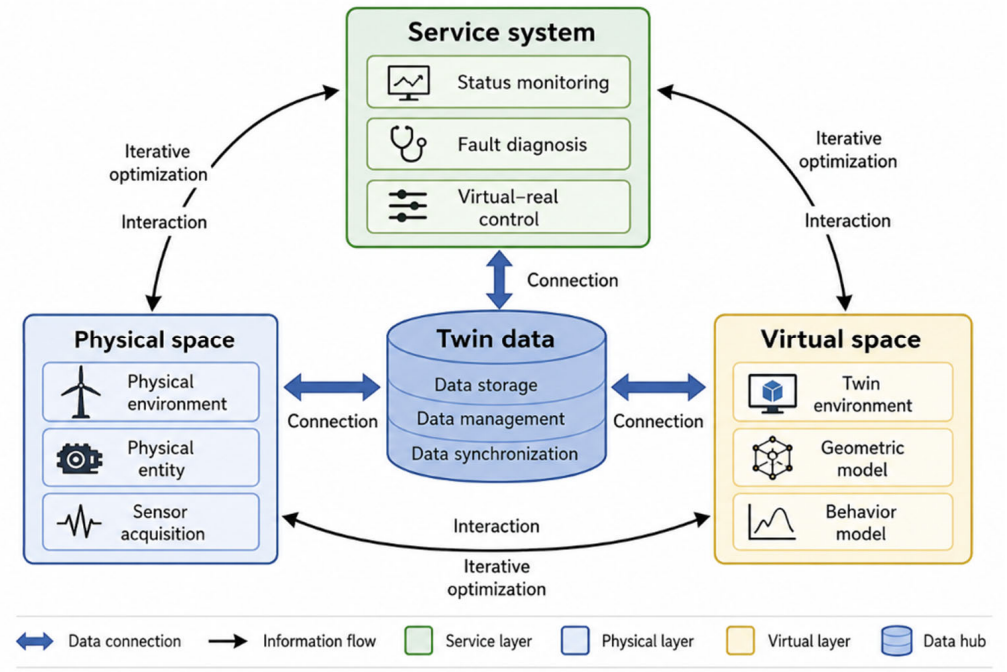

Figure 15. Digital twin basic workflow (recreated from [131]).

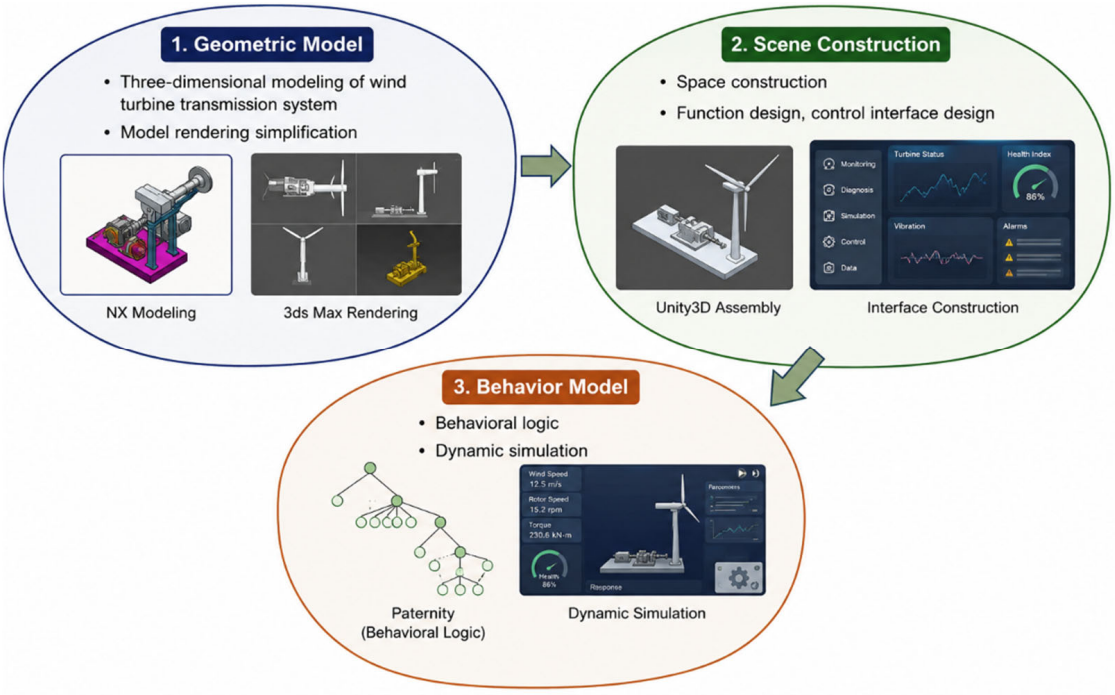

Figure 16. Digital twin for wind turbine fault analysis (recreated from [131]).

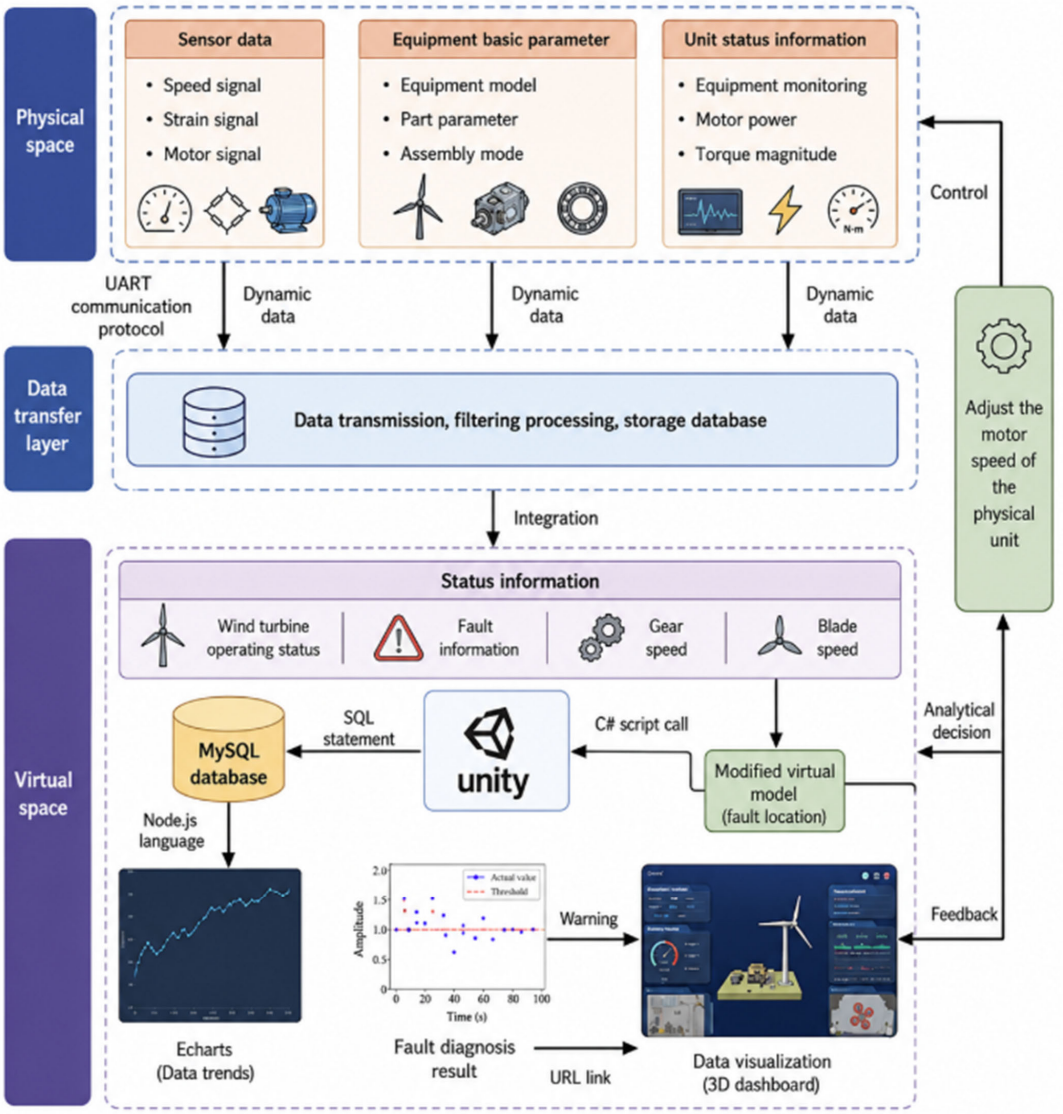

Figure 17. Digital twin architecture for wind turbine (recreated from [131]).

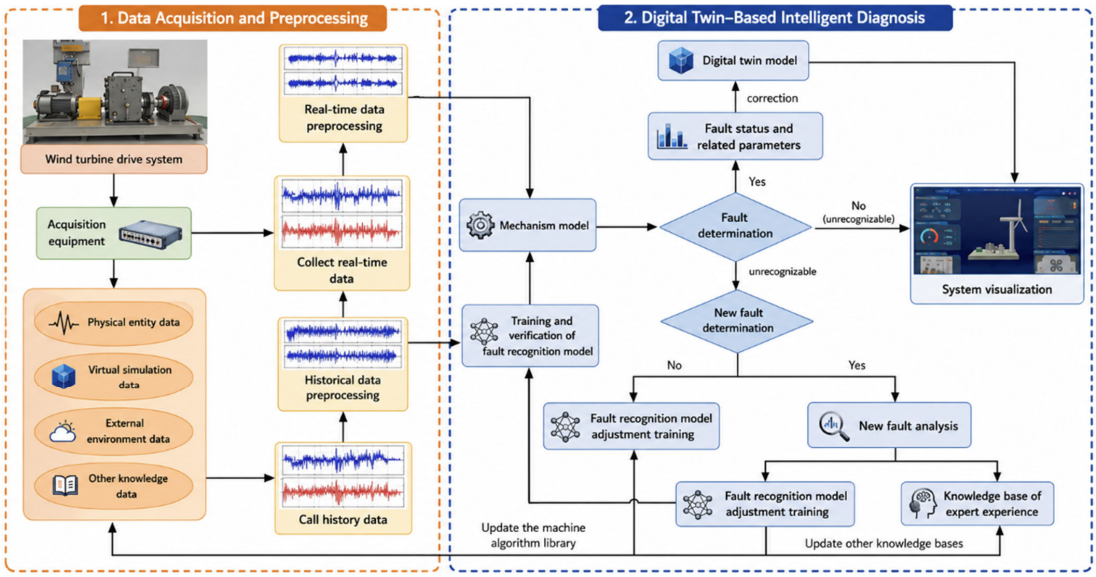

Figure 18. Intelligent diagnosis process for planetary gear of wind turbine (recreated from [131]).

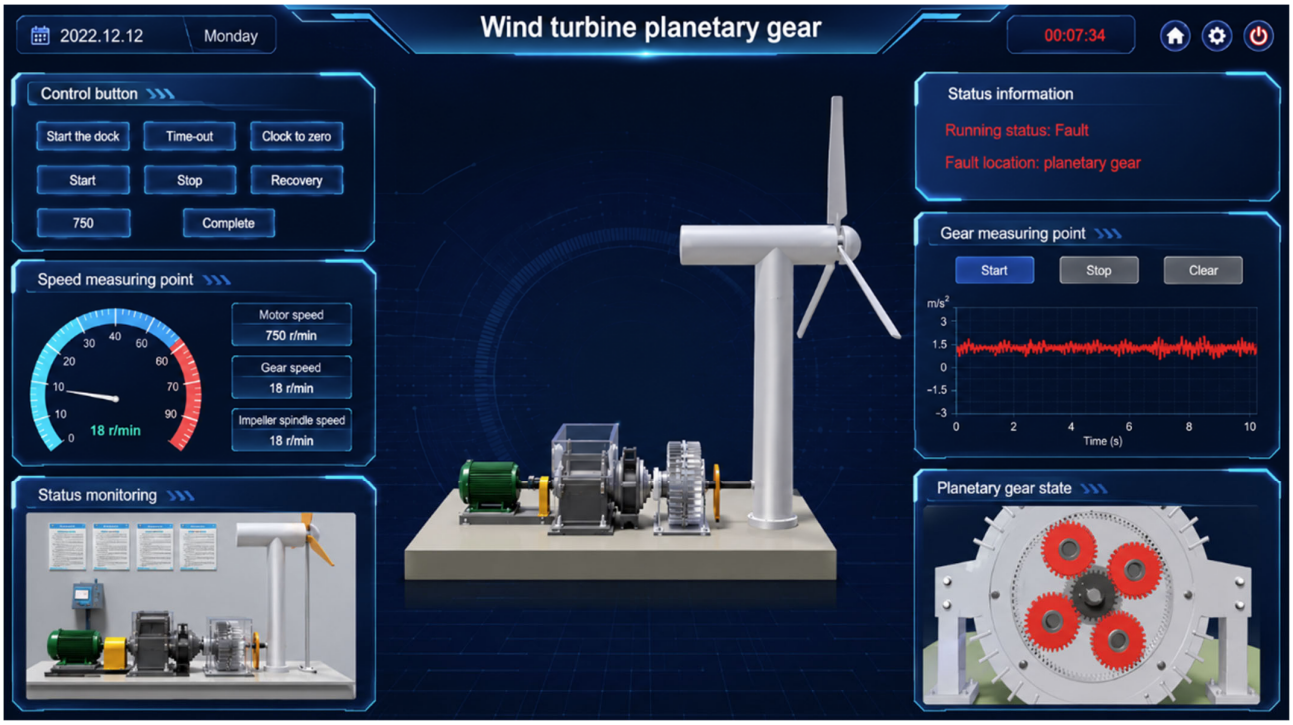

Figure 19. Digital twin-based fault diagnosis mechanism of WT gear system (recreated from [131]).

3.6. Integrated SHM/PHM Architecture for Wind Turbine Reliability

The reviewed literature shows that individual monitoring methods are usually developed for specific components or signals, such as vibration-based gearbox diagnosis, acoustic-emission-based crack detection, SCADA-based anomaly detection, or vision-based blade inspection. However, wind turbine reliability management requires integration across components, sensors, models, and maintenance decisions. To clarify the cross-component synthesis proposed in this review, Figure 20 presents an original integrated SHM/PHM architecture for wind turbine reliability and predictive maintenance. The architecture connects drivetrain and structural components with heterogeneous monitoring data, feature extraction, physics-based and data-driven models, digital twin updating, and maintenance decision support. This system-level representation is intended to show how component-level diagnosis can be converted into actionable reliability management for large-scale and offshore wind turbines.

Figure 20 illustrates that wind turbine reliability assessment cannot rely on a single sensor type or diagnostic algorithm. Drivetrain components such as gearboxes and bearings require high-frequency vibration, acoustic emission, oil-debris, temperature, and SCADA data, while blades, towers, flange joints, and support structures require strain, ultrasonic, thermographic, visual, impedance-based, and corrosion-related monitoring. These heterogeneous data streams must first be cleaned, synchronized, normalized for operating and environmental conditions, and converted into damage-sensitive features. The diagnostic and prognostic layer then combines physics-based models, statistical reliability methods, residual-based fault detection, machine learning, deep learning, anomaly detection, and RUL estimation. The digital twin or data-fusion layer updates component health states, assigns risk or confidence scores, and supports maintenance prioritization. This architecture therefore substantiates the integrated scope of the present review by linking failure mechanisms, measurable indicators, modeling approaches, and maintenance decisions within a single reliability-management pathway.

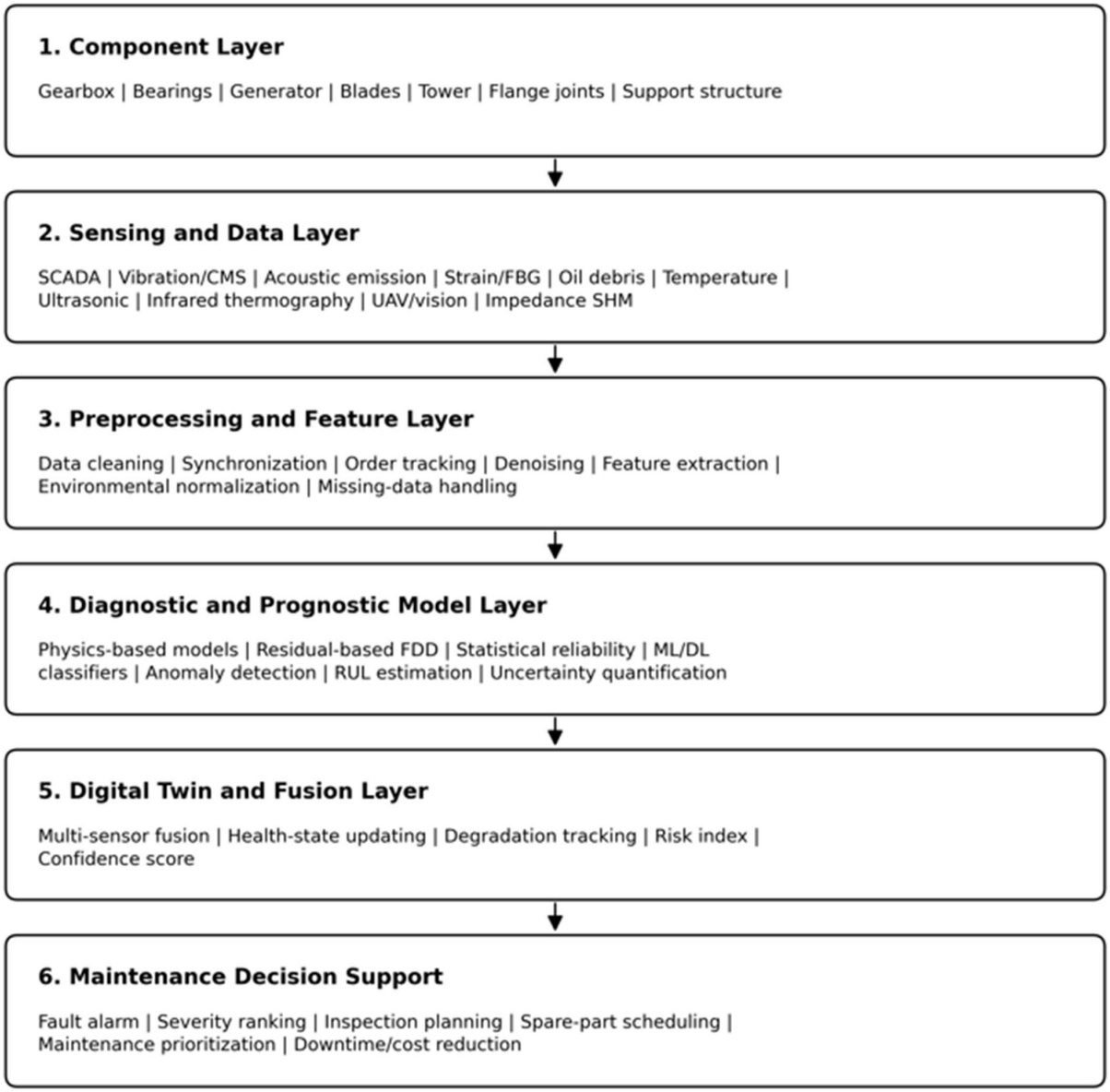

Figure 20. Integrated multi-component SHM/PHM architecture for wind turbine reliability and predictive maintenance.

(R1) Impedance-based SHM studies are directly related to the damage-index formulation in Equation (13), where the current electromechanical impedance signature is compared with the healthy baseline. This mathematical link explains the high sensitivity of impedance methods to local stiffness changes, bolt loosening, cracks, and bonded-joint degradation, while also emphasizing the need for temperature and environmental compensation.

4. Case Studies and Real-World Applications of Wind Turbine PHM

Practical PHM deployment in wind turbines is strongly influenced by the type of turbine, sensor configuration, monitoring duration, data quality, diagnostic algorithm, and the extent to which the diagnostic result can be converted into a maintenance decision. Many published studies report high diagnostic performance, but only a smaller number provide sufficient information on field deployment, operational duration, maintenance outcome, or economic benefit. Therefore, Table 8 summarizes representative field, semi-field, and operational-data-based studies that illustrate how PHM methods have been applied to wind turbine components. The purpose is not to rank all studies by accuracy,

but to identify what type of evidence is available for real-world implementation and what information is still missing.

Table 8. Representative field and semi-field PHM applications for wind turbines.

Application/Study Type	Component	Turbine/Dataset Type	Sensor or Data Source	Method/Algorithm	Reported Performance or Outcome	Maintenance/Economic Information	Main Limitation
SCADA-based early fault detection	Gearbox/generator/turbine subsystem	Operational wind turbine SCADA data	10 min SCADA signals such as power, wind speed, temperature, rotor speed, and alarms	Normal-behavior modeling, ANN, statistical residuals, anomaly detection	Early warning of abnormal thermal or performance behavior before failure	Maintenance benefit usually discussed qualitatively; exact cost saving often not reported	Low sampling frequency limits localization and early mechanical fault sensitivity
SCADA-based condition monitoring review/applications	Multiple turbine subsystems	Wind farm operational datasets	SCADA records and alarm logs	Data-driven condition monitoring, machine learning, performance-curve analysis	Demonstrated usefulness for fleet-level monitoring and early warning	O&M decision support discussed, but economic metrics are inconsistently reported	Missing data, imbalance, turbine-to-turbine variability, and inconsistent labels remain major barriers
Gearbox condition monitoring field case	Gearbox planetary stage/gear-bearing system	Industrial wind farm case	Vibration, SCADA, and multi-scale operational data	Multi-scale signal-processing and data-fusion diagnosis	Severe gearbox fault was identified through combined diagnostic interpretation when standard monitoring alone was insufficient	Demonstrates practical diagnostic value for avoiding prolonged downtime, but exact cost saving was not fully quantified	Single-case evidence; diagnosis depends on data availability and expert interpretation
Main bearing fault prognosis	Main bearing	Operational wind turbine data	SCADA and/or condition-monitoring variables	Fault prognosis/machine-learning model	Fault progression predicted in advance, enabling planning before severe failure	Supports maintenance planning; exact downtime or cost reduction varies by case and is not always reported	Generalization to other turbine types requires validation
Gearbox and bearing test-rig diagnosis	Gearbox gears and bearings	Laboratory or semi-field test rigs	Vibration, acoustic emission, speed, torque	VMD, entropy features, transfer learning, SVM, ANN, CNN, or hybrid classifiers	Frequently reports high diagnostic accuracy, often above 90% under controlled conditions	Maintenance outcome generally not evaluated because studies are diagnostic experiments	Artificial faults, balanced datasets, and controlled speeds may overestimate field performance
Blade inspection using UAV and computer vision	Blade surface defects, cracks, erosion, coating damage	Field blade images/UAV inspection datasets	RGB images, UAV photographs, visual inspection records	CNN, YOLO-type detection, semantic segmentation, image classification	Effective detection and localization of visible blade surface defects; recent studies report improved detection accuracy and inference speed	Can reduce manual inspection exposure and inspection time; exact cost benefit often not reported	Performance depends on lighting, resolution, weather, image angle, and annotation quality
Blade internal damage inspection	Blade delamination, debonding, moisture ingress	Field inspection or laboratory blade sections	Ultrasonic testing, thermography, acoustic emission, strain	NDT interpretation, thermal contrast analysis, AE feature analysis	Useful for detecting internal or near-surface composite defects	Supports targeted repair decisions, but long-term automated PHM evidence is limited	Requires access, environmental control, and skilled interpretation
Tower and welded-joint monitoring	Tower fatigue cracking, weld defects, corrosion-assisted damage	Field monitoring or structural inspection cases	Strain gauges, accelerometers, AE sensors, ultrasonic thickness, corrosion inspection	Modal tracking, strain-cycle monitoring, AE event detection, ultrasonic inspection	Enables identification of fatigue-sensitive regions and local degradation	Useful for inspection prioritization; quantitative cost savings rarely reported	Long-term sensor durability and environmental compensation remain difficult
Flange bolt monitoring	Bolt loosening and preload loss	Laboratory joint tests and limited field-oriented studies	Impedance sensors, strain gauges, torque/preload measurements	Impedance-based damage index, preload monitoring, baseline comparison	Sensitive to local stiffness change and bolt loosening	Can support targeted bolt inspection and retightening	Temperature compensation, baseline drift, and sensor bonding reliability are key issues
Digital twin/data-fusion PHM	Whole turbine or multiple subsystems	Conceptual, simulation-supported, or limited field datasets	SCADA, CMS, inspection records, physical models	Digital twin updating, data fusion, reliability and RUL models	Supports system-level health-state tracking and maintenance prioritization	Potential O&M benefit is high, but field-validated economic evidence remains limited	Requires interoperable data, model calibration, uncertainty quantification, and confirmed fault labels

Table 8 shows that real-world PHM evidence is uneven across wind turbine components and monitoring technologies. SCADA-based methods are mature for fleet-level screening because they use existing turbine data, but their low sampling frequency limits fault localization and early mechanical damage detection. Vibration, acoustic emission, and oil-debris methods provide stronger diagnostic sensitivity for gearbox and bearing faults, but they require additional sensors, high-frequency acquisition, and careful interpretation under variable speed and load. UAV and machine-vision methods are increasingly practical for blade surface inspection, while ultrasonic, thermographic, strain-based, and impedance-based methods are more suitable for internal structural damage, welded joints, towers, and flange connections. The table also shows that many studies report diagnostic accuracy or early warning performance, but fewer provide complete maintenance outcomes, avoided downtime, or economic benefit. This gap indicates that future PHM studies should report not only diagnostic performance but also deployment duration, turbine type, sensor layout, data quality, maintenance action, and cost or availability impact.

The case study evidence also highlights the difference between diagnostic feasibility and deployable PHM. Laboratory studies are useful for validating feature sensitivity and algorithm behavior, but they often use artificial faults, balanced datasets, controlled speeds, and high signal-to-noise ratios. Field studies are more valuable for deployment assessment because

they include operational variability, environmental noise, missing data, sensor degradation, and uncertain labels. However, field studies frequently lack ground-truth failure confirmation, economic metrics, and standardized reporting. Therefore, a practical PHM case study should ideally report the turbine type or capacity, component monitored, monitoring duration, sensor placement, sampling frequency, data preprocessing steps, diagnostic algorithm, performance metric, maintenance decision, and economic or availability outcome.

The significance of case studies in proving the real-world effectiveness of fault identification and PHM in wind turbines needs to be emphasized [132–136]. Recently, a significant example of this is that comprehensive research was being conducted [137]. Advanced vibration analysis techniques were used to monitor the condition of wind turbine gears and bearings. This program resulted in the early detection of possible breakdowns, enabling prompt maintenance interventions. This solution was not only successful in preventing serious problems, but it also greatly reduced maintenance and operational costs. This case demonstrates how conceptual advances in PHM can be effectively turned into tangible, real-world advantages.

Another excellent example comes from an offshore wind farm that used acoustic emission detectors to monitor the gearbox's performance [138]. This approach proved to be extremely effective in early failure diagnosis, outperforming traditional vibration evaluation methods. The sensors were capable of detecting minute acoustic signals caused by emerging flaws, providing a more sensitive and precise diagnostic tool. This application demonstrated the potential for improved sensing technologies to improve the dependability and effectiveness of PHM systems in wind turbines.

These examples [139–143] provide useful information on the practical obstacles and advantages of deploying advanced PHM technologies. They explain how these innovations can help reduce unexpected downtime, extend machine life, and optimize maintenance schedules. Furthermore, these practical applications [48,144–150] serve as standards for future executions, providing a road map for the effective integration of cutting-edge diagnostic and predictive techniques into the wind energy industry. Table 9 summarizes the most prominent and relevant studies conducted recently.

Table 9. Summary of studies on PHM of wind turbine components.

Reference	Authors	Year	Key Contributions
[127]	[Zhang et al.]	2023	Bearing diagnostics in the presence of strong operational and non-stationarity conditions
[128]	[Xiong et al.]	2022	Vibration condition monitoring system for wind turbine bearings using noise suppression and multi-point data fusion.
[129]	[Guo et al.]	2021	A recurrent neural network-based health indicator for remaining useful life prediction of bearings
[130]	[Shangguan et al.]	2020	Prognosis of the remaining useful life of bearings in a wind turbine gearbox
[131]	[Wang et al.]	2023	Wind turbine high-speed shaft bearing health prognosis through a spectral Kurtosis-derived indices and SVR
[132]	[Zimroz et al.]	2014	Online automatic diagnosis of wind turbine bearing progressive degradations under real experimental conditions
[133]	[Yang et al.]	2016	A hybrid DBN-SOM-PF-based prognostic approach of remaining useful life for wind turbine gearbox
[134]	[Guo et al.]	2017	A fiber Bragg grating sensor system monitors operational load in a wind turbine rotor blade
[135]	[Teng et al.]	2016	Double-fed induction generator shaft misalignment monitoring by FBG frame strain sensing
[136]	[Saidi et al.]	2017	Damage detection based on static strain responses using FBG in a wind turbine blade
[137]	[Ali et al.]	2018	Damage and nonlinearities detection in wind turbine based on strain field pattern recognition
[138]	[Pan et al.]	2020	Experimental wind tunnel study of a smart sensing skin for condition evaluation of a wind turbine
[139]	[Schroeder et al.]	2006	Feasibility study on a strain-based deflection monitoring system for wind turbine
[140]	[Wang et al.]	2020	Monitoring loads for a floating wind turbine in wave basin model tests using Fiber Bragg Grating sensors
[141]	[Tian et al.]	2015	Bi-axial neutral axis tracking for damage detection in wind-turbine
[142]	[Sierra-Pérez]	2016	Structural Health Monitoring system based on FBG sensors to offshore wind turbine
[143]	[Downey]	2017	Vibration-based condition monitoring of wind turbine gearboxes based on cyclo-stationary analysis
[144]	[Lee et al.]	2017	Prognosis of a wind turbine gearbox bearing using supervised machine learning
[145]	[Wen et al.]	2020	Integrated condition monitoring scheme for bearing fault diagnosis of a wind turbine gearbox
[146]	[Soman et al].	2016	Blind filters based on envelope spectrum sparsity indicators for bearing and gear vibration-based condition monitoring

5. Towers

5.1. Major Failure Modes

The wind turbine tower is one of the most structurally critical components, as it cannot be replaced or modified in the same manner as many mechanical or electrical subsystems. Because the tower is susceptible to fatigue-related degradation [151], cracking, and corrosion, the mechanisms driving these failures must be regularly evaluated through systematic inspection and continuous monitoring [152]. Although utility-scale wind turbines are designed for an operational life of about 25 years, actual operating conditions can impose loads and hazards beyond those anticipated during design. Events such as earthquakes, severe storms, and abnormal structural loading sequences are examples that may elevate structural risk [153].

In practice, substantial variations often arise between the environmental and loading conditions considered during tower design and those encountered in real operation. These discrepancies can intensify deterioration mechanisms—particularly corrosion–fatigue interaction—thereby increasing the overall risk level. Consequently, frequent inspections and the use of structural health monitoring systems (SHMS) are strongly recommended from the early operational stages to ensure that deviations from design assumptions are detected and mitigated promptly [154].

As stated in [155], cyclic load-bearing capacity must remain sufficient to withstand long-term external cyclic loading while maintaining tower deformations within acceptable limits. Moreover, the tower must be designed to accommodate uncertainties in material properties, modeling accuracy, and load estimations, all of which contribute to variations between predicted and realized structural behavior. As highlighted in [156], discrepancies between assumed and actual conditions should be minimized and effectively managed throughout the design and operational phases.

Because of the tower's critical role in overall structural stability, risk mitigation relies on periodic inspections focused on structural integrity, corrosion progression, weld conditions, climbing and safety systems, and coating performance. Maintenance activities generally include visual inspections, NDT techniques, restoration of protective coatings, removal of surface contaminants, and localized repairs where required.

Table 10 shows a consolidated summary of major structural failure modes observed in wind turbine towers, highlighting the locations where they typically occur, the associated driving mechanisms, and their operational consequences. The table also outlines the diagnostic methods most commonly used in practice, providing a comprehensive overview of how each failure mode is identified and monitored within industry applications.

Table 10. Common failure modes in wind turbine towers [151–156].

Failure Mode	Typical Location	Primary Causes	Key Consequences	Detection/Monitoring Methods
Circumferential weld cracking	Base, mid-tower	High-cycle fatigue, poor weld quality	Progressive crack growth leads to collapse risk	Strain gauges, FBG sensors, dye-penetrant testing
Longitudinal seam cracking	Upper- and mid-tower	Stress concentration, weld defects	Loss of shell stability	Ultrasonic testing, UAV-visual mapping
Local buckling	Near tower base or door opening	Overturning moments, corrosion-thinning	Plastic deformation leads to collapse	Shell-thickness scans, modal testing
Corrosion-assisted cracking	Entire tower, esp. splash zone	Marine exposure, coating failure	Accelerated fatigue and section loss	Coating inspection, corrosion sensors
Flange bolt loosening and ovalization	Tower base and segment flanges	Improper pretension, cyclic bending	Connection slip leads to misalignment which leads to cracks	Bolt-torque logging, vibration monitoring
Tower collapse under extreme wind	Global	Extreme gusts, yaw misalignment	Complete structural failure	SHM, SCADA load events analysis

Figure 21 shows the distribution of major failure modes observed in wind turbine towers based on reported field data. Weld-related fatigue cracking represents the dominant failure mechanism, accounting for approximately 36% of cases, followed by corrosion and coating degradation at 22% and local buckling or shell instability at 18%. Flange and bolt-related failures contribute about 14% of observed incidents, while complete tower collapse under extreme wind conditions constitutes the remaining 10%, highlighting the critical role of fatigue and environmental degradation in tower reliability.

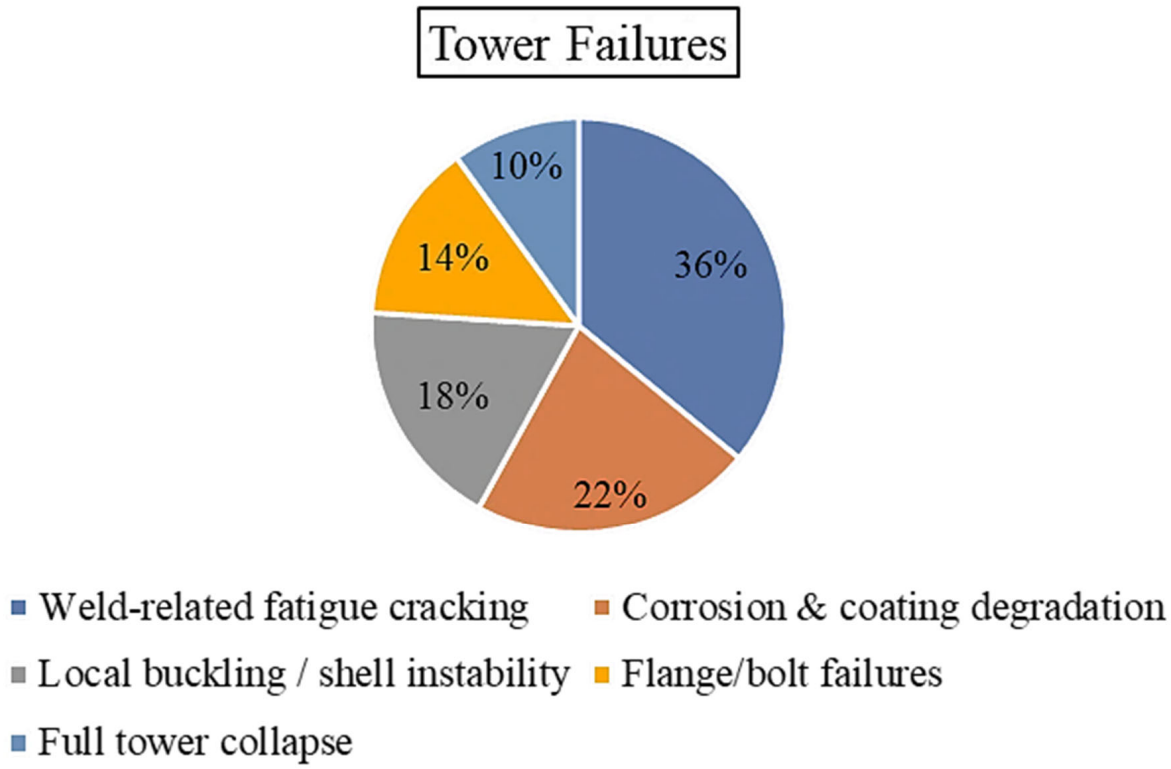

Figure 21. Major failure modes in wind turbine towers.

5.2. Failure Case Studies

Figure 22 shows a severe wind turbine tower failure caused by global shell buckling, where the steel tubular tower experienced catastrophic instability and collapse. This type of failure is primarily associated with insufficient strength or stiffness of the tower cross-section, leading to an inability to resist extreme compressive and bending stresses. Such buckling events are often aggravated by resonance effects, where dynamic excitation approaches the tower's natural frequencies, amplifying structural response. The figure highlights the importance of rigorous shell-buckling design criteria, adequate stiffness provision, and the careful evaluation of dynamic behavior during both design and operational phases.

Figure 23 shows a concrete wind turbine tower failure characterized by severe structural collapse near the base region. This failure is primarily attributed to insufficient strength and stiffness of the concrete tower cross-section, leading to inadequate resistance against combined bending and compressive loads. Such failures are often associated with deficiencies in flexural capacity, suboptimal reinforcement detailing, or inadequate load redistribution mechanisms.



Figure 22. Wind turbine tower failure due to shell buckling [157].



Figure 23. Concrete tower failure [158].

5.3. Condition Monitoring and SHM

Tower SHM is critical because the wind turbine tower functions as the primary load transfer and stability-providing component, continuously subjected to stochastic wind loading, operational vibrations, and environmental degradation throughout its service life. Due to its large slenderness ratio and extensive welded connections, the tower is highly vulnerable to fatigue damage, local buckling initiation, and corrosion-induced stiffness loss, particularly in flange regions and weld seams. Undetected damage in the tower can propagate rapidly and compromise the global dynamic behavior of the entire wind turbine system, leading to increased operational risk and maintenance costs. Consequently, tower-specific SHM and PHM strategies are essential for early damage identification, degradation tracking, and reliable lifetime management of modern wind turbines.

Regarding the use of robotized inspection in tower structural health monitoring, unmanned aerial vehicles (UAVs) have emerged as the predominant solution for visual inspection of external tower surfaces, welds, and flange regions. Compared to UAV-based approaches, non-flying robotic inspection systems remain relatively uncommon and have received limited attention from both industry practitioners and researchers. For

example, Lim et al. [159] proposed an inchworm-like robot with telescopic motion for visual inspection (VI), originally intended for blade inspection, which can be conceptually extended to tower surface inspections where stable contact-based mobility is required. The proposed system is designed to carry multiple sensors, including cameras, enabling damage detection and the localization of surface cracks through computer vision techniques and blob labeling algorithms.

In the context of automated visual inspection and damage identification for tower structures, deep neural networks (DNNs) constitute the most widely adopted approach, particularly region-based convolutional neural networks such as Fast R-CNN [160] and related variants. These architectures are extensively employed to automatically detect, localize, and assess the severity of surface-level defects on tower shells, including fatigue cracks, corrosion pits, coating degradation, and oil or rust stains. In most applications, robust R-CNN-based architectures pre-trained on large generic image datasets are adapted through transfer learning, fine-tuning, or retraining using tower-specific inspection datasets, many of which are increasingly available. Depending on the damage typologies incorporated during training, AI-based models can distinguish between multiple tower-related defects such as cracks, material loss, breakages, and surface contamination [161]. Representative pre-trained models frequently adopted in tower visual inspection include VGG-16 [162], ResNetv2 [163], Inceptionv4 [164], YOLOv5 [165], and Efficient Net [166], along with hybrid architectures such as Inception-ResNet-v2 [164]. A recent application of such AI-driven visual inspection techniques can be found in Ref. [167], highlighting their growing relevance for automated tower SHM and PHM frameworks.

Table 11 provides a comprehensive overview of structural health monitoring techniques applicable to wind turbine towers, covering optical, laser-based, thermal, microwave, terahertz, and electromagnetic approaches. The table highlights how non-contact and full-field techniques such as DIC, PBMM, LiDAR, and shearography enable deformation and vibration-based assessment of tower integrity, while infrared thermography and electromagnetic methods are particularly effective for detecting corrosion, weld defects, and subsurface anomalies in steel tower structures. Microwave and terahertz technologies further extend inspection capabilities beneath protective coatings and insulation layers, addressing key challenges in harsh offshore and atmospheric environments.

Table 11. Structural health monitoring techniques for wind turbine towers.

SHM Technique Category	Specific Methods	Measured Quantity/Data Type	Targeted Tower Damage or Phenomenon	Key Advantages	Main Limitations	References
Optical Measurement Techniques	Digital Image Correlation (DIC)	Full-field strain, displacement	Local strain concentration, deformation, fatigue-prone zones	Non-contact, full-field measurement, high spatial resolution	Sensitive to illumination, limited large-scale field deployment	[168–170]
Optical Measurement Techniques	Stereophotogrammetry	Three-dimensional displacement, strain	Global and local deformation of tower shells	Suitable for large structures, compatible with UAV imaging	Requires multiple cameras, calibration complexity	[171,172]
Video-Based Optical Techniques	Phase-Based Motion Magnification (PBMM)	Amplified vibration response, modal parameters	Global stiffness degradation, dynamic property variation	Extracts imperceptible vibrations, no physical sensors	Limited to visible spectrum, sensitive to noise	[173–176]
Laser-Based Techniques	Laser Doppler Velocimetry (LDV)	Velocity time histories	Vibration-based damage detection, modal analysis	High accuracy, non-contact	Point-wise measurement, high cost	[177]
Laser-Based Techniques	UAV-mounted LiDAR	Three-dimensional geometry, surface mapping	Geometric distortion, structural deformation	Large-area coverage, remote inspection	Limited damage sensitivity, expensive hardware	[178]
Laser-Based NDT	Shearography Testing (ST)	Surface deformation anomalies	Subsurface defects, debonding, structural anomalies	Full-field, real-time, non-contact	High cost, complex setup, limited field use	[179–184]

Table 11. *Cont.*

SHM Technique Category	Specific Methods	Measured Quantity/Data Type	Targeted Tower Damage or Phenomenon	Key Advantages	Main Limitations	References
Infrared Thermography (IRT)	Pulsed Thermography	Thermal response, defect contrast	Corrosion, bonding defects, subsurface anomalies	Fast inspection, large-area coverage	Depth resolution limits, environmental sensitivity	[185–189]
Infrared Thermography (IRT)	Pulsed Phase Thermography	Phase delay, thermal wave propagation	Deep defects, delamination-like features	Improved depth discrimination	Complex signal processing	[189]
Infrared Thermography (IRT)	Eddy Current (EC) Pulsed Thermography	Induced thermal patterns	Corrosion, surface and subsurface defects in steel	Suitable for metallic towers, corrosion-sensitive	Lift-off effects, limited depth resolution	[190–197]
Infrared Thermography (IRT)	Lock-in/Vibrothermography	Periodic thermal response	Internal inhomogeneities, fatigue damage	High defect sensitivity	Requires controlled excitation	[198–201]
Infrared Thermography (IRT)	Line Scanning Thermography	Continuous thermal imaging	Manufacturing and in-service defects	High scanning speed	Specialized equipment	[202,203]
Microwave Testing	Microwave Radar/Imaging	Electromagnetic reflection	Corrosion under coatings, hidden steel degradation	Penetrates coatings, remote sensing	Limited spatial resolution	[204,205]
Terahertz (THz) Testing	THz Imaging	Subsurface material response	Corrosion under insulation, moisture ingress	High resolution compared to ultrasound	Limited penetration depth	[206,207]
Electromagnetic Testing (ET)	Eddy Current (EC) Testing	Electrical conductivity variation	Weld cracks, corrosion, surface-breaking defects	Mature technology, industry-ready	Limited penetration depth	[208,209]
Electromagnetic Testing (ET)	Pulsed Eddy Currents	Transient electromagnetic response	Corrosion in splash zone, thickness loss	Suitable for coated steel	Signal interpretation complexity	[210,211]
Electromagnetic Testing (ET)	RF Eddy Currents	High-frequency EM response	Material degradation, microstructural anomalies	Enhanced sensitivity for low conductivity materials	Limited SHM adoption	[212–214]

The Ping Monitor represents an emerging class of acoustic-based structural health monitoring devices for wind turbine towers, designed for rapid deployment and long-term, maintenance-free operation. Magnetically mounted directly onto the metallic tower surface, the device is self-powered through an integrated solar panel and incorporates an Intelligent Listening Sensor consisting of a microphone coupled with an embedded ARM processor. After installation, the system establishes a baseline acoustic signature of the operating turbine by continuously recording structural and operational sounds over an initial learning period, while actively filtering out unrelated ambient noise sources such as wind and traffic. Deviations from this baseline are then tracked to identify abnormal acoustic patterns, whose intensity and temporal evolution can be correlated with structural anomalies and damage progression relevant to tower-related reliability assessment, as well as turbine-wide degradation mechanisms. By analyzing sound variation trends over time, the Ping Monitor enables condition-based and predictive maintenance, with processed data transmitted to a cloud-based platform for remote monitoring and decision support by wind farm operators (Figures 24 and 25 [215]).

Figure 26 illustrates the regions of the electromagnetic spectrum that are relevant to the structural health monitoring of wind turbine towers, highlighting the complementary roles of optical, thermal, microwave, and terahertz-based inspection techniques. Optical methods such as digital imaging, multi- and hyper-spectral imaging, and infrared thermography operate mainly within the visible and infrared bands, enabling non-contact detection of surface-level defects, coating degradation, and thermal anomalies on tower shells. The infrared domain is further divided into near-, short-, mid-, and long-wave infrared ranges, each offering different sensitivity to temperature gradients and subsurface features associated with corrosion or bonding irregularities. In contrast, microwave and terahertz techniques occupy longer-wavelength, lower-frequency regions of the spectrum,

allowing penetration through protective coatings and insulating layers commonly applied to steel towers, thereby supporting the detection of hidden corrosion and material degradation. By mapping wavelength, frequency, and energy levels, the figure emphasizes how multi-spectral inspection strategies can be combined to address both surface and subsurface damage mechanisms in tower SHM applications [216].



Figure 24. Ping monitor magnetically mounted on a turbine tower [215].

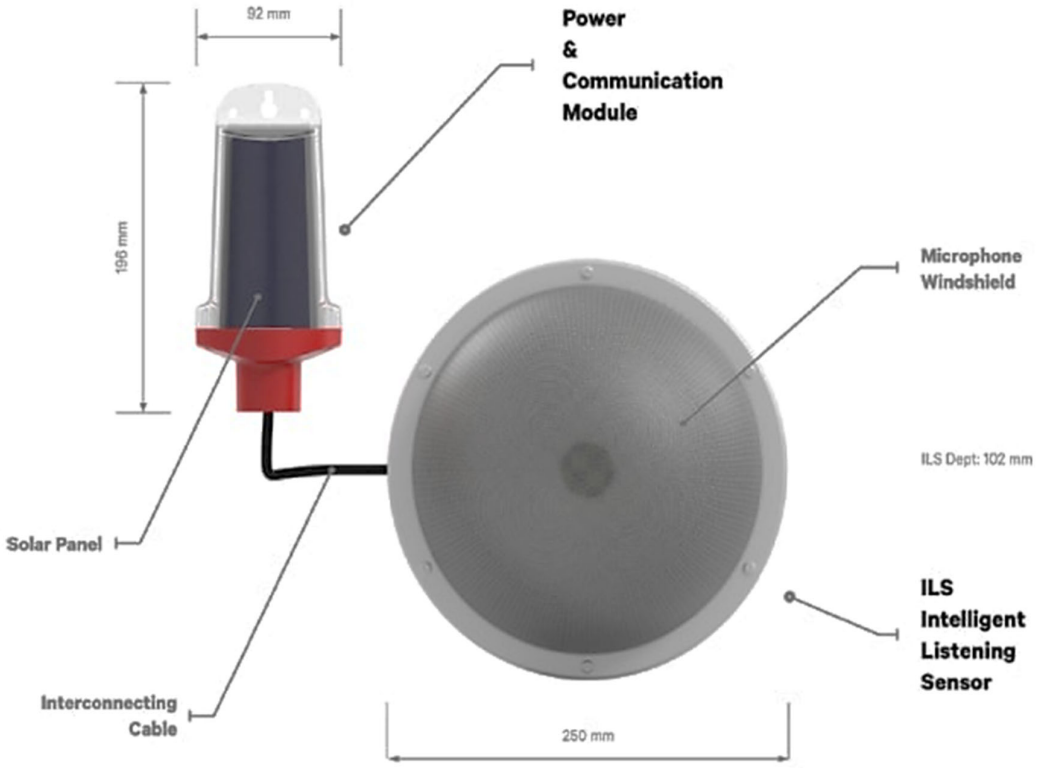

Figure 25. Ping monitor's main components [215].

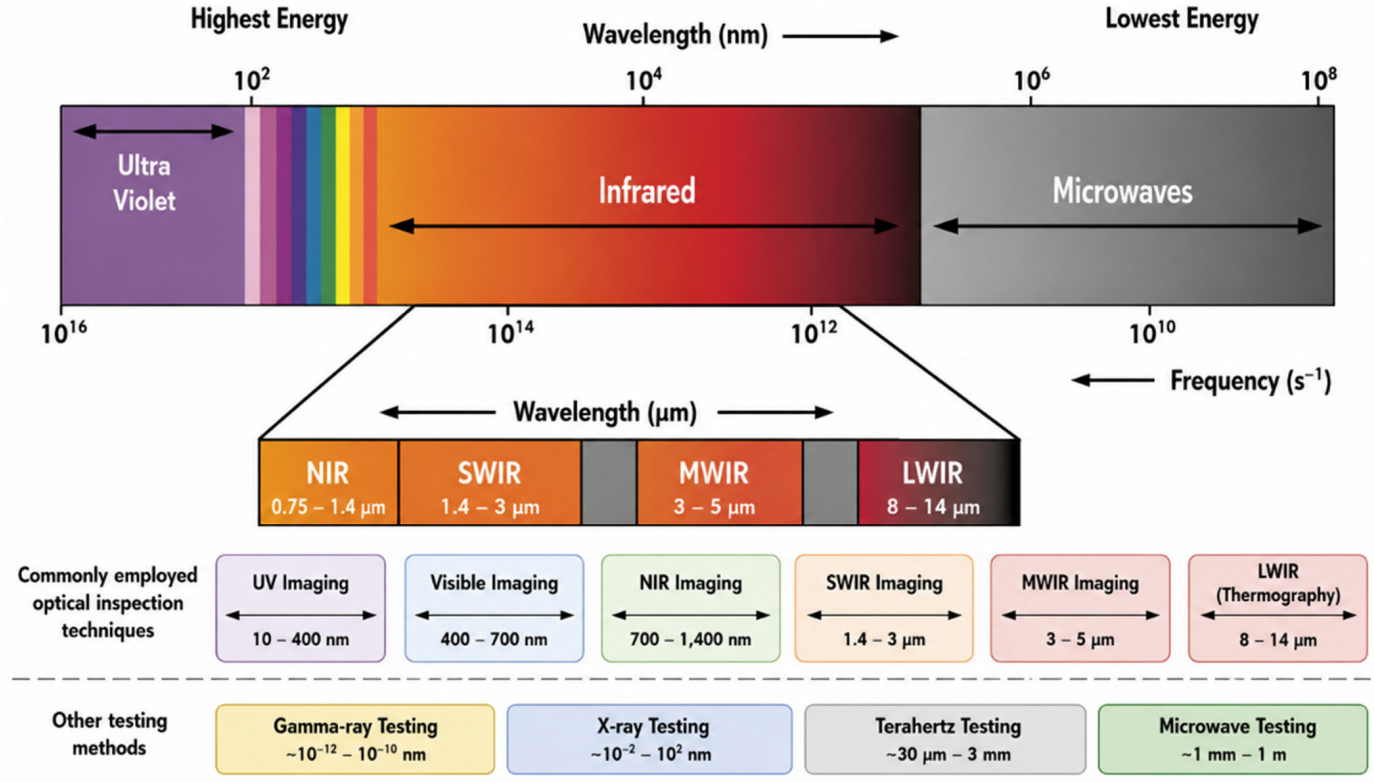

Figure 26. Coverage of the electromagnetic spectrum by commonly employed optical inspection techniques (digital imaging, multi- and hyper-spectral imaging, and thermography), alongside the spectral ranges associated with Gamma-ray, X-ray, microwave, and terahertz testing methods (recreated from [216]).

Figure 27 schematically illustrates the fundamental ultrasonic testing (UT) principles as applied to wind turbine tower inspection. In the conventional through-thickness configuration, ultrasonic waves are introduced and received by a single transducer operating in reflection mode, enabling the detection and localization of internal flaws such as cracks or inclusions within the tower wall. In contrast, the guided-wave approach employs separate transmitting and receiving transducers to propagate ultrasonic energy over longer distances along the tower shell in through-transmission mode, allowing extended structural coverage and the identification of defects over large areas with a reduced number of sensing locations.

Figure 28 provides a qualitative comparison of different non-destructive testing (NDT) techniques in terms of deployment extent and associated costs within the context of wind turbine tower structural health monitoring. Low-cost and widely deployable approaches, such as visual inspection and temperature-based analysis, are positioned toward higher deployment levels but offer limited damage sensitivity. Conventional NDT methods, including ultrasonic testing, occupy an intermediate range, balancing inspection capability and implementation cost, while requiring localized access to the tower surface. In contrast, advanced techniques such as acoustic emission monitoring and infrared thermography exhibit higher costs but enable broader structural coverage and enhanced damage sensitivity, particularly when integrated with embedded sensors, vibration-based analysis, and machine-learning-driven frameworks. Overall, the figure highlights the trade-off between cost and deployment scalability, emphasizing the need for hybrid SHM strategies to achieve effective and economically viable tower monitoring solutions [217–219].

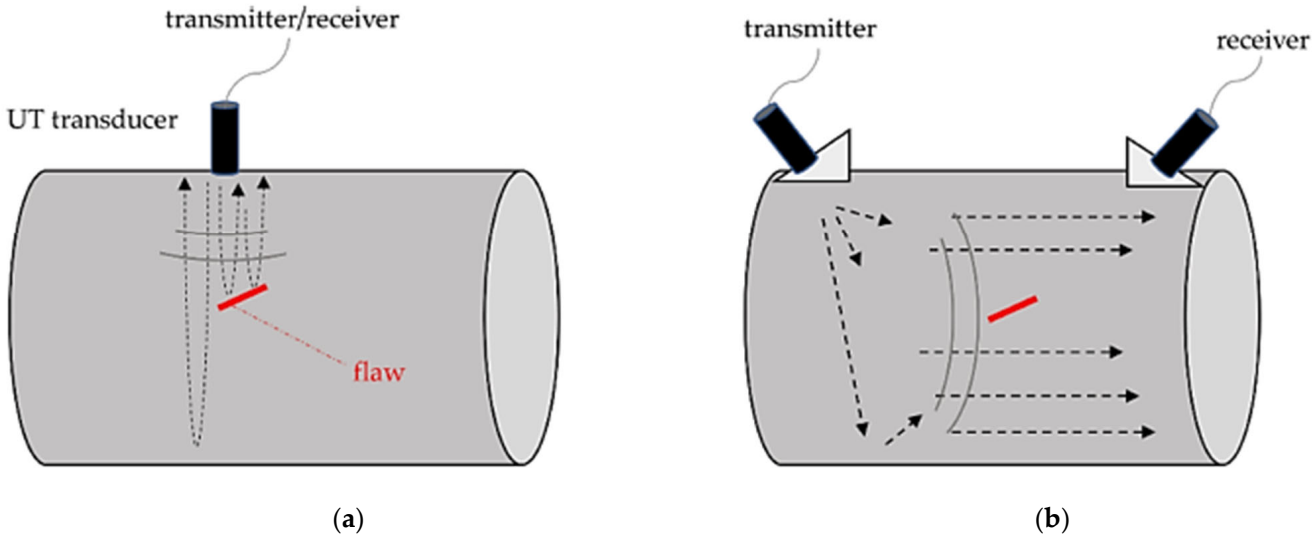

Figure 27. Schematic illustration of the fundamental principles of ultrasonic testing (UT): (**a**) conventional through-thickness inspection operating in reflection mode; (**b**) guided-wave-based inspection employing through-transmission mode for extended structural coverage.

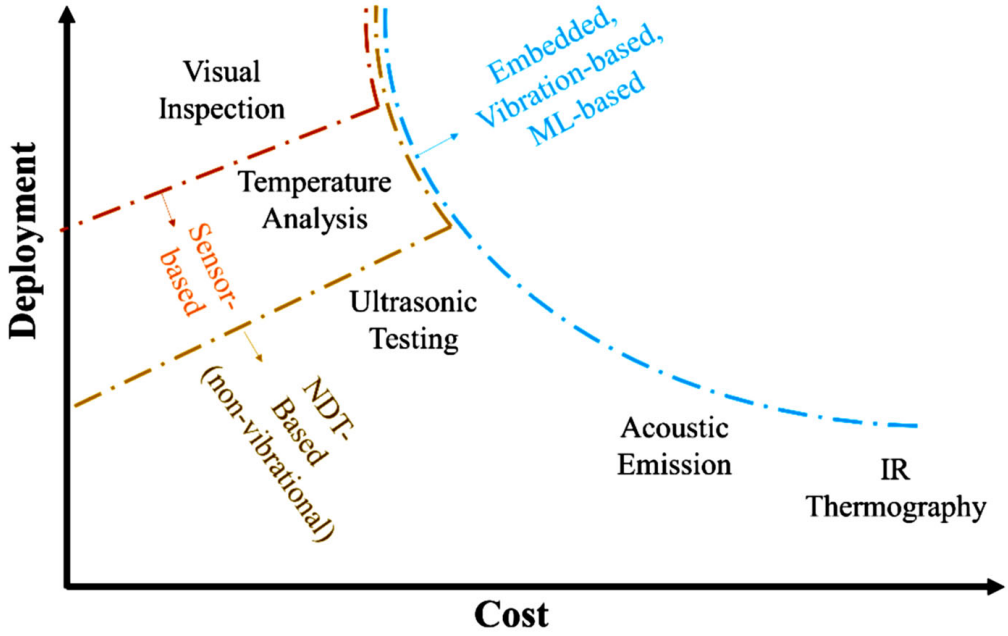

Figure 28. Qualitative comparison of deployment extent and associated costs for different non-destructive testing (NDT) techniques.

Table 12 summarizes the key sensing technologies used in structural health monitoring of wind turbine towers, classified according to sensor type, monitoring function, and diagnostic capability. Accelerometers and strain gauges form the backbone of tower SHM, enabling vibration-based assessment and fatigue monitoring at critical shell and welded regions. Acoustic emission and ultrasonic sensors allow the early identification of crack initiation, weld defects, and corrosion activity within tower steel. Distributed fiber-optic sensing offers continuous, full-height coverage of strain and temperature variations, while SCADA-based virtual sensing and emerging microwave-based techniques complement physical sensors by enabling trend-based diagnostics and the detection of hidden degradation beneath protective coatings.

Table 12. SHM Sensors and data collection methods for wind turbine tower [159–219].

Sensor Type	Image	Primary Application	Technical Coverage	Key Detection/Advantage
Accelerometers		Vibration monitoring, modal analysis	Foundation, tower	Detect cracks, looseness, resonance
Strain gauges	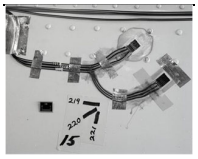	Fatigue load monitoring	Yield points: tower joints	Crack, plasticity, overload, repair data
Inclinometers		Tilt and basement rotation	Tower base	Scour, settlement, soil slip, tilt
Acoustic emission		Crack/growth detection	Tower foundations, TP interfaces	Microcrack/initiation, corrosion
Fiber-optic/Distributed sensing		Full-structure strain, temp, acoustic	Entire tower	Distributed crack/deformation
Ultrasonic (US)		Local flaw/joint weld	Joints, interfaces	Weld cracks, voids, corrosion pockets
SCADA virtual sensors		Performance, alarm diagnosis	All main components	Vibration, overload, trend prediction
Microwave/Radar		Cracks detection, interface	TP connections	Washout, separation, loss of preload

6. Blades

6.1. Major Failure Modes

Wind turbine blades are exposed to a wide range of environmental and mechanical loads throughout their operational life, including cyclic structural deformation, rain and sand erosion, and the accumulation of surface contaminants. Additional degradation mechanisms arise from icing, elevated moisture levels, and temperature fluctuations, while

rare but severe events such as transportation-induced damage, lightning strikes, and bird impacts can further compromise blade integrity.

Leading edge erosion is one of the most prevalent degradation mechanisms affecting wind turbine blades, particularly in offshore and high-precipitation environments. It is primarily caused by repeated impacts from rain droplets and airborne particles, which progressively damage the protective coating systems applied to the blade surface [220]. As erosion advances, the exposed laminate becomes susceptible to further material loss and surface roughness development, leading to aerodynamic performance deterioration [221]. Experimental and field-based studies have demonstrated that even moderate erosion can significantly reduce lift-to-drag ratios, resulting in measurable annual energy production losses [222]. In addition to aerodynamic penalties, leading edge erosion has been shown to accelerate fatigue damage in downstream structural regions due to altered load distributions along the blade span [223].

Tapered blade sections containing ply drop transitions represent critical zones where abrupt changes in laminate thickness introduce localized stress concentrations. These stress gradients promote matrix cracking and interlaminar damage under cyclic flap-wise and edgewise bending loads [224]. Numerical investigations have shown that ply drop configurations strongly influence delamination initiation, particularly under variable-amplitude loading conditions [225]. Manufacturing-induced imperfections, such as misaligned ply terminations, further exacerbate damage sensitivity in these regions [226]. Full-scale blade testing has confirmed that fatigue damage in tapered areas often precedes more extensive structural degradation [227]. Consequently, optimized ply drop design and strict quality control during manufacturing are essential for improving blade durability [228].

Structural collapse and buckling constitute catastrophic blade failure modes that typically occur under extreme loading scenarios, including severe storms or emergency shutdown events [229]. These failures are often associated with the compressive instability of spar caps and the global buckling of blade shell panels when critical load thresholds are exceeded [230]. Large-scale experimental studies have demonstrated that accumulated fatigue damage significantly reduces buckling resistance over the blade service life [231]. Material imperfections, such as fiber waviness and resin-rich zones, further compromise compressive strength [232]. Numerical simulations have also highlighted the role of dynamic amplification and resonance effects in triggering instability-driven failures [233]. As blade lengths continue to increase, ensuring sufficient buckling margins has become a key challenge in next-generation blade design [234].

Adhesive joints within the spar cap and shear web region are essential for effective load transfer across the blade cross-section. Failure in these joints commonly initiates as adhesive debonding or cohesive cracking under long-term cyclic bending loads [235]. Experimental investigations have shown that bond-line thickness variations and void formation significantly reduce joint fatigue strength [236]. Environmental exposure, including moisture ingress and temperature cycling, further accelerates adhesive degradation [237]. Full-scale blade fatigue tests have revealed that spar area joint failures can propagate rapidly once initiated, compromising overall structural integrity [238]. Advanced numerical models have been developed to predict mixed-mode fracture behavior in these joints [239]. Field inspections have confirmed that undetected spar-joint damage often precedes major blade failures [240]. As a result, improved joint design and in situ monitoring techniques are increasingly recommended [241].

Adhesive joints along the trailing and leading edges are particularly vulnerable due to their slender geometry and exposure to complex aerodynamic loading. Trailing-edge cracking has been widely reported in operational turbines and is commonly linked to cyclic peel stresses acting on the bonded interface [242]. Laboratory fatigue tests have shown that

adhesive aging significantly reduces fracture toughness in these regions [243]. Manufacturing inconsistencies, such as uneven bond thickness, further contribute to premature crack initiation [244]. Field surveys indicate that trailing-edge joint failures are among the most frequently repaired blade defects worldwide [245]. Leading-edge bond failures may interact with surface erosion damage, accelerating structural deterioration [246]. Environmental factors such as moisture and ultraviolet exposure exacerbate adhesive degradation over time [247]. Numerical analyses have demonstrated strong coupling between aerodynamic excitation and joint fatigue response [248]. Consequently, improved joint materials and enhanced inspection strategies are critical for long-term blade reliability [249].

The blade root region serves as the primary load transfer interface between the blade and the hub, making it highly susceptible to fatigue-driven damage. Failures in this region often involve laminate cracking, adhesive degradation, or bolt loosening around insert interfaces subjected to high cyclic loads [250]. Stress concentration at the root transition zone has been shown to accelerate damage accumulation, particularly under variable operational loading [251]. Although less frequent than surface or trailing-edge failures, root-region damage poses a severe safety risk due to its direct impact on blade retention and overall turbine integrity [252].

Table 13 shows the most common failure modes observed in wind turbine blades, together with their typical locations, underlying causes, and structural consequences. The table highlights that blade failures arise from a combination of environmental exposure, manufacturing imperfections, and cyclic operational loading, affecting both surface integrity and internal load-carrying components. It also summarizes the primary inspection and monitoring techniques used in practice to detect early-stage blade damage and mitigate the risk of progressive or catastrophic failure.

Table 13. Common failure modes in wind turbine blades [220–252].

Failure Mode	Typical Location	Primary Causes	Key Consequences	Detection/Monitoring Methods
Leading edge erosion	Blade leading edge (outer span)	Rain, hail, airborne particles, salt spray	Aerodynamic efficiency loss, increased fatigue loads	Visual inspection, UAV imaging, surface roughness monitoring
Ply drop damage in tapered areas	Tapered sections along blade span	Stress concentration, laminate thickness variation	Delamination, matrix cracking, fatigue initiation	Ultrasonic testing, thermography
Structural buckling/collapse	Spar caps, blade shell panels	Extreme loads, compressive instability, fatigue degradation	Catastrophic blade failure	Full-scale testing, strain monitoring, modal analysis
Spar area adhesive joint failure	Spar cap–shear web interface	Cyclic bending, adhesive defects, environmental degradation	Loss of load transfer, progressive structural failure	Acoustic emission, ultrasonic inspection
Trailing/leading edge joint failure	Blade trailing and leading edges	Peel stresses, adhesive aging, manufacturing inconsistencies	Crack propagation, reduced stiffness	Visual inspection, infrared thermography
Root region failure	Blade root and insert zones	High cyclic loads, bolt loosening, laminate cracking	Blade–hub connection failure	Bolt preload monitoring, NDT, vibration analysis

Figure 29 shows the variation in wind turbine blade failure mechanisms as a function of operational time [253]. Surface damages and lightning-related cracks dominate during the early- to mid-life stages of operation, particularly within the first 3–5 years, reflecting the influence of environmental exposure and external impact events. Manufacturing defects and structural cracks are more pronounced in the initial years, while lightning-related failures remain significant in later stages, indicating cumulative damage effects and long-term exposure risks as turbines age.

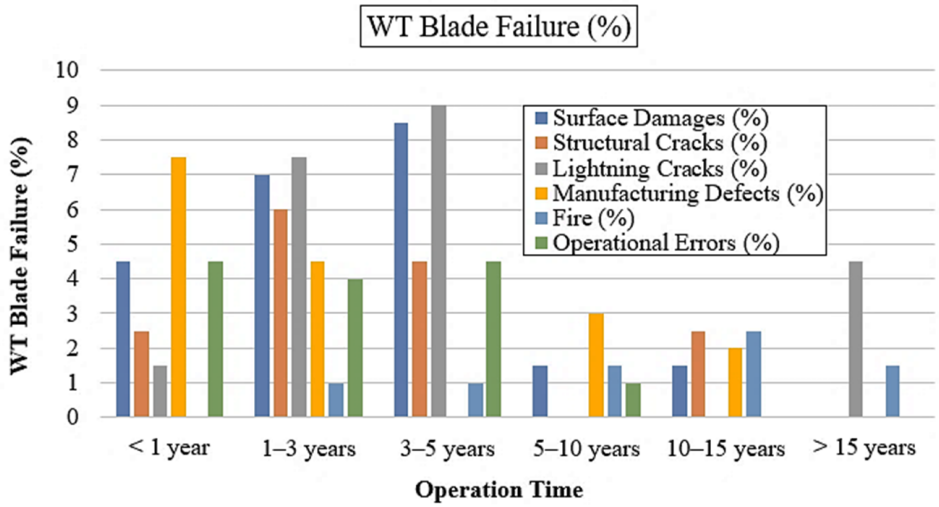

Figure 29. WT blade failure according to operation time for different faults.

6.2. Failure Case Studies

Figure 30 shows wind turbine blade failure caused by severe erosion and wear concentrated along the leading edge region. The progressive loss of protective coatings and laminate material due to repeated rain and particle impacts degrades the blade surface, leading to aerodynamic inefficiency and increased structural loading. As erosion advances, the exposed composite layers become more susceptible to fatigue damage and crack initiation.

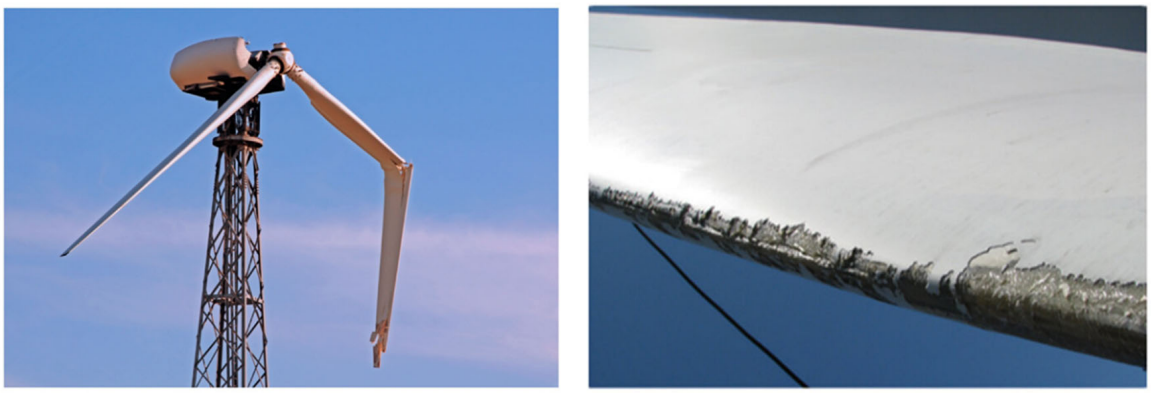

Figure 30. WT blade failure due to erosion and wear [254].

Figure 31 shows wind turbine blade failure induced by gust impact, characterized by severe delamination and localized structural damage within the composite laminate. Sudden aerodynamic load amplification during extreme gust events generates high interlaminar stresses, leading to resin cracking, fiber–matrix debonding, and progressive delamination growth. Such impact-related damage significantly reduces load-carrying capacity and stiffness, increasing the likelihood of subsequent fatigue-driven failure.

Figure 32 shows wind turbine blade failure caused by direct object impact, resulting in localized structural damage and material loss along the blade surface. Impacts from birds, hail, or airborne debris induce high contact stresses that lead to laminate cracking, fiber breakage, and surface penetration of the composite structure. Such localized damage can act as a trigger for moisture ingress and subsequent fatigue crack propagation if left unaddressed. The figure highlights the importance of impact-resistant surface coatings, protective design measures, and routine inspections to mitigate object-induced blade damage.

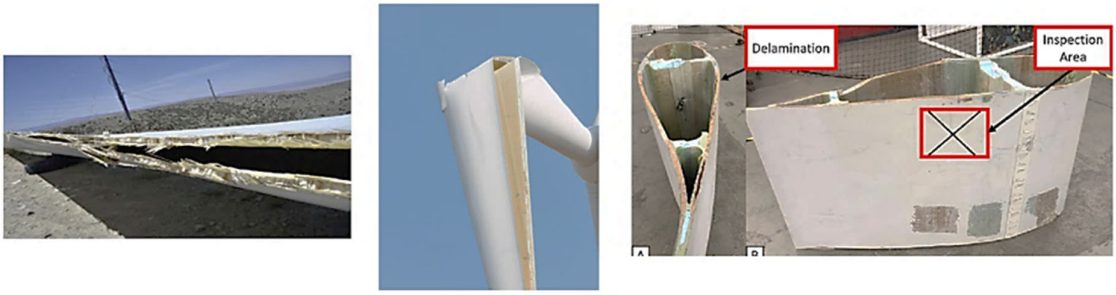

Figure 31. WT blade failure due to gust impact [254].



Figure 32. WT blade failure due to object impact [255].

Figure 33 shows wind turbine blade failure characterized by surface and subsurface cracking accompanied by local material splitting within the composite laminate. Such cracks typically initiate due to accumulated fatigue loading, material defects, or stress concentration under cyclic aerodynamic forces. Once formed, cracks facilitate moisture ingress and progressive delamination, accelerating structural degradation if not addressed promptly. This failure mode emphasizes the importance of appropriate material selection, stringent quality control during manufacturing, continuous stress monitoring, and timely repair to prevent crack propagation and loss of blade integrity.



Figure 33. WT blade failure due to cracks [255].

Figure 34 shows wind turbine blade failure caused by overspeed conditions, resulting in severe blade strike, imbalance, and structural rupture near the hub region. Overspeed events generate excessive centrifugal and aerodynamic forces that exceed the blade's design limits, often triggered by pitch system malfunction or inadequate braking response. Such failures lead to rapid load redistribution and catastrophic blade damage, posing significant safety risks to the entire turbine system.



Figure 34. WT blade failure due to overspeed [256].

6.3. Condition Monitoring and SHM

Blade SHM is critical because wind turbine blades are continuously exposed to highly variable aerodynamic loading, environmental effects, and impact events that directly govern energy production and structural reliability. Owing to their large size, composite material construction, and complex aeroelastic behavior, blades are particularly susceptible to fatigue damage, delamination, leading-edge erosion, and lightning-induced defects. Damage initiation and progression in blades can significantly alter aerodynamic performance and induce load redistribution across the turbine system if not detected at an early stage. Consequently, blade-specific SHM and PHM approaches are essential for timely damage detection, degradation tracking, and remaining useful life estimation in modern wind turbines.

The structural health monitoring of wind turbine blades relies on a diverse set of sensing and diagnostic technologies due to the complex damage mechanisms inherent to large composite structures. Strain-based SHM is among the most widely adopted approaches, as it directly measures local deformation and stress redistribution in blade laminates. By capturing strain evolution over time, this method is particularly effective for fatigue monitoring and the early detection of stiffness degradation near critical regions such as spar caps and root joints [141,144,257,258]. However, because strain measurements are inherently localized, reliable blade-scale assessment requires dense sensor networks and careful sensor placement informed by prior structural analysis.

Acoustic emission (AE) techniques provide a complementary capability by detecting transient elastic waves generated by damage events such as matrix cracking, fiber breakage, and delamination growth. AE-based SHM is especially valuable for blades because it enables continuous, real-time monitoring and early-stage damage detection before macroscopic stiffness changes become measurable [259–262]. The high sensitivity of AE allows precise damage localization when multiple sensors are deployed; however, the

interpretation of high-frequency signals in large composite blades remains challenging due to attenuation, dispersion, and environmental noise.

Global vibration-based SHM approaches exploit changes in modal parameters—such as natural frequencies, mode shapes, and damping—to infer structural degradation at the blade level. These techniques are attractive because they are non-destructive and scalable to large blades, offering insight into damage severity and progression without direct access to internal structures [263–266]. Nevertheless, blade vibration responses are strongly influenced by aerodynamic loading, operational conditions, and environmental variability, making early damage detection and reliable damage discrimination difficult without advanced signal-processing or machine-learning-based compensation strategies.

To address subsurface damage in composite blades, ultrasonic guided waves and infrared thermography (IRT) are frequently employed. Guided-wave ultrasonic enables the detection of delamination, debonding, and internal flaws over relatively long distances within blade laminates [267–270]. However, strong wave scattering and attenuation in composite materials limit spatial resolution and complicate signal interpretation. IRT, on the other hand, provides non-contact, full-field inspection capability and is effective for identifying subsurface defects and fatigue-induced thermal anomalies across large blade surfaces [271–274]. Its effectiveness, however, is sensitive to environmental conditions and typically requires controlled excitation and advanced image processing.

Machine vision techniques—often integrated with AI and deep learning—have rapidly gained prominence for blade SHM due to their ability to automate surface damage detection, including cracks, erosion, and lightning strike marks [275–278]. These approaches significantly reduce inspection time and human exposure when deployed via UAVs, although they remain limited to surface-visible damage and require high-quality datasets for robust performance. Finally, radiographic and electromagnetic wave-based methods offer high-resolution internal inspection and real-time monitoring capabilities, respectively, but their adoption in blade SHM is constrained by safety concerns, equipment cost, and complex data interpretation requirements [279–285].

Table 14 provides a structured comparison of the principal structural health monitoring techniques applied to wind turbine blades, emphasizing their sensing principles, detectable damage mechanisms, and practical deployment characteristics. The table highlights the complementary roles of local sensing methods—such as strain measurement and acoustic emission—for early damage detection, and global approaches, such as vibration-based monitoring and infrared thermography, for blade-scale condition assessment. Advanced techniques including machine vision, radiography, and electromagnetic sensing further extend SHM capability toward automated inspection and internal defect detection.

Figure 35 illustrates the application of infrared thermography for the structural health monitoring of wind turbine blades, where an infrared camera is used to capture temperature distributions over multiple blade sections during inspection. The blade is divided into five thermographic sections along its span, and the corresponding thermal images are stitched together to form a continuous temperature map, enabling the comprehensive assessment of thermal anomalies over the entire blade surface. Such temperature variations are indicative of subsurface defects, material inhomogeneities, delamination, or fatigue-related damage, which alter local heat transfer characteristics. By combining infrared imaging with visible-camera observations, this approach allows non-contact, full-field detection of damage-prone regions and supports rapid screening of large composite blades, making it particularly suitable for in situ blade SHM and condition-based maintenance.

Figures 36 and 37 also show wind turbine blade health monitoring using infrared cameras in different cases.

Table 14. SHM techniques for wind turbine blades.

SHM Technique	Sensing Principle	Typical Damage Types	Key Measured Features	Deployment Scale	Advantages (Reduced)	Disadvantages (Reduced)	References
Strain Measurement	Local deformation sensing	Fatigue damage, stiffness loss	Strain range, stress cycles	Local	Direct fatigue insight; low power	Point-wise; sensor degradation	[141,144,257,258]
Acoustic Emission	Transient elastic waves	Cracks, delamination, fiber breakage	Hit rate, energy, arrival time	Local–Global	Early damage detection; high sensitivity	Noise-sensitive; complex processing	[259–262]
Vibration-Based	Modal response variation	Global damage, stiffness reduction	Frequency shift, mode shapes	Global	Scalable; non-invasive	Operational variability effects	[263–266]
Ultrasonic Guided Waves	Wave propagation in laminates	Delamination, debonding	Time-of-flight, attenuation	Regional	Subsurface defect detection	Limited resolution in composites	[267–270]
Infrared Thermography	Thermal response imaging	Delamination, fatigue hot spots	Thermal contrast, phase lag	Global	Full-field; non-contact	Environmentally sensitive	[271–274]
Machine Vision	Optical image analysis	Surface cracks, erosion	Crack geometry, texture features	Global	Automated; UAV-compatible	Surface-only detection	[275–278]
Radiography	X-ray/Gamma-ray penetration	Internal cracks, delamination	Density contrast	Local	High-resolution internal imaging	Safety and cost constraints	[279–282]
Electromagnetic Waves	EM field interaction	Material inhomogeneity	Signal reflection, phase shift	Local–Regional	Real-time; non-invasive	Interference; calibration needs	[283–285]

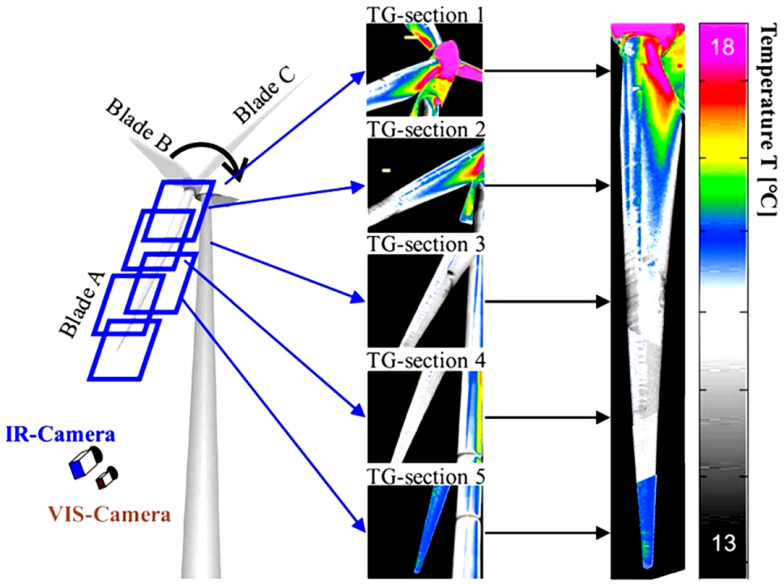

Figure 35. Thermal inspection of a wind turbine blade using infrared cameras with five-section thermograms stitched into a single image for comprehensive analysis [286].

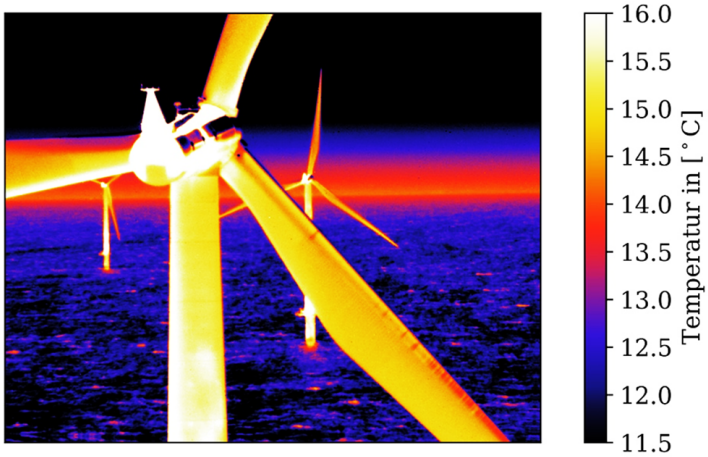

Figure 36. Passive thermography for the detection of rotor blade damage on wind turbines [287].

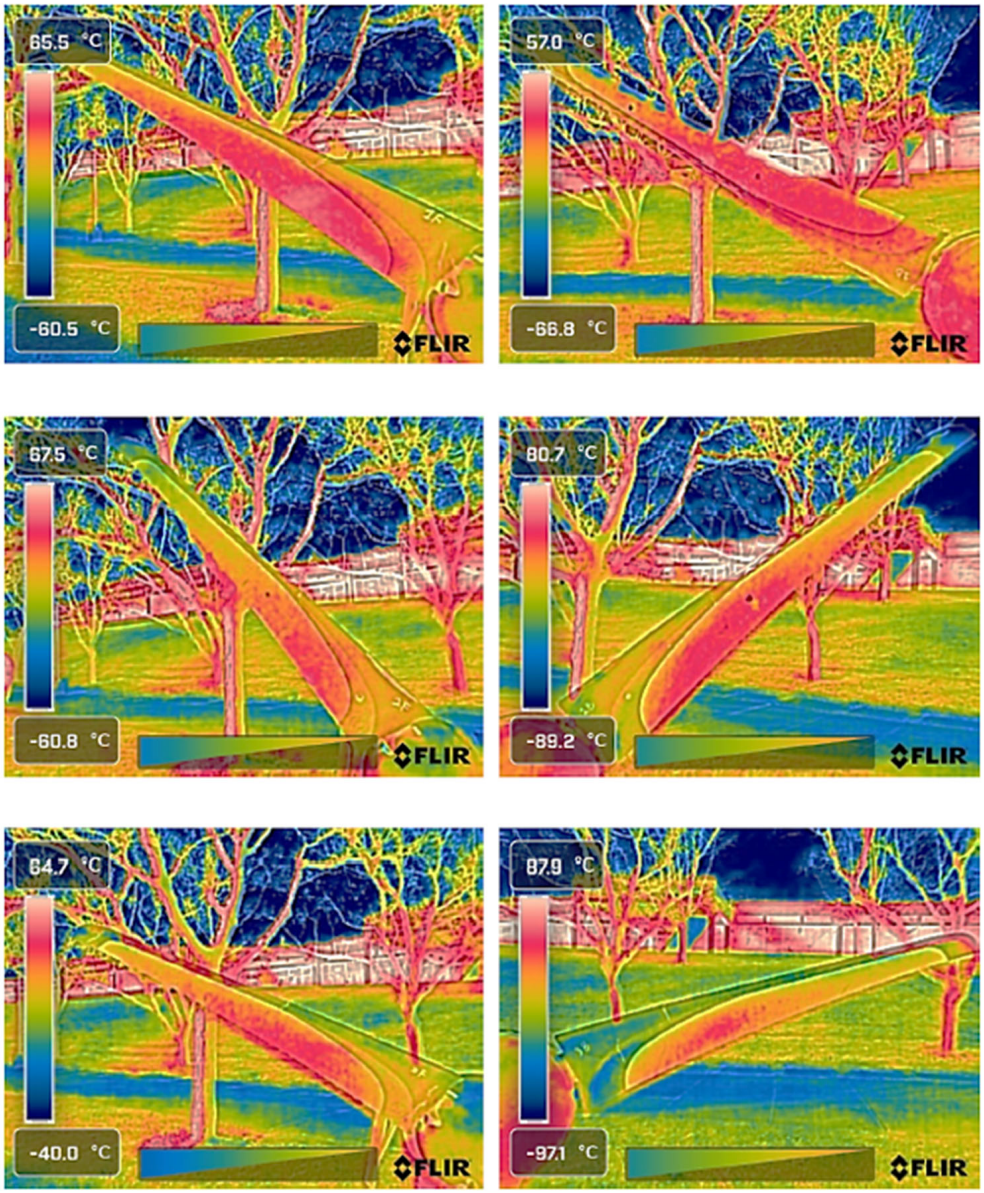

Figure 37. Infrared thermal images of small-scale wind turbine blades captured from both front and rear perspectives, processed using FLIR Thermal Studio with Digital Detail Enhancement to enhance defect visibility and improve interpretability of damage features [288].

Figure 38 schematically illustrates a machine-vision-based structural health monitoring (SHM) configuration for wind turbine blades, where multiple cameras are strategically positioned to capture synchronized images of the blade surface during inspection. By employing two cameras with overlapping fields of view, the system enables geometric reconstruction and surface feature tracking of the blade through stereo or multiview vision principles. This configuration allows accurate detection and localization of surface-level defects such as cracks, erosion, and geometric irregularities by analyzing image features, texture variations, and edge discontinuities. The non-contact nature of machine vision makes it well-suited for blade SHM, particularly when integrated with automated image processing and AI-based algorithms, enabling remote, repeatable, and scalable inspection of large composite blades without interrupting turbine operation.

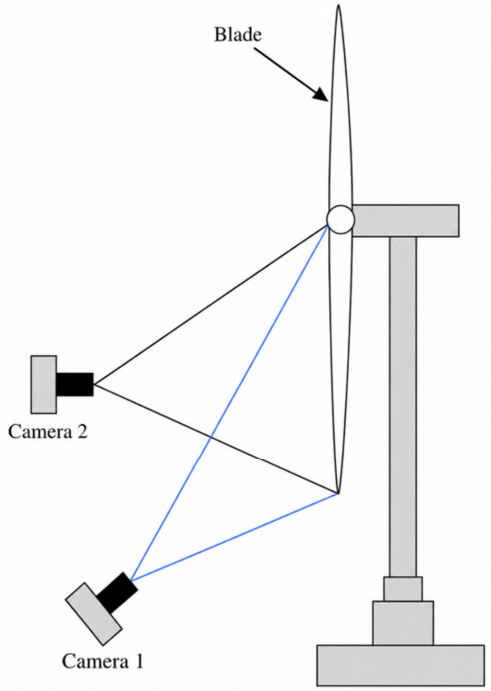

Figure 38. Machine vision technique for wind turbine blade SHM (recreated from [289]).

Figure 39 shows the experimental setup developed by researchers at Zhejiang University (Hangzhou, China) for monitoring wind turbine blade performance under operational conditions using stereo digital image correlation (DIC). The system employs synchronized cameras, optical components, and on-site data acquisition hardware to capture full-field deformation and displacement of large blades during real operation. By enabling non-contact, in situ measurement of blade structural response, this approach improves the accuracy and practicality of blade SHM compared to conventional offline inspection methods [290].

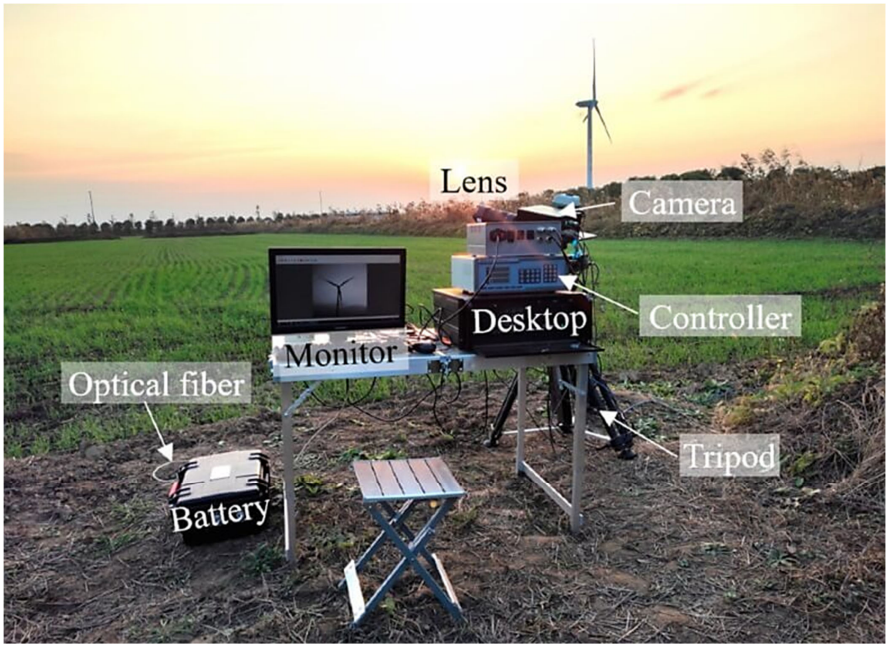

Figure 39. Experimental setup for monitoring blade performance in operational condition using stereo digital image correlation (DIC) [290].

Figure 40 illustrates the application of an impedance-based SHM technique for wind turbine blades, where piezoelectric (PZT) transducers are bonded to critical blade com-

ponents such as the skin, spar, and carbon laminate regions [291]. By exciting the PZT sensors over a frequency range and analyzing changes in the electromechanical impedance signature, local stiffness variations associated with damage initiation and progression can be identified. The method is capable of detecting both indirectly induced damage (e.g., added mass or clamping effects) and actual structural damage, with progressive degradation clearly reflected through shifts in impedance–frequency responses and RMSD-based damage indices. This approach is particularly effective for blade SHM because of its high sensitivity to localized damage in composite structures and its suitability for early-stage damage detection.

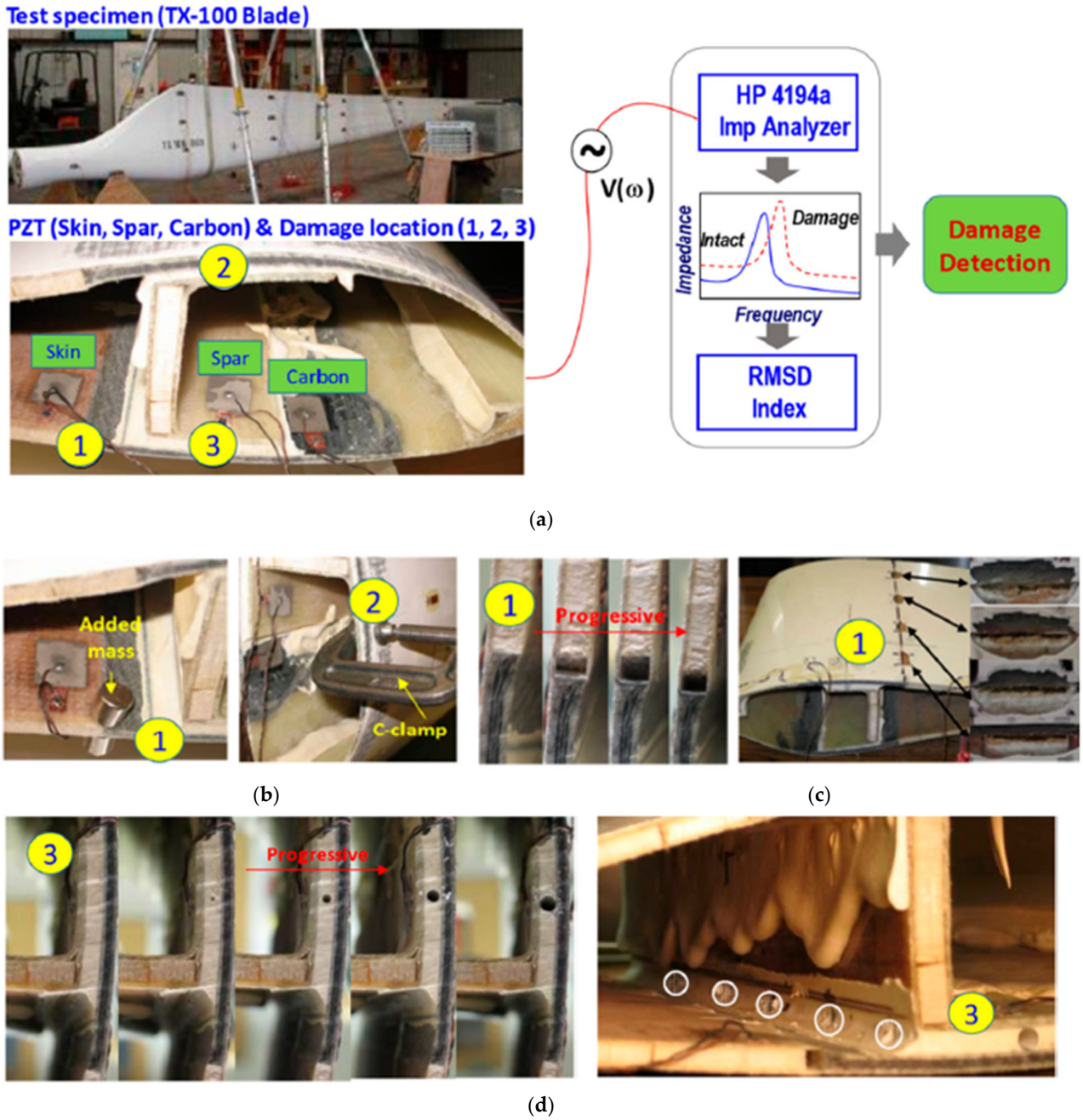

Figure 40. Identification of structural damage in the spar and skin regions of a wind turbine blade segment using an impedance-based monitoring approach [291]: (**a**) test specimen configuration and experimental procedure; (**b**) indirect damage simulation; (**c**) validation through actual damage testing at location 1; (**d**) progressive damage assessment at location 3.

7. Flange Joint

7.1. Major Failure Modes

Wind turbine flange joints play a critical role in transferring axial forces and bending moments between major structural components, such as tower segments and the nacelle interface. Due to their reliance on bolted connections and sustained exposure to cyclic loading and environmental effects, flange joints are particularly vulnerable to progressive degradation and failure during long-term operation. Figure 41 shows the application of flange joints in wind turbine towers, illustrating how tower sections are connected through bolted flange interfaces to transfer axial forces and bending moments. This figure highlights the load transmission mechanism within the flange–bolt assembly, where bolt pretension and contact pressure govern joint stiffness and structural integrity.

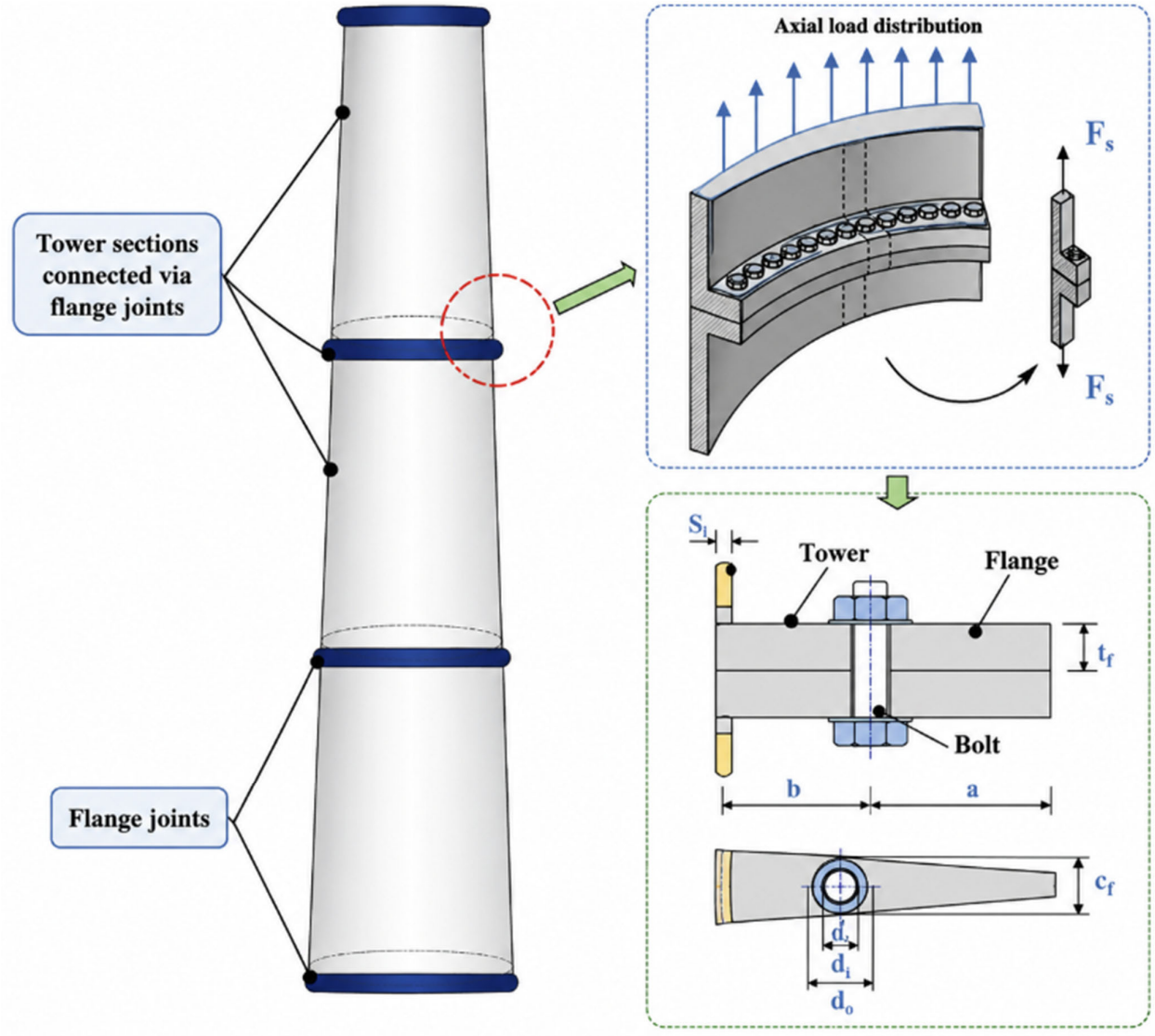

Figure 41. Flange joint application in wind turbine tower (recreated from [292]).

Self-loosening is one of the most commonly reported failure mechanisms in wind turbine flange joints, particularly under cyclic axial and bending loads. Dynamic excitation arising from wind-induced vibrations and operational transients can progressively reduce bolt preload through micro-slip at the thread and bearing interfaces [293]. Experimental studies have shown that insufficient initial pretension significantly accelerates preload loss under transverse vibration [294]. The presence of joint flexibility and non-uniform load

distribution further promotes relative motion between connected components [295]. Field inspections have confirmed that self-loosening often precedes more severe damage modes, such as fatigue cracking and flange misalignment, if not detected early [296].

Fatigue failure in flange joints primarily occurs due to repeated cyclic stress variations in bolts subjected to fluctuating axial forces and bending moments. Stress concentration at the first engaged thread and at the bolt–nut interface has been identified as a critical initiation point for fatigue cracks [297]. Long-term operational loading, combined with partial preload loss, significantly increases stress amplitudes experienced by individual bolts [298]. Numerical and experimental investigations have demonstrated that uneven load sharing among bolts further accelerates fatigue damage accumulation [299]. Several reported wind turbine failures indicate that the fatigue fracture of flange–bolts can lead to progressive joint degradation and, in extreme cases, complete structural separation [300].

Corrosion represents a major durability concern for flange joints, especially in offshore and coastal wind turbines exposed to humid and saline environments. Electrochemical reactions driven by moisture ingress and coating degradation result in material loss at bolt threads and flange contact surfaces [301]. Corrosion products increase surface roughness and alter frictional behavior, which can directly influence preload retention and promote self-loosening [302]. Studies have also shown that corrosion pits act as stress raisers, significantly reducing fatigue strength under cyclic loading [303]. Inspection reports from offshore wind farms indicate that corrosion-related bolt failures often occur earlier than predicted when environmental effects are underestimated during design [304].

Galling is a surface damage mechanism characterized by the adhesive wear between mating metallic surfaces under high contact pressure and relative sliding. In wind turbine flange joints, galling commonly occurs at bolt threads or nut interfaces during installation or retightening operations [305]. Inadequate lubrication and the use of similar material pairs significantly increase susceptibility to adhesive material transfer and surface tearing [306]. Once galling initiates, it can prevent proper preload application and compromise joint integrity [307]. Field maintenance records have shown that galling-related damage often necessitates bolt replacement and increases downtime if not mitigated through appropriate material selection and surface treatment [308].

Table 15 shows the primary failure modes observed in wind turbine flange joints, along with their typical locations, underlying causes, and resulting structural consequences. The table illustrates that flange joint failures are driven by the combined effects of cyclic loading, environmental exposure, and installation-related issues, which directly influence preload retention and load transfer efficiency.

Table 15. Common failure modes in wind turbine flange joints [292–308].

Failure Mode	Typical Location	Primary Causes	Key Consequences	Detection/Monitoring Methods
Self-loosening	Tower–tower segment flanges, tower–nacelle interface	Cyclic loading, insufficient pretension, joint flexibility	Loss of preload, joint separation, misalignment	Bolt torque checks, vibration monitoring
Fatigue failure	Bolts and first engaged threads	Cyclic axial and bending stresses, uneven load sharing	Bolt fracture, progressive joint degradation	Strain monitoring, ultrasonic inspection
Corrosion	Bolt threads, flange contact surfaces	Moisture ingress, saline exposure, coating degradation	Section loss, reduced fatigue strength	Visual inspection, corrosion sensors
Galling	Bolt threads and nut interfaces	High contact pressure, inadequate lubrication	Impaired tightening, preload loss	Installation torque monitoring, surface inspection

Figure 42 shows the statistical distribution of major failure modes observed in wind turbine flange joints based on reported field data and literature. Self-loosening is the most dominant failure mechanism, accounting for approximately 35% of cases, followed by fatigue failure at 30%, which reflects the influence of long-term cyclic loading. Corrosion

contributes about 20% of flange joint failures, particularly in offshore and humid environments, while galling represents the remaining 15%, primarily associated with installation and maintenance operations.

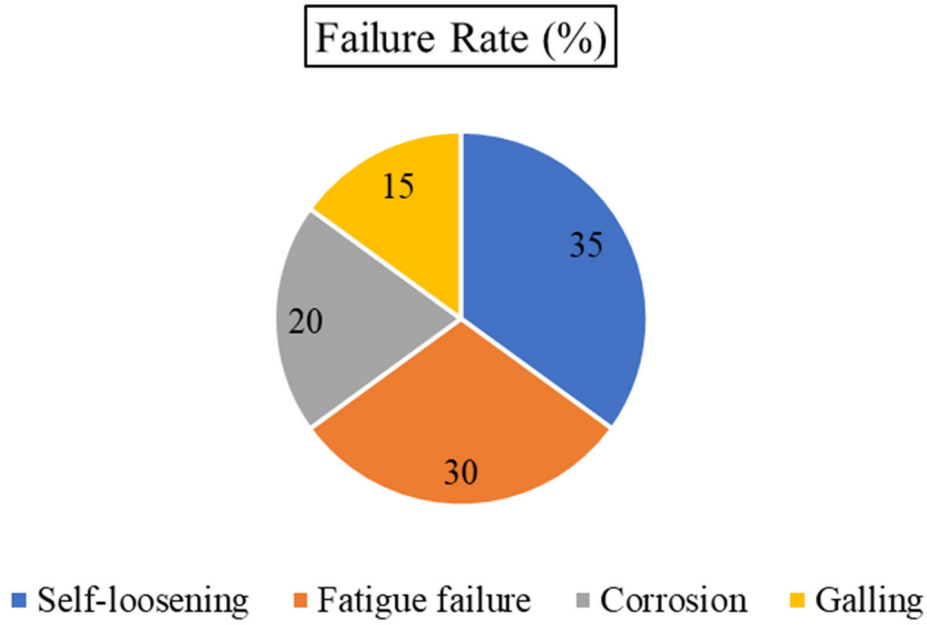

Figure 42. Major failure modes in wind turbine flange joint.

7.2. Failure Case Studies

Figure 43 shows a catastrophic wind turbine tower collapse triggered by failure of a flange joint connection between tower segments. The localized failure of bolted flange components led to loss of load transfer capacity, causing progressive instability and eventual global collapse of the tower structure.



Figure 43. WT tower collapse due to flange joint failure [309].

7.3. Condition Monitoring and SHM

Flange joint structural health monitoring (SHM) is critical because flange connections represent mechanically discontinuous regions in wind turbine structures where loads are transferred through bolted interfaces under combined cyclic, dynamic, and environmental actions. These joints are particularly susceptible to preload loss, bolt fatigue, fretting, corrosion, and local slip, all of which can progressively degrade joint stiffness and compromise global structural integrity. Undetected degradation in flange joints can lead to load redistribution, increased vibration levels, and accelerated damage in adjacent structural components. Therefore, flange joint-specific SHM and prognostics and health management (PHM) strategies are essential for early fault detection, the reliable assessment of joint condition, and the prevention of sudden connection failures in modern wind turbines.

To date, impedance-based structural health monitoring (SHM) of wind turbine flange joints has received limited attention, despite flange connections being highly susceptible to bolt preload loss, joint stiffness degradation, and fretting-induced damage under cyclic loading. Nguyen et al. [310] conducted one of the earliest investigations into the feasibility of impedance-based SHM for monitoring bolt looseness in wind turbine tower flange joints (Figure 44). In their study, piezoelectric (PZT) transducers were installed on bolted flange interfaces, and joint degradation was introduced by sequential bolt loosening. The impedance responses measured in the high-frequency range were shown to be highly sensitive to local joint resonance characteristics, enabling the identification of bolt looseness through statistical damage indices such as RMSD and CCD. Their work further demonstrated that combining impedance-based sensing with vibration-based monitoring can enhance damage detectability in flange-type connections. However, the applicability of the approach to realistic tubular wind turbine flange joints remains limited, and the influence of operational loading and temperature variations on impedance signatures was not fully addressed.

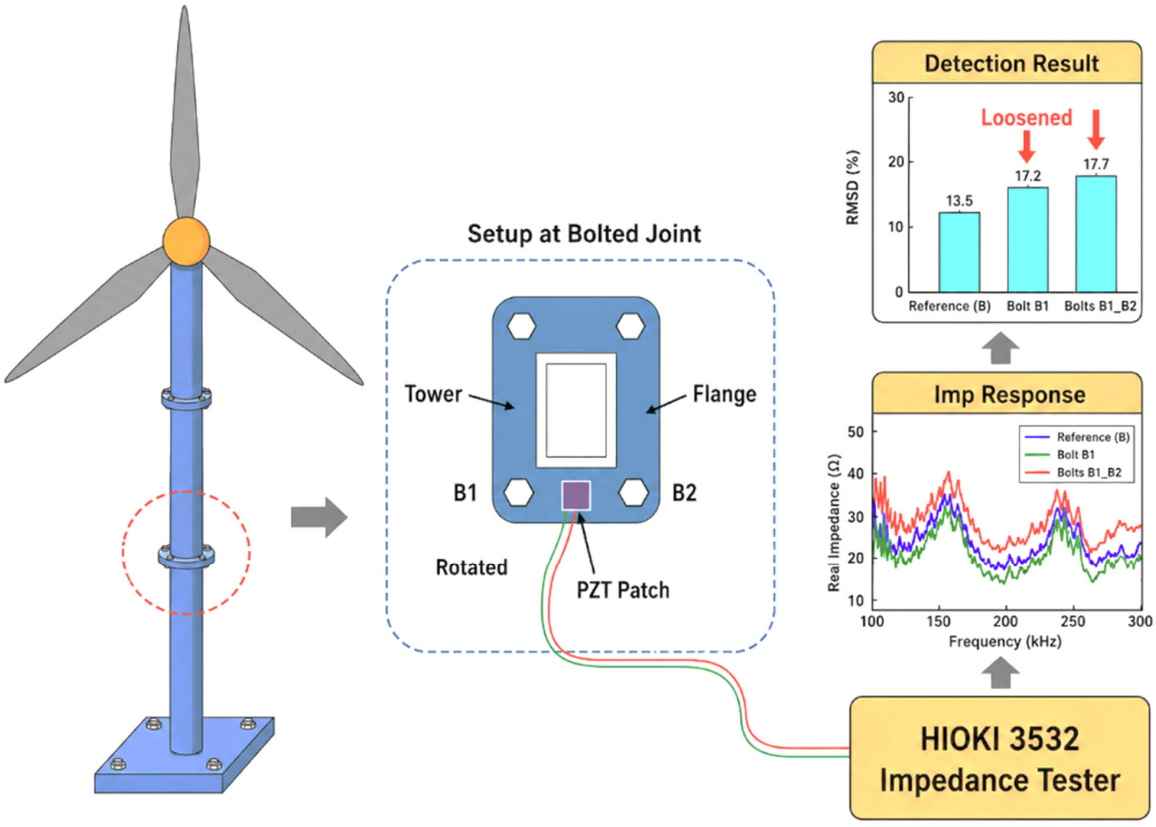

Figure 44. Experimental implementation of impedance-based SHM for flange joint condition assessment in a lab-scale wind turbine model (recreated from [310]).

Beyond direct wind turbine applications, impedance-based SHM has also been explored in structural configurations with geometrical similarity to wind turbine flange joints. Jiang et al. [311] investigated the detection of minor bolt looseness in a multi-bolt tubular flange using PZT-based impedance measurements under controlled torque reductions (Figure 45). Their results highlighted the vulnerability of traditional impedance damage indices, such as RMSD, MAPD, CCD, and RMSCR, to measurement noise, particularly when identifying small preload losses. To overcome this limitation, a new damage metric (T index) was proposed, demonstrating improved robustness in distinguishing minor bolt looseness from noise-contaminated signals. This study provided important insight into the challenges of flange joint SHM, emphasizing the need for noise-resilient damage features when monitoring subtle degradation in bolted interfaces.

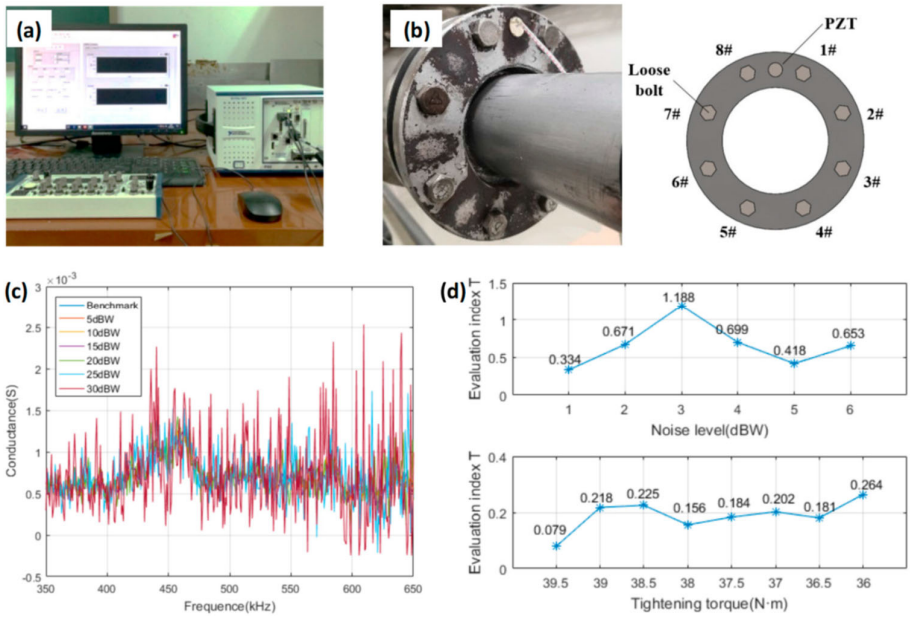

Figure 45. Impedance-based SHM for flange joint condition assessment: (**a**) impedance analyzer; (**b**) PZT transducer mounted on an eight-bolt flange joint with layout schematic; (**c**) influence of measurement noise on conductance response; (**d**) damage evaluation indices under different operating conditions [311].

To improve practicality and field applicability, Wang et al. [312] developed a wearable impedance-based sensing device for monitoring bolt preload variations in flange joints (Figure 46). The device integrates PZT transducers within a mechanically clamped housing, allowing non-permanent attachment to flange surfaces without adhesive bonding. This design enables repeated installation and removal, making it particularly suitable for wind turbine flange joints that require maintainability and adaptability. Experimental results demonstrated a clear correlation between impedance-based damage indices and bolt torque variations over a wide frequency range, confirming the capability of wearable impedance sensing to detect preload changes in multi-bolt flange assemblies. Such developments represent a promising step toward deployable, flange-specific SHM systems for wind turbine applications.

Table 16 summarizes the principal impedance-based and hybrid SHM techniques developed for monitoring wind turbine flange joints, with emphasis on bolt preload loss and joint stiffness degradation. The table highlights how conventional impedance metrics offer high sensitivity to local joint damage but suffer from noise and environmental effects, motivating the development of noise-resilient indices and hybrid monitoring frameworks. Wearable impedance sensor systems further enhance practical deployment by enabling

non-invasive, repeatable monitoring of flange joints. Overall, the table demonstrates that impedance-based SHM represents a promising yet evolving approach for flange joint health assessment, requiring further integration with operational-condition compensation and long-term prognostic frameworks.

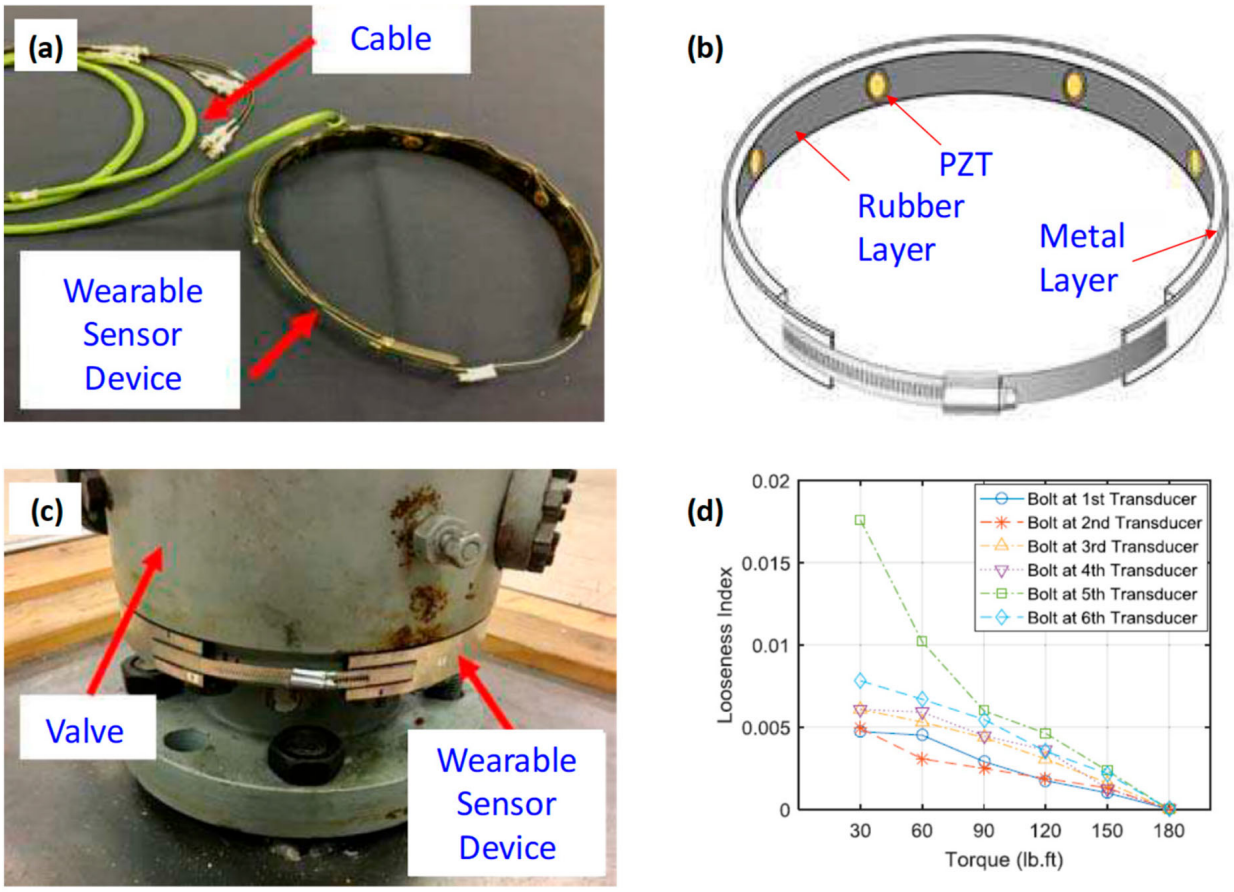

Figure 46. Wearable impedance-based SHM for flange joint condition assessment: (**a**) wearable sensor device; (**b**) device configuration and layout; (**c**) sensor mounted on a flanged valve joint; (**d**) relationship between bolt loosening index and applied bolt torque [312].

Table 16. SHM techniques for wind turbine flange joints.

SHM Technique	Sensing Principle	Targeted Flange Joint Faults	Key Features/Indices	Deployment Type	Pros	Cons	Reference
Impedance-Based SHM	Electromechanical impedance variation	Bolt looseness, stiffness degradation	RMSD, CCD, MAPD, RMSCR	Local	High sensitivity to local damage	Sensitive to temperature, noise	[310]
Hybrid Impedance-Vibration SHM	Local impedance + global dynamics	Bolt looseness, joint degradation	RMSD, modal changes	Local–Global	Improved detectability	Increased system complexity	[310]
Noise-Resilient Impedance SHM	Statistical separation of damage and noise	Minor bolt preload loss	T index	Local	Robust to excitation noise	Threshold calibration needed	[311]
Wearable Impedance Sensors	Clamped PZT impedance sensing	Bolt preload variation	Normalized RMSD	Local	Non-permanent, portable	Requires proper clamping force	[312]

Figure 47 illustrates the application of impedance-based structural health monitoring across key wind turbine components, highlighting its versatility for blade, tower, and flange joint condition assessment [313]. Piezoelectric (PZT)-based impedance sensing is shown to be deployable at different structural locations, where changes in local electromechanical impedance reflect stiffness degradation, damage initiation, or connection deterioration. For blade SHM, the technique enables the detection of localized damage within composite skin

and spar regions, while tower SHM benefits from sensitivity to local structural changes near critical sections. In the context of flange joint SHM, impedance-based monitoring is particularly effective for identifying bolt looseness, corrosion, and contact degradation at bolted interfaces. Overall, the figure demonstrates that impedance-based SHM provides a unified, high-sensitivity framework for multi-component monitoring of wind turbine structures, supporting early damage detection and condition-based maintenance strategies.

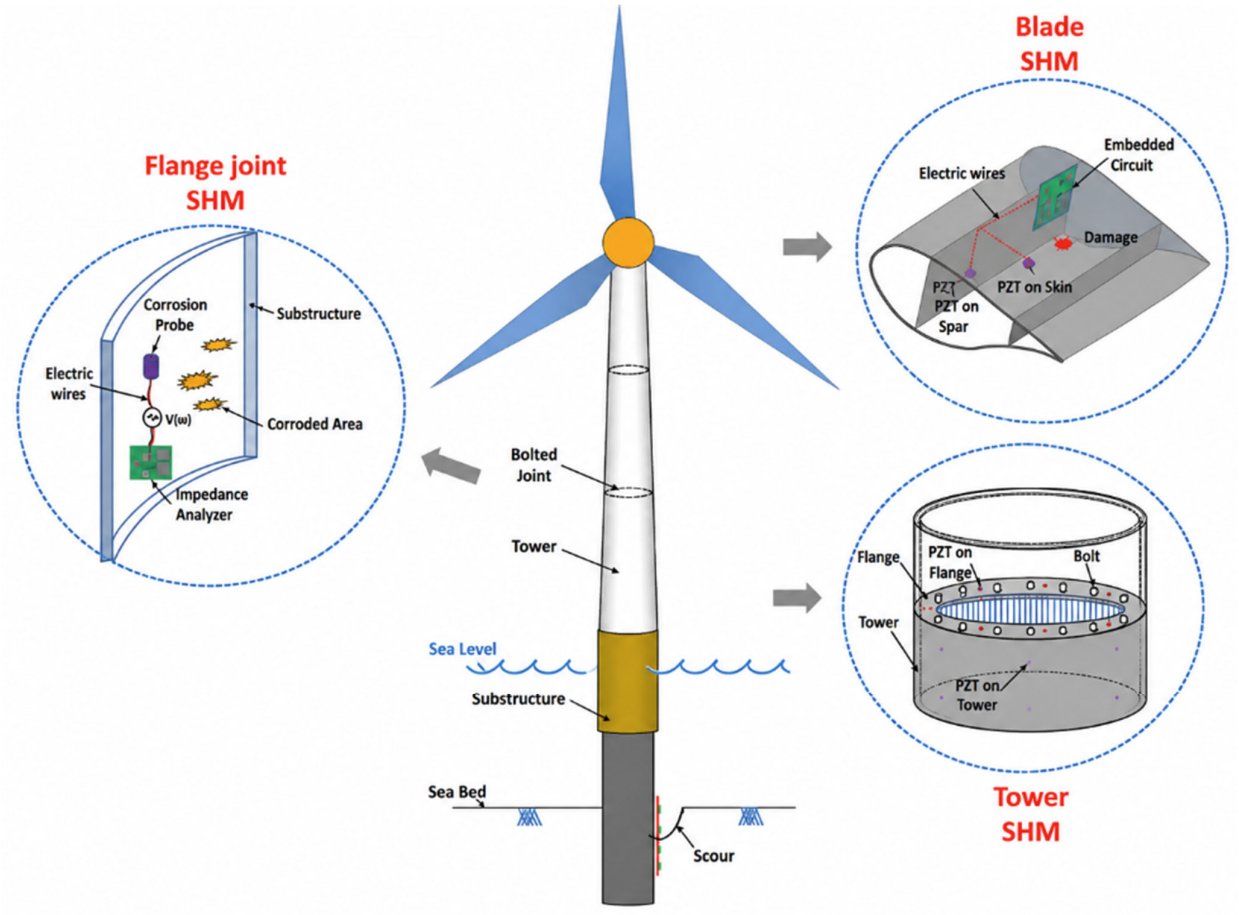

Figure 47. Application of impedance-based SHM for wind turbine components (recreated from [313]).

Welded regions in wind turbine towers and flange joints are sensitive to local microstructural change, residual stress, coating degradation, and corrosion-assisted fatigue. The welded-steel study by Ziat et al. [314] showed that surface treatment and epoxy/alumina coating strongly influence corrosion resistance and impedance response in corrosive media. This supports the need to consider surface state, corrosion protection, and impedance-sensitive monitoring when evaluating welded tower and flange joint reliability in offshore wind turbines.

8. Discussion

The monitoring techniques reviewed in the previous sections differ substantially in their sensing principle, detectable damage type, data requirement, field applicability, and maturity level. Therefore, a direct comparison is necessary to avoid treating all monitoring methods as equally suitable for wind turbine reliability assessment. Table 17 summarizes the main advantages, limitations, applicable conditions, and field-deployment challenges of widely used wind turbine condition monitoring, structural health monitoring, and PHM-related sensing technologies. The comparison shows that no single method can fully cover all drivetrain and structural failure modes. Vibration and acoustic emission methods are

effective for drivetrain and early crack-related damage, but they require appropriate sensor placement and high-frequency data acquisition. SCADA-based diagnostics provide fleet-wide low-cost monitoring, but their low sampling frequency limits early fault sensitivity. Vision, thermography, ultrasonic testing, impedance-based SHM, strain sensing, and oil-debris monitoring each provide different levels of spatial coverage, damage sensitivity, and deployment practicality. This confirms the need for multi-sensor data fusion and component-specific monitoring design.

Table 17. Critical comparison of monitoring technologies for wind turbine reliability assessment.

Monitoring Method	Detectable Failure Mechanisms	Typical Data/Features	Advantages	Limitations	Best Application Conditions	Field-Deployment Challenges	Maturity Level
Vibration analysis	Gear tooth pitting, bearing spalling, shaft misalignment, imbalance, looseness	RMS, kurtosis, crest factor, gear-mesh frequency, bearing fault frequencies, envelope spectrum, sidebands	High sensitivity to rotating-component defects; strong diagnostic foundation; suitable for online CMS	Sensitive to speed/load variation; requires high-frequency sensors; fault signatures may overlap	Gearboxes, main bearings, generator bearings, drivetrain monitoring	Sensor mounting, noise, variable-speed operation, non-stationarity, data volume	High
Acoustic emission	Early cracking, bearing defects, gear tooth damage, frictional events, impact-related damage	AE counts, energy, amplitude, hit rate, frequency content, rise time	Sensitive to early-stage microcracks and high-frequency transient events	Strong attenuation; short sensing range; high sampling rate; expensive sensor network	Localized gearbox, bearing, blade, and welded-joint monitoring	Sensor coupling, attenuation, noise filtering, source localization	Medium to high
Oil debris and lubricant monitoring	Gear wear, bearing wear, scuffing, lubrication degradation, contamination	Particle count, particle size, ferrous debris, viscosity, moisture, oil temperature	Direct indication of wear and lubricant health; useful for drivetrain degradation	Limited to lubricated components; offline sampling may miss rapid damage evolution	Gearbox and bearing lubrication systems	Sampling interval, sensor fouling, interpretation of debris source	High
Temperature and thermal monitoring	Overheating, lubrication failure, electrical faults, frictional heating, blade surface anomalies	Oil temperature, bearing temperature, winding temperature, thermal images	Low cost; easy integration with SCADA; useful as supporting indicator	Slow response; weak early fault sensitivity; affected by ambient temperature and load	Gearbox, generator, bearings, electrical systems, blade surface inspection	Environmental compensation, low specificity, delayed detection	Medium
SCADA-based diagnostics	Power underperformance, yaw/pitch faults, thermal anomalies, drivetrain performance degradation	Power, wind speed, rotor speed, pitch angle, temperature, current, voltage, alarms	Uses existing turbine data; fleet-wide applicability; low additional cost	Low sampling rate; limited early damage sensitivity; weak localization	Fleet-level anomaly detection and performance monitoring	Missing data, operational variability, false alarms, limited labels	High for screening; medium for diagnosis
Ultrasonic testing	Blade delamination, adhesive defects, wall-thickness loss, cracks, corrosion-assisted damage	Time-of-flight, reflected amplitude, attenuation, C-scan features	Strong internal defect detection; useful for thickness and crack assessment	Usually inspection-based rather than continuous; requires access and coupling	Blade inspection, tower welds, flange zones, metallic structures	Access difficulty, operator dependence, coupling condition	High for inspection
Infrared thermography	Blade delamination, debonding, moisture ingress, surface heating, electrical faults	Thermal contrast, temperature gradients, hot spots	Non-contact inspection; useful for blades and electrical components	Sensitive to weather, solar radiation, surface emissivity; limited depth	Blade surface and near-surface inspection; electrical cabinets	Environmental correction, inspection timing, defect-depth limitation	Medium
Machine vision and UAV inspection	Blade erosion, cracks, coating loss, lightning damage, tower surface corrosion, external defects	RGB images, defect segmentation, texture, edge features, object detection outputs	Large-area inspection; safer than manual inspection; compatible with AI image analysis	Mainly surface-visible defects; performance depends on lighting and image quality	Blade and tower external inspection	Image quality, weather, annotation cost, false positives	Medium to high
Strain gauges and FBG sensors	Fatigue loading, tower bending, blade strain, flange/joint load redistribution	Strain range, load cycles, modal response, curvature, strain spectra	Direct structural response measurement; useful for fatigue and load monitoring	Requires installation and protection; limited spatial coverage	Towers, blades, foundations, flange/joint regions	Sensor durability, calibration drift, cable routing, environmental protection	Medium to high
Impedance-based SHM	Bolt loosening, local stiffness loss, small cracks, adhesive degradation, local joint damage	Electrical impedance/admittance signatures, resonance shifts, damage index	Highly sensitivity to local stiffness changes; suitable for bolts and joints	Local sensing range; temperature sensitivity; requires baseline comparison	Flange joints, bolted joints, bonded areas, local welded regions	Environmental compensation, sensor bonding durability, baseline drift	Medium
Electromagnetic and Eddy Current methods	Surface/subsurface cracks, corrosion, metallic discontinuities, bolt/flange defects	Impedance change, magnetic flux leakage, eddy current response	Effective for metallic components and near-surface defects	Limited penetration depth; mainly inspection-based; material-dependent	Tower welds, flange regions, bolts, metallic drivetrain parts	Access, geometry effects, coating influence, calibration	Medium
Digital twin/data-fusion monitoring	System-level degradation, multi-component fault interaction, RUL estimation, maintenance prioritization	Combined SCADA, CMS, strain, AE, vision, inspection, and model outputs	Integrates heterogeneous data; supports predictive maintenance and decision-making	Requires model calibration, data quality, uncertainty quantification, computational resources	Fleet-level PHM and long-term reliability management	Data interoperability, validation, explainability, cyber/data governance	Emerging

A major requirement for practical wind turbine SHM and PHM is the direct connection between the physical failure mechanism and the measurable monitoring indicator. A diagnostic method is useful only when the sensor output can be linked to a specific degradation process, such as gear tooth pitting, bearing spalling, blade delamination, tower fatigue cracking, or flange bolt loosening. Therefore, failure diagnosis should not be treated only as a signal-classification problem; it must also be interpreted through the physics of damage initiation, propagation, and load transfer. Table 18 maps representative wind turbine failure mechanisms to their measurable indicators and suitable diagnostic methods. This mapping helps identify which monitoring technologies are physically meaningful for each component and clarifies why multi-sensor monitoring is often required in real operating environments.

Table 18. Failure mechanisms, measurable indicators, and suitable diagnostic methods for major wind turbine components.

Component	Failure Mechanism	Physical Degradation Process	Measurable Monitoring Indicators	Suitable Diagnostic Methods	Practical Limitation
Gearbox gears	Gear tooth pitting	Repeated contact stress causes surface fatigue and local material removal on gear teeth	Gear-mesh frequency sidebands, vibration kurtosis, RMS increase, oil debris particles	Vibration analysis, envelope analysis, oil-debris monitoring, acoustic emission	Load/speed variation can mask sidebands; oil debris source may be difficult to localize
Gearbox gears	Tooth bending fatigue or cracking	Cyclic root bending stress initiates cracks near the tooth root and propagates under repeated torque	Impulsive vibration, modulation sidebands, AE bursts, abnormal torque fluctuation	Vibration analysis, order tracking, acoustic emission, model-based residuals	Early cracks produce weak signals under variable-speed operation
Gearbox gears	Scuffing and lubrication failure	Breakdown of lubricant film causes sliding damage, frictional heating, and surface roughening	Oil temperature rise, viscosity change, metallic debris, high-frequency AE activity	Lubricant monitoring, temperature monitoring, acoustic emission, vibration analysis	Temperature response may be delayed and affected by ambient conditions
Bearings	Outer-race spalling	Rolling contact fatigue produces localized material loss on the stationary raceway	BPFO component, envelope spectrum peaks, AE energy, impact repetition	Vibration envelope analysis, acoustic emission, spectral kurtosis	Bearing fault frequencies vary with speed and load; early damage may be buried in noise
Bearings	Inner-race spalling	Local raceway defect interacts with rolling elements and rotating load zone	BPFI component, amplitude modulation, sidebands around shaft frequency	Vibration analysis, order tracking, AE monitoring, current-based monitoring	Non-stationary speed requires resampling or order-domain processing
Bearings	Cage damage or fracture	Cage wear, cracking, or instability alters rolling element spacing and motion	Low-frequency modulation, irregular impacts, cage-frequency components, temperature rise	Vibration analysis, AE monitoring, temperature monitoring	Cage faults are difficult to isolate from lubrication and misalignment effects
Bearings/gearbox	Lubricant contamination	Water, dust, wear particles, or degraded oil accelerates abrasion and contact fatigue	Particle count, moisture content, viscosity change, oil dielectric properties	Online/offline oil monitoring, particle counting, ferrography	Sampling interval and sensor fouling can reduce reliability
Blades	Delamination	Interlaminar stresses separate composite layers and reduce local stiffness	AE events, ultrasonic reflection, thermal contrast, modal frequency shift, strain redistribution	Acoustic emission, ultrasonic testing, infrared thermography, strain sensing, modal analysis	Internal defects may be difficult to detect from the surface; inspection access is limited
Blades	Leading-edge erosion	Rain, hail, particles, and salt spray remove coating and roughen the blade surface	Image texture change, surface roughness, power-curve deviation, aerodynamic loss	UAV/machine vision, thermography, SCADA performance monitoring	Image quality depends on lighting/weather; SCADA indicators are indirect
Blades	Lightning damage	High-current strike causes burns, punctures, internal delamination, and conductor damage	Visible burn marks, AE activity, thermal anomalies, conductivity/resistance change	Visual/UAV inspection, thermography, electrical continuity testing, AE	Damage may extend internally beyond visible surface marks
Tower	Fatigue cracking	Cyclic bending and welded-detail stress concentration initiate and grow cracks	Strain range increase, AE events, modal frequency shift, crack indication, local stiffness loss	Strain gauges, AE monitoring, modal analysis, ultrasonic testing	Low crack-growth rates require long-term monitoring and environmental compensation
Tower	Corrosion-assisted degradation	Marine humidity, coating damage, and cyclic stress cause wall-thickness loss and crack acceleration	Thickness reduction, corrosion potential, impedance change, visual rusting, strain redistribution	Ultrasonic thickness testing, visual inspection, corrosion sensors, impedance-based SHM	Coating condition and access constraints affect inspection quality
Flange joints	Bolt loosening/preload loss	Cyclic loading, relaxation, embedding, and vibration reduce bolt clamping force	Preload reduction, local stiffness loss, impedance signature shift, strain redistribution	Bolt tension monitoring, torque checks, impedance-based SHM, strain sensing	Local damage sensitivity requires baseline data and temperature compensation
Flange joints	Fretting fatigue	Micro-slip at contact interfaces causes surface damage and crack initiation	Local vibration change, AE events, surface wear debris, bolt-load variation	AE monitoring, vibration analysis, visual inspection, impedance-based SHM	Fretting signatures can be confused with bolt loosening or general vibration
Welded joints	Weld toe cracking	Stress concentration and cyclic load initiate cracks at weld toes or heat-affected zones	AE hits, strain concentration, ultrasonic crack signal, impedance damage index	AE, strain gauges, ultrasonic testing, impedance-based SHM	Sensor placement strongly affects detection sensitivity
Generator/electrical system	Electrical insulation degradation	Thermal aging, moisture, and electrical stress degrade insulation material	Temperature rise, partial discharge, current harmonics, insulation resistance change	Electrical monitoring, temperature monitoring, partial discharge monitoring, SCADA	Fault signatures can be affected by grid events and converter operation

AI-based models have shown strong potential for wind turbine fault diagnosis and PHM, particularly in studies using vibration, acoustic emission, SCADA, image, and multi-sensor datasets. However, reported diagnostic performance must be interpreted carefully

because many high classification accuracies are obtained under controlled laboratory conditions, balanced datasets, artificial fault injection, or limited operating variability. In real wind farms, fault diagnosis is more difficult because turbines operate under variable wind speed, turbulence, temperature, humidity, yaw error, pitch control action, drivetrain load variation, and sensor noise. In addition, healthy data usually dominate the dataset, while true fault data are rare, incomplete, and unevenly distributed among failure classes. Therefore, a model that achieves high overall accuracy may still perform poorly in detecting rare but critical faults.

The main field-deployment limitations of AI-based PHM include small labeled datasets, severe class imbalance, domain shift between turbines and wind farms, inconsistent sensor placement, different sampling rates, missing data, environmental variability, lack of failure labels, overfitting to test-rig data, limited interpretability, and insufficient uncertainty quantification. These limitations are particularly important for offshore wind turbines, where access constraints make labeled failure confirmation expensive and where models trained on one turbine type, site, or operating regime may not transfer reliably to another. Therefore, AI-based PHM should be evaluated not only by classification accuracy, but also by metrics that are robust to imbalanced data and by validation under realistic field conditions.

To avoid misleading interpretation under imbalanced data conditions, diagnostic performance should be evaluated using confusion-matrix-based metrics. For a binary fault-detection problem, precision, recall, F1-score, and balanced accuracy are defined as

$$\text{Precision} = \frac{TP}{TP + FP} \tag{14}$$

$$\text{Recall} = \frac{TP}{TP + FN} \tag{15}$$

$$F_1 = 2\frac{\text{Precision} \times \text{Recall}}{\text{Precision} + \text{Recall}} \tag{16}$$

$$\text{Balanced Accuracy} = \frac{1}{2}\left(\frac{TP}{TP + FN} + \frac{TN}{TN + FP}\right) \tag{17}$$

where TP, TN, FP, and FN denote true positives, true negatives, false positives, and false negatives, respectively. Precision measures how many predicted fault cases are correct, while recall measures how many actual fault cases are successfully detected. The F1-score combines precision and recall and is more informative than accuracy when fault cases are rare. Balanced accuracy accounts for both fault and healthy classes and is therefore more suitable than ordinary accuracy for highly imbalanced wind turbine datasets.

Table 19 shows that accuracy alone is insufficient for evaluating AI-based wind turbine fault-diagnosis models, especially when fault samples are rare compared with healthy operating data. For example, a model can achieve high accuracy by correctly classifying healthy data while still missing early bearing spalling, gearbox pitting, blade delamination, or flange loosening events. Precision and recall are therefore necessary to distinguish false alarms from missed detections, while F1-score and balanced accuracy provide more meaningful performance measures under class imbalance. PR-AUC is particularly useful for rare-fault detection because it focuses on the trade-off between fault-alarm reliability and fault-detection sensitivity. These metrics should be reported together with dataset type, turbine operating condition, sensor type, fault severity, and validation strategy to determine whether an AI model is suitable for field deployment.

Table 19. AI diagnostic evaluation metrics and relevance for imbalanced wind turbine fault datasets.

Metric	Formula/Definition	Strength	Limitation	Recommended Use in Wind Turbine PHM
Accuracy	((TP + TN)/(TP + TN + FP + FN))	Simple and widely reported	Misleading when healthy data dominate; rare faults may be missed	Use only with balanced datasets or together with other metrics
Precision	(TP/(TP + FP))	Measures reliability of fault alarms	Does not show how many real faults are missed	Important when false alarms increase inspection and maintenance cost
Recall/sensitivity	(TP/(TP + FN))	Measures fault-detection ability	High recall may increase false alarms	Important for safety-critical faults where missed detection is costly
F1-score	Harmonic mean of precision and recall	Balances false alarms and missed detections	Does not include true negatives	Recommended for imbalanced fault-classification problems
Specificity	(TN/(TN + FP))	Measures correct healthy-state identification	Does not measure fault detection directly	Useful when false alarms affect turbine availability
Balanced accuracy	Average of recall and specificity	Accounts for imbalance between healthy and fault classes	Less informative for multi-class severity ranking	Recommended for healthy/fault datasets with unequal class distribution
ROC-AUC	Area under true-positive vs. false-positive curve	Threshold-independent comparison	Can be optimistic under severe imbalance	Useful for model comparison, but should be paired with PR-AUC
PR-AUC	Area under precision–recall curve	More sensitive to rare-fault performance	Depends strongly on class prevalence	Recommended for rare-fault detection and early-warning models
Confusion matrix	Class-wise TP, TN, FP, FN distribution	Shows which classes are confused	Requires enough labeled examples per class	Essential for multi-class gearbox, bearing, blade, and tower fault diagnosis
Calibration/uncertainty	Agreement between predicted probability and observed frequency	Supports risk-based maintenance decisions	Often not reported in AI fault-diagnosis studies	Needed for PHM decision support and maintenance prioritization

A further limitation is the difference between controlled laboratory datasets and field data from operating wind turbines. Laboratory datasets often contain clear fault labels, controlled speed/load conditions, high signal-to-noise ratio, and artificially introduced damage. In contrast, field datasets are affected by non-stationary wind speed, variable rotational speed, turbulence, control action, sensor drift, missing data, and mixed fault signatures. This creates domain shift between training and deployment conditions. Consequently, AI models trained on laboratory or single-turbine datasets may lose accuracy when applied to different turbine capacities, drivetrain configurations, wind farms, seasons, or sensor layouts. Transfer learning, domain adaptation, physics-informed learning, uncertainty quantification, and continual model updating are therefore important research directions for making AI-based PHM reliable under real wind turbine operating environments.

9. Future Directions and Open Research Questions

Despite substantial advances in understanding wind turbine failure mechanisms and in developing structural health monitoring (SHM) and prognostics and health management (PHM) techniques, several challenges remain unresolved, particularly for large-scale and offshore wind turbines. The increasing complexity of modern wind energy systems, combined with harsher operating environments and higher reliability requirements, demands the evolution of SHM from isolated component-level monitoring toward integrated, scalable, uncertainty-aware, and decision-oriented frameworks. Addressing these challenges requires coordinated progress in sensing technologies, data analytics, reliability modeling, artificial intelligence, digital twins, and maintenance decision support, as well as a clearer understanding of the limitations of current laboratory-based and component-specific methodologies. The following points summarize the key future research directions and open questions identified through this review.

9.1. Future Directions

Development of scalable SHM and PHM frameworks validated on full-scale, large-capacity onshore and offshore wind turbines under realistic operational and environmental conditions, especially for turbines of 10 MW class and above.

Integration of multi-sensor and multi-physics monitoring systems that combine vibration, strain, acoustic emission, impedance, thermal, electromagnetic, ultrasonic, SCADA, and vision-based data across drivetrain and structural components.

Advancement of physics-informed artificial intelligence and hybrid digital twin approaches to improve robustness, interpretability, uncertainty quantification, and generalization capability of data-driven SHM and PHM models.

Expansion of SHM objectives from qualitative damage detection toward quantitative remaining useful life estimation, risk-based maintenance planning, and decision-oriented PHM.

Increased emphasis on blade, tower, welded-joint, and flange joint monitoring, particularly for fatigue cracking, corrosion-assisted degradation, bolt-preload loss, local stiffness reduction, and long-term environmental deterioration in large-diameter structures.

Development of durable, self-powered, wireless, and minimally invasive sensing technologies suitable for long-term deployment in offshore and harsh operating environments.

Standardization of field datasets, failure labels, maintenance records, and performance metrics so that AI-based PHM models can be compared using not only accuracy, but also precision, recall, F1-score, balanced accuracy, uncertainty calibration, and maintenance relevance.

Greater reporting of real-world deployment outcomes, including turbine type, sensor layout, monitoring duration, data quality, diagnostic performance, false-alarm behavior, maintenance action, downtime reduction, and economic benefit.

9.2. Open Research Questions

How can SHM techniques validated at laboratory or sub-component scale be reliably transferred to full-scale wind turbines operating under variable aerodynamic, mechanical, thermal, and environmental loading?

What are the most effective strategies for data fusion, feature extraction, and damage representation when combining heterogeneous SHM signals across multiple turbine components?

How can AI-based SHM and PHM models maintain accuracy, robustness, and interpretability under unseen operating conditions, different turbine designs, site-specific environmental variability, and rare but critical failure events?

How can the limited availability of labeled failure data, particularly for tower cracking, flange joint loosening, blade internal damage, and offshore structural degradation, be mitigated using simulation-based learning, synthetic data generation, transfer learning, domain adaptation, or physics-informed modeling?

How can SHM outputs be systematically integrated with probabilistic reliability models, risk assessment, digital twin updating, inspection planning, and maintenance decision-making frameworks?

What compensation strategies are required to address environmental and operational variability, such as temperature, humidity, corrosion, biofouling, rotor-speed variation, load fluctuation, and sensor aging, that affects long-term sensor performance and data quality?

The open research questions summarized in this section show that wind turbine reliability improvement requires more than higher diagnostic accuracy. Future PHM systems must connect physical failure mechanisms, sensor selection, uncertainty-aware data analytics, field validation, and maintenance decision-making. This motivates the concluding synthesis, where the main findings of the review are summarized in terms of component reliability, monitoring technology, AI limitations, and integrated SHM/PHM deployment needs.

10. Conclusions

This review has presented a comprehensive assessment of major failure modes and monitoring strategies associated with principal wind turbine components, including gearboxes, bearings, blades, towers, and flange joints. The collected evidence confirms that drivetrain components remain dominant contributors to operational interruption, with gearboxes and bearings responsible for approximately 30–40% of unplanned downtime, while blade-related failures account for roughly 20–25% of reported failure events. At the same time, the increasing scale of modern turbines, especially in offshore environments, has amplified the importance of structural degradation mechanisms such as tower fatigue cracking, corrosion-assisted deterioration, local buckling, adhesive joint degradation, welded-detail damage, and flange joint bolt-preload loss. These findings demonstrate that wind turbine reliability can no longer be treated only as a drivetrain issue, but must be addressed as a coupled system-level challenge involving both mechanical and structural subsystems.

The review further shows that no single monitoring technique is sufficient to capture the full range of wind turbine damage mechanisms. Vibration-based methods remain highly effective for drivetrain diagnostics and global condition assessment, while acoustic emission, ultrasonic testing, infrared thermography, impedance-based sensing, electromagnetic methods, strain sensing, SCADA-based diagnostics, and vision-based inspection provide complementary capabilities for detecting localized, subsurface, or progressive damage in blades, towers, welded joints, and flange joints. In particular, impedance-based approaches show strong sensitivity to local stiffness changes and bolt looseness, whereas machine-vision and infrared methods offer practical advantages for the rapid, non-contact inspection of large surfaces. The mechanism-to-indicator mapping discussed in this review confirms that sensor selection should be guided by the physical degradation process, expected measurable features, accessibility, environmental sensitivity, and required detection stage. Therefore, future monitoring frameworks should increasingly rely on hybrid, multi-sensor strategies that combine global and local diagnostic information rather than depending on isolated sensing methods.

Recent advances in artificial intelligence and data-driven diagnostics have significantly improved fault recognition capability, with many controlled or semi-controlled studies reporting classification accuracies above 90%. However, practical deployment of these models remains constrained by limited labeled failure data, severe class imbalance, operational variability, environmental noise, domain shift among turbine types and sites, model interpretability, and insufficient field validation. Therefore, AI should not be treated as a standalone solution. It should be integrated with physics-based understanding, statistical reliability models, uncertainty quantification, and robust field measurements. In particular, performance assessment should move beyond accuracy alone and include precision, recall, F1-score, balanced accuracy, PR-AUC, confusion matrices, and uncertainty calibration, especially when fault samples are rare compared with healthy operating data.

Overall, the main value of this review lies in its integrated applied synthesis of failure mechanisms, monitoring indicators, diagnostic technologies, AI-enabled PHM limitations, and predictive-maintenance decision needs across both drivetrain and structural components. The conceptual multi-component SHM/PHM architecture developed in this review provides a pathway for linking heterogeneous data sources, including SCADA, CMS, vibration, acoustic emission, strain/FBG, oil-debris, temperature, ultrasonic, thermographic, vision, and impedance-based monitoring, with preprocessing, feature extraction, physics-based models, statistical reliability methods, machine-learning classifiers, anomaly detection, remaining useful life estimation, digital twin updating, and maintenance decision support. This integration is necessary to move wind turbine reliability assessment

from isolated component diagnostics toward system-level health-state tracking and maintenance prioritization.

Despite major progress, important research gaps remain. More field-validated datasets are needed for large-scale and offshore turbines, especially datasets that include confirmed failure labels, sensor placement, monitoring duration, environmental conditions, maintenance actions, and cost or downtime impacts. Future research should focus on physics-informed AI, transfer learning, domain adaptation, uncertainty-aware digital twins, standardized reliability-data reporting, robust sensor compensation under environmental variability, and interpretable decision-support systems. Therefore, future SHM and PHM development should move beyond isolated fault classification toward field-validated, uncertainty-aware, and maintenance-linked reliability frameworks capable of reducing operational risk and improving the long-term availability of wind energy systems.

Author Contributions: Conceptualization, S.A. and D.L.; methodology, S.A.; software, S.A.; validation, S.A. and M.W.; formal analysis, S.A.; investigation, S.A.; resources, S.A.; data curation, D.L.; writing—original draft preparation, S.A.; writing—review and editing, D.L.; visualization, M.W.; supervision, D.L.; project administration, D.L.; funding acquisition, D.L. All authors have read and agreed to the published version of the manuscript.

Funding: This work was supported by the Human Resources Development of the Korea Institute of Energy Technology Evaluation and Planning (KETEP) grant funded by the Korea government Ministry of Trade, Industry and Energy (RS-2021-KP002506). This research was supported by the Basic Science Research Program through the National Research Foundation of Korea (NRF) funded by the Ministry of Education (RS-2021-NR060134).

Institutional Review Board Statement: Not applicable.

Informed Consent Statement: Not applicable.

Data Availability Statement: The data presented in this study are available on request from the corresponding author.

Acknowledgments: The authors would like to express their gratitude to KMA for providing the wind and wave datasets.

Conflicts of Interest: The authors declare no conflicts of interest.

Abbreviations

The following abbreviations are used in this manuscript:

Abbreviation	Full term	Use in manuscript
WT	Wind turbine	General term for wind turbine systems
HAWT	Horizontal-axis wind turbine	Used only when specifically referring to horizontal-axis turbines
O&M	Operation and maintenance	Maintenance cost, downtime, and service planning
CM	Condition monitoring	General monitoring of operational and health-related signals
CMS	Condition monitoring system	Installed monitoring system, usually high-frequency vibration/CMS hardware
SHM	Structural health monitoring	Monitoring of structural components such as blades, towers, flange joints, foundations, and welded details
PHM	Prognostics and health management	Diagnosis, prognosis, RUL estimation, and maintenance decision support
FDD	Fault detection and diagnosis	Detection and classification of fault type or abnormal condition
RUL	Remaining useful life	Estimated remaining time or cycles before failure threshold
SCADA	Supervisory control and data acquisition	Low-frequency operational turbine data
AI	Artificial intelligence	Broad class of intelligent computational methods
ML	Machine learning	Data-driven algorithms such as SVM, RF, and ANN

DL	Deep learning	Neural-network-based models such as CNN, DBN, LSTM, and autoencoders
ANN	Artificial neural network	Neural-network model used for diagnosis or prognosis
CNN	Convolutional neural network	Deep-learning model often used for images or transformed signals
DBN	Deep belief network	Layered probabilistic deep-learning model
LSTM	Long short-term memory	Recurrent neural network for time-series modeling
SVM	Support vector machine	Supervised classifier based on margin maximization
AE	Acoustic emission	High-frequency elastic-wave sensing
UT	Ultrasonic testing	Non-destructive inspection using ultrasonic waves
IR	Infrared thermography	Thermal inspection method
EMI	Electromechanical impedance	Impedance-based local SHM method
FBG	Fiber Bragg grating	Optical-fiber strain/temperature sensor
RMS	Root mean square	Time-domain signal amplitude feature
FFT	Fast Fourier transform	Frequency-domain signal-processing method
VMD	Variational mode decomposition	Signal decomposition method
HHT	Hilbert–Huang transform	Time–frequency analysis method
PR-AUC	Precision–recall area under curve	Performance metric for imbalanced fault detection
ROC-AUC	Receiver operating characteristic area under curve	Threshold-independent classification metric
F1-score	Harmonic mean of precision and recall	Useful metric for imbalanced fault classification

References

1. Verbruggen, T. *Wind Turbine Operation & Maintenance Based on Condition Monitoring WT-Ω*; Final Report; Energy Research Centre of the Netherlands (ECN): Petten, The Netherlands, 2003.
2. Carroll, J.; McDonald, A.; McMillan, D. Failure rate, repair time and unscheduled O&M cost analysis of offshore wind turbines. *Wind Energy* **2016**, *19*, 1107–1119.
3. Blaabjerg, F.; Ma, K. Wind energy systems. *Proc. IEEE* **2017**, *105*, 2116–2131. [CrossRef]
4. Franko, J.; Du, S.; Kallweit, S.; Duelberg, E.; Engemann, H. Design of a multi-robot system for wind turbine maintenance. *Energies* **2020**, *13*, 2552. [CrossRef]
5. Erlich, I.; Shewarega, F.; Feltes, C.; Koch, F.W.; Fortmann, J. Offshore wind power generation technologies. *Proc. IEEE* **2013**, *101*, 891–905. [CrossRef]
6. Li, J.; Wang, G.; Li, Z.; Yang, S.; Chong, W.T.; Xiang, X. A review on development of offshore wind energy conversion system. *Int. J. Energy Res.* **2020**, *44*, 9283–9297. [CrossRef]
7. Pérez, J.M.P.; Márquez, F.P.G.; Tobias, A.; Papaelias, M. Wind turbine reliability analysis. *Renew. Sustain. Energy Rev.* **2013**, *23*, 463–472. [CrossRef]
8. Dao, C.; Kazemtabrizi, B.; Crabtree, C. Wind turbine reliability data review and impacts on levelised cost of energy. *Wind Energy* **2019**, *22*, 1848–1871. [CrossRef]
9. Hahn, B.; Durstewitz, M.; Rohrig, K. Reliability of wind turbines. In *Wind Energy: Proceedings of the Euromech Colloquium*; Springer: Berlin/Heidelberg, Germany, 2007; pp. 329–332.
10. International Renewable Energy Agency (IRENA). *Renewable Energy Technologies: Cost Analysis Series, Wind Power*; International Renewable Energy Agency (IRENA): Abu Dhabi, United Arab Emirates, 2012.
11. Dalgic, Y.; Lazakis, I.; Dinwoodie, I.; McMillan, D.; Revie, M. Advanced logistics planning for offshore wind farm operation and maintenance activities. *Ocean Eng.* **2015**, *101*, 211–226. [CrossRef]
12. Singh, S. Technical Aspects of Different Grid Connected Wind Energy Conversion System Configurations in Wind Farm. *Int. J. Eng. Adv. Technol. (IJEAT)* **2019**, *9*, 3949–3955. [CrossRef]
13. Faulstich, S.; Hahn, B.; Tavner, P.J. Wind turbine downtime and its importance for offshore deployment. *Wind Energy* **2011**, *14*, 327–337. [CrossRef]
14. Spinato, F.; Tavner, P.J.; van Bussel, G.J.W.; Koutoulakos, E. Reliability of Wind Turbine Subassemblies. *IET Renew. Power Gener.* **2008**, *3*, 387–401.
15. Sheng, S. *Gearbox Typical Failure Modes, Detection and Mitigation Methods*; National Renewable Energy Laboratory, National Wind Technology Center: Boulder, CO, USA, 2014.
16. Jin, X.; Cheng, F.; Peng, Y.; Qiao, W.; Qu, L. A comparative study on vibration-and current-based approaches for drivetrain gearbox fault diagnosis. In *2016 IEEE Industry Applications Society Annual Meeting*; IEEE: Piscataway, NJ, USA, 2016; pp. 1–8.

17. Sanchez, P.; Mendizabal, D.; Gonzalez, K.; Zamarreño, C.R.; Hernaez, M.; Matias, I.R.; Arregui, F.J. Wind turbines lubricant gearbox degradation detection by means of a lossy mode resonance based optical fiber refractometer. *Microsyst. Technol.* **2016**, *22*, 1619–1625.
18. Hossain, M.M.; Ali, M.H. Future research directions for the wind turbine generator system. *Renew. Sustain. Energy Rev.* **2015**, *49*, 481–489. [CrossRef]
19. Qiao, W.; Lu, D. A survey on wind turbine condition monitoring and fault diagnosis-Part I: Components and subsystems. *IEEE Trans. Ind. Electron.* **2015**, *62*, 6536–6545. [CrossRef]
20. Research and Markets. *Wind Turbine Gearbox and Direct-Drive Systems, 2014 Update—Global Market Size, Gearbox Refurbishments, Competitive Landscape and Key Country Analysis to 2020*; Technical Report 2974385; Research and Markets: Dublin, Ireland, 2014.
21. Igba, J.; Alemzadeh, K.; Durugbo, C.; Henningsen, K. Performance assessment of wind turbine gearboxes using in-service data: Current approaches and future trends. *Renew. Sustain. Energy Rev.* **2015**, *50*, 144–159. [CrossRef]
22. Yoon, J.; He, D.; Van Hecke, B. On the use of a single piezoelectric strain sensor for wind turbine planetary gearbox fault diagnosis. *IEEE Trans. Ind. Electron.* **2015**, *62*, 6585–6593. [CrossRef]
23. Blesa, J.; Jiménez, P.; Rotondo, D.; Nejjari, F.; Puig, V. An interval NLPV parity equations approach for fault detection and isolation of a wind farm. *IEEE Trans. Ind. Electron.* **2014**, *62*, 3794–3805. [CrossRef]
24. Sheng, S. *Report on Wind Turbine Subsystem Reliability—A Survey of Various Databases (Presentation)*; No. NREL/PR-5000-59111; National Renewable Energy Laboratory (NREL): Golden, CO, USA, 2013.
25. de Azevedo, H.D.M.; Araújo, A.M.; Bouchonneau, N. A review of wind turbine bearing condition monitoring: State of the art and challenges. *Renew. Sustain. Energy Rev.* **2016**, *56*, 368–379. [CrossRef]
26. Fierro, T. Extending Bearing Life in Wind Turbine Mainshafts. Power Engineering, 23 August 2016. Available online: https://www.power-eng.com/coal/extending-bearing-life-in-wind-turbine-mainshafts/#gref (accessed on 28 December 2025).
27. Page, M.J.; McKenzie, J.E.; Bossuyt, P.M.; Boutron, I.; Hoffmann, T.C.; Mulrow, C.D.; Shamseer, L.; Tetzlaff, J.M.; Akl, E.A.; Brennan, S.E.; et al. The PRISMA 2020 statement: An updated guideline for reporting systematic reviews. *BMJ* **2021**, *372*, 71. [CrossRef] [PubMed]
28. Fernandes, C.M.; Blazquez, L.; Sanesteban, J.; Martins, R.C.; Seabra, J.H. Energy efficiency tests in a full scale wind turbine gearbox. *Tribol. Int.* **2016**, *101*, 375–382. [CrossRef]
29. He, G.; Ding, K.; Li, W.; Jiao, X. A novel order tracking method for wind turbine planetary gearbox vibration analysis based on discrete spectrum correction technique. *Renew. Energy* **2016**, *87*, 364–375. [CrossRef]
30. Feng, Y.; Qiu, Y.; Crabtree, C.J.; Long, H.; Tavner, P.J. Monitoring wind turbine gearboxes. *Wind Energy* **2013**, *16*, 728–740.
31. Cibulka, J.; Ebbesen, M.K.; Hovland, G.; Robbersmyr, K.G.; Hansen, M.R. A review on approaches for condition based maintenance in applications with induction machines located offshore. *Model. Identif. Control* **2012**, *33*, 69–86. [CrossRef]
32. Gu, H.; Liu, W.Y.; Gao, Q.W.; Zhang, Y. A review on wind turbines gearbox fault diagnosis methods. *J. Vibroeng.* **2021**, *23*, 26–43. [CrossRef]
33. Özgüven, H.N.; Houser, D.R. Mathematical models used in gear dynamics-a review. *J. Sound Vib.* **1988**, *121*, 383–411. [CrossRef]
34. Parey, A.; Tandon, N. Spur gear dynamic models including defects: A review. *Shock. Vib. Dig.* **2003**, *35*, 465–478. [CrossRef]
35. Wang, J.; Li, R.; Peng, X. Survey of nonlinear vibration of gear transmission systems. *Appl. Mech. Rev.* **2003**, *56*, 309–329. [CrossRef]
36. Cooley, C.G.; Parker, R.G. A review of planetary and epicyclic gear dynamics and vibrations research. *Appl. Mech. Rev.* **2014**, *66*, 040804. [CrossRef]
37. Li, F.; Qin, Y.; Ge, L.; Pang, Z.; Liu, S.; Lin, D. Influences of planetary gear parameters on the dynamic characteristics-a review. *J. Vibroeng.* **2015**, *17*, 574–586.
38. Ma, H.; Zeng, J.; Feng, R.; Pang, X.; Wang, Q.; Wen, B. Review on dynamics of cracked gear systems. *Eng. Fail. Anal.* **2015**, *55*, 224–245. [CrossRef]
39. Liang, X.; Zuo, M.J.; Feng, Z. Dynamic modeling of gearbox faults: A review. *Mech. Syst. Signal Process.* **2018**, *98*, 852–876. [CrossRef]
40. Lei, Y.; Lin, J.; Zuo, M.J.; He, Z. Condition monitoring and fault diagnosis of planetary gearboxes: A review. *Measurement* **2014**, *48*, 292–305. [CrossRef]
41. Peng, Z.K.; Chu, F.L. Application of the wavelet transform in machine condition monitoring and fault diagnostics: A review with bibliography. *Mech. Syst. Signal Process.* **2004**, *18*, 199–221. [CrossRef]
42. Wang, D.; Tsui, K.L.; Miao, Q. Prognostics and health management: A review of vibration based bearing and gear health indicators. *IEEE Access* **2017**, *6*, 665–676. [CrossRef]
43. Feng, K.; Wang, K.; Zhang, M.; Ni, Q.; Zuo, M.J. A diagnostic signal selection scheme for planetary gearbox vibration monitoring under non-stationary operational conditions. *Meas. Sci. Technol.* **2017**, *28*, 035003. [CrossRef]
44. Sharma, V.; Parey, A. Case study on the effectiveness of gear fault diagnosis technique for gear tooth defects under fluctuating speed. *IET Renew. Power Gener.* **2017**, *11*, 1841–1849. [CrossRef]
45. Qiao, W.; Lu, D. A survey on wind turbine condition monitoring and fault diagnosis-Part II: Signals and signal processing methods. *IEEE Trans. Ind. Electron.* **2015**, *62*, 6546–6557. [CrossRef]

46. Wymore, M.L.; Van Dam, J.E.; Ceylan, H.; Qiao, D. A survey of health monitoring systems for wind turbines. *Renew. Sustain. Energy Rev.* **2015**, *52*, 976–990. [CrossRef]
47. Ren, H.; Liu, W.; Shan, M.; Wang, X. A new wind turbine health condition monitoring method based on VMD-MPE and feature-based transfer learning. *Measurement* **2019**, *148*, 106906. [CrossRef]
48. Elasha, F.; Shanbr, S.; Li, X.; Mba, D. Prognosis of a wind turbine gearbox bearing using supervised machine learning. *Sensors* **2019**, *19*, 3092. [CrossRef] [PubMed]
49. Liu, X.; Du, J.; Ye, Z.S. A condition monitoring and fault isolation system for wind turbine based on SCADA data. *IEEE Trans. Ind. Inform.* **2021**, *18*, 986–995. [CrossRef]
50. Han, H.; Yang, D.; Ni, X. Application of Sparse Representation in SCADA: Wind Turbine Fault Diagnosis Based on K-SVD. In *2021 CAA Symposium on Fault Detection, Supervision, and Safety for Technical Processes (SAFEPROCESS)*; IEEE: Piscataway, NJ, USA, 2021; pp. 1–6.
51. Jiang, Z.; Cao, Y.; Hong, H.; Yang, Q. Fault detection and diagnosis of wind turbine gearbox based on acoustic analysis. In *2021 International Conference on Power System Technology (POWERCON)*; IEEE: Piscataway, NJ, USA, 2021; pp. 2047–2052.
52. Yoshioka, T.; Fujiwara, T. Application of acoustic emission technique to detection of rolling bearing failure. *Am. Soc. Mech. Eng.* **1984**, *14*, 55–76.
53. Tandon, N.; Yadava, G.S.; Ramakrishna, A.K. A comparison of some condition monitoring techniques for the detection of defect in induction motor ball bearings. *Mech. Syst. Signal Process.* **2007**, *21*, 244–256. [CrossRef]
54. Elasha, F.; Greaves, M.; Mba, D.; Fang, D. A comparative study of the effectiveness of vibration and acoustic emission in diagnosing a defective bearing in a planetry gearbox. *Appl. Acoust.* **2017**, *115*, 181–195. [CrossRef]
55. König, F.; Marheineke, J.; Jacobs, G.; Sous, C.; Zuo, M.J.; Tian, Z. Data-driven wear monitoring for sliding bearings using acoustic emission signals and long short-term memory neural networks. *Wear* **2021**, *476*, 203616. [CrossRef]
56. Tan, C.K.; Irving, P.; Mba, D. A comparative experimental study on the diagnostic and prognostic capabilities of acoustics emission, vibration and spectrometric oil analysis for spur gears. *Mech. Syst. Signal Process.* **2007**, *21*, 208–233. [CrossRef]
57. Márquez, F.P.G.; Tobias, A.M.; Pérez, J.M.P.; Papaelias, M. Condition monitoring of wind turbines: Techniques and methods. *Renew. Energy* **2012**, *46*, 169–178. [CrossRef]
58. Jayaswal, P.; Wadhwani, A.K.; Mulchandani, K.B. Machine fault signature analysis. *Int. J. Rotating Mach.* **2008**, *2008*, 583982. [CrossRef]
59. Lu, L.; He, Y.; Ruan, Y.; Yuan, W. Wind turbine planetary gearbox condition monitoring method based on wireless sensor and deep learning approach. *IEEE Trans. Instrum. Meas.* **2020**, *70*, 3503016.
60. Sarma, N.; Tuohy, P.M.; Djurović, S. Stator Electrical Fault Detection in DFIGs Using Wide-Band Analysis of the Embedded Signals from the Controllers. *IEEE Trans. Energy Convers.* **2020**, *36*, 800–811. [CrossRef]
61. Gong, X. Online Nonintrusive Condition Monitoring and Fault Detection for Wind Turbines. Ph.D. Thesis, The University of Nebraska-Lincoln, Lincoln, NE, USA, 2012.
62. Rezamand, M.; Kordestani, M.; Carriveau, R.; Ting, D.S.K.; Orchard, M.E.; Saif, M. Critical wind turbine components prognostics: A comprehensive review. *IEEE Trans. Instrum. Meas.* **2020**, *69*, 9306–9328. [CrossRef]
63. Yang, T.; Teng, J.; Li, C.; Feng, Y. Wind turbine fault detection and diagnosis using LSTM neural network. In *2020 39th Chinese Control Conference (CCC)*; IEEE: Piscataway, NJ, USA, 2020; pp. 4042–4047.
64. Lin, Z.; Duan, D.; Yang, Q.; Hong, X.; Cheng, X.; Yang, L.; Cui, S. One-class classifier based fault detection in distribution systems with varying penetration levels of distributed energy resources. *IEEE Access* **2020**, *8*, 130023–130035. [CrossRef]
65. Bangalore, P.; Letzgus, S.; Karlsson, D.; Patriksson, M. An artificial neural network-based condition monitoring method for wind turbines, with application to the monitoring of the gearbox. *Wind Energy* **2017**, *20*, 1421–1438. [CrossRef]
66. Alkhadafe, H.; Al-Habaibeh, A.; Lotfi, A. Condition monitoring of helical gears using automated selection of features and sensors. *Measurement* **2016**, *93*, 164–177. [CrossRef]
67. Xu, X.; Huang, X.; Bian, H.; Wu, J.; Liang, C.; Cong, F. Total process of fault diagnosis for wind turbine gearbox, from the perspective of combination with feature extraction and machine learning: A review. *Energy AI* **2023**, *15*, 100318. [CrossRef]
68. An, X.; Jiang, D.; Chen, J.; Liu, C. Application of the intrinsic time-scale decomposition method to fault diagnosis of wind turbine bearing. *J. Vib. Control.* **2012**, *18*, 240–245.
69. Xin, W.; Liu, Y.; He, Y.; Su, B. Amplitude envelope analysis for feature extraction of direct-driven wind turbine bearing failure. In *Proceedings of the 10th World Congress on Intelligent Control and Automation*; IEEE: Piscataway, NJ, USA, 2012; pp. 3173–3176.
70. Pan, Z.; Liang, S.; Liu, Y.; Liang, P. Spectral correlation feature analysis for rolling bearing fault of wind turbine generator. In *International Conference on Renewable Power Generation (RPG 2015)*; IET: London, UK, 2015; pp. 1–5.
71. Zhang, L.; Lang, Z.Q.; Papaelias, M. Generalized transmissibility damage indicator with application to wind turbine component condition monitoring. *IEEE Trans. Ind. Electron.* **2016**, *63*, 6347–6359. [CrossRef]
72. Bodla, M.K.; Malik, S.M.; Rasheed, M.T.; Numan, M.; Ali, M.Z.; Brima, J.B. Logistic regression and feature extraction based fault diagnosis of main bearing of wind turbines. In *2016 IEEE 11th Conference on Industrial Electronics and Applications (ICIEA)*; IEEE: Piscataway, NJ, USA, 2016; pp. 1628–1633.

73. Chen, C.; Sun, X.; Gu, Q.; Zhou, B.; Gu, Y. Wavelet-based multifractal analysis of large scale wind turbine main bearing. *J. Renew. Sustain. Energy* **2013**, *5*, 013102. [CrossRef]
74. Purarjomandlangrudi, A.; Nourbakhsh, G.; Ghaemmaghami, H.; Tan, A. Application of anomaly technique in wind turbine bearing fault detection. In *IECON 2014-40th Annual Conference of the IEEE Industrial Electronics Society*; IEEE: Piscataway, NJ, USA, 2014; pp. 1984–1988.
75. Zhang, L.; Lang, Z.Q. Wavelet energy transmissibility function and its application to wind turbine bearing condition monitoring. *IEEE Trans. Sustain. Energy* **2018**, *9*, 1833–1843. [CrossRef]
76. Han, T.; Liu, Q.; Zhang, L.; Tan, A.C. Fault feature extraction of low speed roller bearing based on Teager energy operator and CEEMD. *Measurement* **2019**, *138*, 400–408. [CrossRef]
77. Gong, X.; Qiao, W.; Zhou, W. Incipient bearing fault detection via wind generator stator current and wavelet filter. In *IECON 2010-36th Annual Conference on IEEE Industrial Electronics Society*; IEEE: Piscataway, NJ, USA, 2010; pp. 2615–2620.
78. Gong, X.; Qiao, W. Bearing fault detection for direct-drive wind turbines via stator current spectrum analysis. In *2011 IEEE Energy Conversion Congress and Exposition*; IEEE: Piscataway, NJ, USA, 2011; pp. 313–318.
79. Gong, X.; Qiao, W. Current-based online bearing fault diagnosis for direct-drive wind turbines via spectrum analysis and impulse detection. In *2012 IEEE Power Electronics and Machines in Wind Applications*; IEEE: Piscataway, NJ, USA, 2012; pp. 1–6.
80. Gong, X.; Qiao, W. Bearing fault diagnosis for direct-drive wind turbines via current-demodulated signals. *IEEE Trans. Ind. Electron.* **2013**, *60*, 3419–3428. [CrossRef]
81. Wang, J.; Peng, Y.; Qiao, W.; Hudgins, J.L. Bearing fault diagnosis of direct-drive wind turbines using multiscale filtering spectrum. *IEEE Trans. Ind. Appl.* **2017**, *53*, 3029–3038. [CrossRef]
82. Wang, J.; Peng, Y.; Qiao, W. Current-aided order tracking of vibration signals for bearing fault diagnosis of direct-drive wind turbines. *IEEE Trans. Ind. Electron.* **2016**, *63*, 6336–6346. [CrossRef]
83. Badihi, H.; Zhang, Y.; Jiang, B.; Pillay, P.; Rakheja, S. A comprehensive review on signal-based and model-based condition monitoring of wind turbines: Fault diagnosis and lifetime prognosis. *Proc. IEEE* **2022**, *110*, 754–806. [CrossRef]
84. Isermann, R. *Fault-Diagnosis Systems: An Introduction from Fault Detection to Fault Tolerance*; Springer Science & Business Media: Berlin/Heidelberg, Germany, 2006.
85. Badihi, H.; Zhang, Y.; Pillay, P.; Rakheja, S. Fault-tolerant individual pitch control for load mitigation in wind turbines with actuator faults. *IEEE Trans. Ind. Electron.* **2020**, *68*, 532–543. [CrossRef]
86. Odgaard, P.F.; Stoustrup, J. Results of a wind turbine FDI competition. *IFAC Proc. Vol.* **2012**, *45*, 102–107. [CrossRef]
87. Chen, J.; Patton, R.J. *Robust Model-Based Fault Diagnosis for Dynamic Systems*; Springer Science & Business Media: Berlin/Heidelberg, Germany, 2012; Volume 3.
88. Chui, C.K.; Chen, G. Kalman filtering with real time applications. *Appl. Opt.* **1989**, *28*, 1841.
89. Jiang, L.L.; Yin, H.K.; Li, X.J.; Tang, S.W. Fault diagnosis of rotating machinery based on multisensor information fusion using SVM and time-domain features. *Shock. Vib.* **2014**, *2014*, 418178. [CrossRef]
90. Cheng, F.; Wang, J.; Qu, L.; Qiao, W. Rotor-current-based fault diagnosis for DFIG wind turbine drivetrain gearboxes using frequency analysis and a deep classifier. *IEEE Trans. Ind. Appl.* **2017**, *54*, 1062–1071.
91. Li, Y.; Li, G.; Yang, Y.; Liang, X.; Xu, M. A fault diagnosis scheme for planetary gearboxes using adaptive multi-scale morphology filter and modified hierarchical permutation entropy. *Mech. Syst. Signal Process.* **2018**, *105*, 319–337. [CrossRef]
92. Liu, S.; Liu, Y.; Wang, B.; Feng, X. An improved hyper-sphere support vector machine. In *Third International Conference on Natural Computation (ICNC 2007)*; IEEE: Piscataway, NJ, USA, 2007; Volume 1, pp. 497–500.
93. Li, Y.; Yang, Y.; Li, G.; Xu, M.; Huang, W. A fault diagnosis scheme for planetary gearboxes using modified multi-scale symbolic dynamic entropy and mRMR feature selection. *Mech. Syst. Signal Process.* **2017**, *91*, 295–312. [CrossRef]
94. Xiao, Y.; Wang, Y.; Mu, H.; Kang, N. Research on misalignment fault isolation of wind turbines based on the mixed-domain features. *Algorithms* **2017**, *10*, 67. [CrossRef]
95. Tyagi, S.; Panigrahi, S.K. An SVM-ANN hybrid classifier for diagnosis of gear fault. *Appl. Artif. Intell.* **2017**, *31*, 209–231. [CrossRef]
96. Xing, Z.; Qu, J.; Chai, Y.; Tang, Q.; Zhou, Y. Gear fault diagnosis under variable conditions with intrinsic time-scale decomposition-singular value decomposition and support vector machine. *J. Mech. Sci. Technol.* **2017**, *31*, 545–553. [CrossRef]
97. Bafroui, H.H.; Ohadi, A. Application of wavelet energy and Shannon entropy for feature extraction in gearbox fault detection under varying speed conditions. *Neurocomputing* **2014**, *133*, 437–445. [CrossRef]
98. Li, H.; Zhang, Y.; Zheng, H. Gear fault detection and diagnosis under speed-up condition based on order cepstrum and radial basis function neural network. *J. Mech. Sci. Technol.* **2009**, *23*, 2780–2789. [CrossRef]
99. Chen, J.; Li, Y.; Ye, F. Uncertain information fusion for gearbox fault diagnosis based on BP neural network and DS evidence theory. In *2016 12th World Congress on Intelligent Control and Automation (WCICA)*; IEEE: Piscataway, NJ, USA, 2016; pp. 1372–1376.
100. Jing, L.; Wang, T.; Zhao, M.; Wang, P. An adaptive multi-sensor data fusion method based on deep convolutional neural networks for fault diagnosis of planetary gearbox. *Sensors* **2017**, *17*, 414. [CrossRef] [PubMed]

101. Liao, Y.; Zeng, X.; Li, W. Wavelet transform based convolutional neural network for gearbox fault classification. In *2017 Prognostics and System Health Management Conference (PHM-Harbin)*; IEEE: Piscataway, NJ, USA, 2017; pp. 1–6.
102. Yu, J.; Bai, M.; Wang, G.; Shi, X. Fault diagnosis of planetary gearbox with incomplete information using assignment reduction and flexible naive Bayesian classifier. *J. Mech. Sci. Technol.* **2018**, *32*, 37–47. [CrossRef]
103. Cerrada, M.; Li, C.; Sánchez, R.V.; Pacheco, F.; Cabrera, D.; de Oliveira, J.V. A fuzzy transition based approach for fault severity prediction in helical gearboxes. *Fuzzy Sets Syst.* **2018**, *337*, 52–73. [CrossRef]
104. Bartelmus, W.; Chaari, F.; Zimroz, R.; Haddar, M. Modelling of gearbox dynamics under time-varying nonstationary load for distributed fault detection and diagnosis. *Eur. J. Mech.-A/Solids* **2010**, *29*, 637–646. [CrossRef]
105. Chaari, F.; Abbes, M.S.; Rueda, F.V.; del Rincon, A.F.; Haddar, M. Analysis of planetary gear transmission in non-stationary operations. *Front. Mech. Eng.* **2013**, *8*, 88–94. [CrossRef]
106. Bouchaala, N.; Chaari, F.; Khabou, M.T.; Fakhfakh, T.; Haddar, M. Influence of the non-linear Hertzian stiffness on the dynamics of a spur gear system under transient regime and tooth defects. *Int. J. Veh. Noise Vib.* **2011**, *7*, 149–177. [CrossRef]
107. Viadero, F.; Fernández, A.; Iglesias, M.; De-Juan, A.; Liaño, E.; Serna, M.A. Non-stationary dynamic analysis of a wind turbine power drivetrain: Offshore considerations. *Appl. Acoust.* **2014**, *77*, 204–211. [CrossRef]
108. Hammami, A.; Fernández, A.; Chaari, F.; Viadero, F.; Haddar, M. Dynamic behaviour of two stages planetary gearbox in non-stationary operations. In Proceedings of the Surveillance 7 International Conference, Chartres, France, 29–30 October 2013; Volume 7.
109. Drago, R.J. The effect of start-up load conditions on gearbox performance and life failure analysis, with supporting case study. In Proceedings of the American Gear Manufacturers Association Fall Technical Meeting, Indianapolis, IN, USA, 13–15 September 2009.
110. Hammami, A.; Del Rincon, A.F.; Chaari, F.; Santamaria, M.I.; Rueda, F.V.; Haddar, M. Effects of variable loading conditions on the dynamic behaviour of planetary gear with power recirculation. *Measurement* **2016**, *94*, 306–315. [CrossRef]
111. Hammami, A.; Del Rincon, A.F.; Chaari, F.; Rueda, F.V.; Haddar, M. Dynamic behaviour of back to back planetary gear in run up and run down transient regimes. *J. Mech.* **2015**, *31*, 481–491. [CrossRef]
112. Srikanth, P.; Sekhar, A.S. Dynamic analysis of wind turbine drive train subjected to nonstationary wind load excitation. *Proc. Inst. Mech. Eng. Part C J. Mech. Eng. Sci.* **2015**, *229*, 429–446.
113. Srikanth, P.; Sekhar, A.S. Wind turbine drive train dynamic characterization using vibration and torque signals. *Mech. Mach. Theory* **2016**, *98*, 2–20. [CrossRef]
114. Mabrouk, I.B.; El Hami, A.; Walha, L.; Zghal, B.; Haddar, M. Dynamic vibrations in wind energy systems: Application to vertical axis wind turbine. *Mech. Syst. Signal Process.* **2017**, *85*, 396–414. [CrossRef]
115. Liu, F.; Zhang, L.; Jiang, H.; Yu, X. Simulation of vibro-impact gear model considering the lubricant influence with a new computational algorithm. *J. Braz. Soc. Mech. Sci. Eng.* **2018**, *40*, 147. [CrossRef]
116. Fang, Y.; Liang, X.; Zuo, M.J. Effect of sliding friction on transient characteristics of a gear transmission under random loading. In *2017 IEEE International Conference on Systems, Man, and Cybernetics (SMC)*; IEEE: Piscataway, NJ, USA, 2017; pp. 2551–2555.
117. Chen, H.; Wang, X.; Gao, H.; Yan, F. Dynamic characteristics of wind turbine gear transmission system with random wind and the effect of random backlash on system stability. *Proc. Inst. Mech. Eng. Part C J. Mech. Eng. Sci.* **2017**, *231*, 2590–2597.
118. Xiao, Z.M.; Huan, L.R. Dynamic analysis of planetary gears with gear crack of semi-direct drive wind turbine. In *2017 International Conference on Applied System Innovation (ICASI)*; IEEE: Piscataway, NJ, USA, 2017; pp. 221–223.
119. Liu, C.; Qin, D.; Liao, Y. Dynamic modeling and analysis of high-speed planetary gear including centrifugal force. *J. Braz. Soc. Mech. Sci. Eng.* **2017**, *39*, 3769–3778. [CrossRef]
120. Wei, J.; Bai, P.; Qin, D.; Lim, T.C.; Yang, P.; Zhang, H. Study on vibration characteristics of fan shaft of geared turbofan engine with sudden imbalance caused by blade off. *J. Vib. Acoust.* **2018**, *140*, 041010. [CrossRef]
121. Brethee, K.F.; Zhen, D.; Gu, F.; Ball, A.D. Helical gear wear monitoring: Modelling and experimental validation. *Mech. Mach. Theory* **2017**, *117*, 210–229. [CrossRef]
122. Lei, Y.; Liu, Z.; Lin, J.; Lu, F. Phenomenological models of vibration signals for condition monitoring and fault diagnosis of epicyclic gearboxes. *J. Sound Vib.* **2016**, *369*, 266–281. [CrossRef]
123. Liu, L.; Liang, X.; Zuo, M.J. Vibration signal modeling of a planetary gear set with transmission path effect analysis. *Measurement* **2016**, *85*, 20–31. [CrossRef]
124. Huang, W.; Sun, H.; Dou, H.; Wang, W. Study of transfer path of wind turbine gearbox fault vibration signal based on power flow finite element method. *Adv. Mech. Eng.* **2017**, *9*, 1687814017703899. [CrossRef]
125. Vanhollebeke, F.; Peeters, J.; Vandepitte, D.; Desmet, W. Using transfer path analysis to assess the influence of bearings on structural vibrations of a wind turbine gearbox. *Wind Energy* **2015**, *18*, 797–810.
126. Bakri, A.E.; Sefriti, S.; Boumhidi, I. A fault detection method for wind turbines based on deep belief network. In *2020 Fourth International Conference on Intelligent Computing in Data Sciences (ICDS)*; IEEE: Piscataway, NJ, USA, 2020; pp. 1–6.
127. Zhang, Y.; Ji, J.C.; Ren, Z.; Ni, Q.; Gu, F.; Feng, K.; Yu, K.; Ge, J.; Lei, Z.; Liu, Z. Digital twin-driven partial domain adaptation network for intelligent fault diagnosis of rolling bearing. *Reliab. Eng. Syst. Saf.* **2023**, *234*, 109186. [CrossRef]

128. Xiong, J.; Ye, H.; Pei, W.; Kong, L.; Huo, Q.; Han, Y. A monitoring and diagnostics method based on FPGA-digital twin for power electronic transformer. *Electr. Power Syst. Res.* **2022**, *210*, 108111. [CrossRef]
129. Guo, K.; Wan, X.; Liu, L.; Gao, Z.; Yang, M. Fault diagnosis of intelligent production line based on digital twin and improved random forest. *Appl. Sci.* **2021**, *11*, 7733. [CrossRef]
130. Shangguan, D.; Chen, L.; Ding, J. A digital twin-based approach for the fault diagnosis and health monitoring of a complex satellite system. *Symmetry* **2020**, *12*, 1307. [CrossRef]
131. Wang, Y.; Sun, W.; Liu, L.; Wang, B.; Bao, S.; Jiang, R. Fault Diagnosis of Wind Turbine Planetary Gear Based on a Digital Twin. *Appl. Sci.* **2023**, *13*, 4776. [CrossRef]
132. Zimroz, R.; Bartelmus, W.; Barszcz, T.; Urbanek, J. Diagnostics of bearings in presence of strong operating conditions non-stationarity-A procedure of load-dependent features processing with application to wind turbine bearings. *Mech. Syst. Signal Process.* **2014**, *46*, 16–27. [CrossRef]
133. Yang, D.; Li, H.; Hu, Y.; Zhao, J.; Xiao, H.; Lan, Y. Vibration condition monitoring system for wind turbine bearings based on noise suppression with multi-point data fusion. *Renew. Energy* **2016**, *92*, 104–116. [CrossRef]
134. Guo, L.; Li, N.; Jia, F.; Lei, Y.; Lin, J. A recurrent neural network based health indicator for remaining useful life prediction of bearings. *Neurocomputing* **2017**, *240*, 98–109. [CrossRef]
135. Teng, W.; Zhang, X.; Liu, Y.; Kusiak, A.; Ma, Z. Prognosis of the remaining useful life of bearings in a wind turbine gearbox. *Energies* **2016**, *10*, 32. [CrossRef]
136. Saidi, L.; Ali, J.B.; Bechhoefer, E.; Benbouzid, M. Wind turbine high-speed shaft bearings health prognosis through a spectral Kurtosis-derived indices and SVR. *Appl. Acoust.* **2017**, *120*, 1–8. [CrossRef]
137. Ali, J.B.; Saidi, L.; Harrath, S.; Bechhoefer, E.; Benbouzid, M. Online automatic diagnosis of wind turbine bearings progressive degradations under real experimental conditions based on unsupervised machine learning. *Appl. Acoust.* **2018**, *132*, 167–181. [CrossRef]
138. Pan, Y.; Hong, R.; Chen, J.; Wu, W. A hybrid DBN-SOM-PF-based prognostic approach of remaining useful life for wind turbine gearbox. *Renew. Energy* **2020**, *152*, 138–154. [CrossRef]
139. Schroeder, K.; Ecke, W.; Apitz, J.; Lembke, E.; Lenschow, G. A fibre Bragg grating sensor system monitors operational load in a wind turbine rotor blade. *Meas. Sci. Technol.* **2006**, *17*, 1167. [CrossRef]
140. Wang, Y.; Mohammed, A.; Sarma, N.; Djurović, S. Double fed induction generator shaft misalignment monitoring by FBG frame strain sensing. *IEEE Sens. J.* **2020**, *20*, 8541–8551. [CrossRef]
141. Tian, S.; Yang, Z.; Chen, X.; Xie, Y. Damage detection based on static strain responses using FBG in a wind turbine blade. *Sensors* **2015**, *15*, 19992–20005. [CrossRef] [PubMed]
142. Sierra-Pérez, J.; Torres-Arredondo, M.A.; Güemes, A. Damage and nonlinearities detection in wind turbine blades based on strain field pattern recognition. FBGs, OBR and strain gauges comparison. *Compos. Struct.* **2016**, *135*, 156–166. [CrossRef]
143. Downey, A.; Laflamme, S.; Ubertini, F. Experimental wind tunnel study of a smart sensing skin for condition evaluation of a wind turbine blade. *Smart Mater. Struct.* **2017**, *26*, 125005. [CrossRef]
144. Lee, K.; Aihara, A.; Puntsagdash, G.; Kawaguchi, T.; Sakamoto, H.; Okuma, M. Feasibility study on a strain based deflection monitoring system for wind turbine blades. *Mech. Syst. Signal Process.* **2017**, *82*, 117–129. [CrossRef]
145. Wen, B.; Tian, X.; Jiang, Z.; Li, Z.; Dong, X.; Peng, Z. Monitoring blade loads for a floating wind turbine in wave basin model tests using Fiber Bragg Grating sensors: A feasibility study. *Mar. Struct.* **2020**, *71*, 102729. [CrossRef]
146. Soman, R.N.; Malinowski, P.H.; Ostachowicz, W.M. Bi-axial neutral axis tracking for damage detection in wind-turbine towers. *Wind Energy* **2016**, *19*, 639–650.
147. Mieloszyk, M.; Ostachowicz, W. An application of Structural Health Monitoring system based on FBG sensors to offshore wind turbine support structure model. *Mar. Struct.* **2017**, *51*, 65–86. [CrossRef]
148. Mauricio, A.; Qi, J.; Gryllias, K. Vibration-based condition monitoring of wind turbine gearboxes based on cyclostationary analysis. *J. Eng. Gas Turbines Power* **2019**, *141*, 031026.
149. Inturi, V.; Sabareesh, G.R.; Supradeepan, K.; Penumakala, P.K. Integrated condition monitoring scheme for bearing fault diagnosis of a wind turbine gearbox. *J. Vib. Control* **2019**, *25*, 1852–1865. [CrossRef]
150. Peeters, C.; Antoni, J.; Helsen, J. Blind filters based on envelope spectrum sparsity indicators for bearing and gear vibration-based condition monitoring. *Mech. Syst. Signal Process.* **2020**, *138*, 106556. [CrossRef]
151. Márquez-Domínguez, S.; Sørensen, J.D. Fatigue reliability and calibration of fatigue design factors for offshore wind turbines. *Energies* **2012**, *5*, 1816–1834. [CrossRef]
152. Sørensen, J.D. Reliability assessment of wind turbines. In Proceedings of the 12th International Conference on Applications of Statistics and Probability in Civil Engineering ICASP12, Vancouver, BC, Canada, 12–15 July 2015; pp. 12–15.
153. Van der Woude, C.; Narasimhan, S. A study on vibration isolation for wind turbine structures. *Eng. Struct.* **2014**, *60*, 223–234. [CrossRef]
154. Fleming, K.; Weltman, A.; Randolph, M.; Elson, K. *Piling Engineering*; CRC Press: Boca Raton, FL, USA, 2009.
155. Andersen, K.H.; Puech, A.A.; Jardine, R.J. Design for cycling loading: Piles and other foundations. In Proceedings of the 18th International Conference on Soil Mechanics and Geotechnical Engineering (ICSMGE), Paris, France, 2–6 September 2013.

156. Brennan, F.; Kolios, A. Structural integrity considerations for the H2Ocean multi modal wind-wave platform. In *European Wind Energy Association Conference and Exhibition 2014, EWEA 2014*; European Wind Energy Association: Brussels, Belgium, 2014.
157. Shreve, E. One Faulty Blade Caused Turbine on Wind Farm to Collapse, TerraForm Power Says. Postmedia Network, 4 April 2018. Available online: https://nationalpost.com/news/canada/one-faulty-blade-caused-turbine-on-wind-farm-to-collapse-terraform-power-says (accessed on 14 August 2025).
158. Hessler, U. German Wind Energy Buildup Collapsing. DW, 9 April 2019. Available online: https://www.dw.com/en/german-wind-energy-stalls-amid-public-resistance-and-regulatory-hurdles/a-50280676 (accessed on 14 August 2025).
159. Lim, S.; Park, C.W.; Hwang, J.H.; Kim, D.Y.; Kim, T.K. The inchworm type blade inspection robot system. In *2012 9th International Conference on Ubiquitous Robots and Ambient Intelligence (URAI)*; IEEE: Piscataway, NJ, USA, 2012; pp. 604–607.
160. Girshick, R. Fast R-CNN. In Proceedings of the IEEE International Conference on Computer Vision, Santiago, Chile, 7–13 December 2015; pp. 1440–1448.
161. Mao, Y.; Wang, S.; Yu, D.; Zhao, J. Automatic image detection of multi-type surface defects on wind turbine blades based on cascade deep learning network. *Intell. Data Anal.* **2021**, *25*, 463–482. [CrossRef]
162. Simonyan, K.; Zisserman, A. Very deep convolutional networks for large-scale image recognition. *arXiv* **2014**, arXiv:1409.1556.
163. He, K.; Zhang, X.; Ren, S.; Sun, J. Identity mappings in deep residual networks. In *European Conference on Computer Vision*; Springer International Publishing: Cham, Switzerland, 2016; pp. 630–645.
164. Szegedy, C.; Ioffe, S.; Vanhoucke, V.; Alemi, A. Inception-v4, inception-resnet and the impact of residual connections on learning. In Proceedings of the AAAI Conference on Artificial Intelligence, San Francisco, CA, USA, 4–9 February 2017; Volume 31.
165. Jocher, G.; Stoken, A.; Chaurasia, A.; Borovec, J.; Kwon, Y.; Michael, K.; Changyu, L.; Fang, J.; Skalski, P.; Hogan, A.; et al. *Ultralytics/Yolov5: V6. 0-YOLOv5n'Nano'Models, Roboflow Integration, TensorFlow Export, OpenCV DNN Support*; Zenodo: Geneva, Switzerland, 2021.
166. Tan, M.; Le, Q. Efficientnet: Rethinking model scaling for convolutional neural networks. In *International Conference on Machine Learning*; PMLR: Cambridge, MA, USA, 2019; pp. 6105–6114.
167. Qiu, Z.; Wang, S.; Zeng, Z.; Yu, D. Automatic visual defects inspection of wind turbine blades via YOLO-based small object detection approach. *J. Electron. Imaging* **2019**, *28*, 043023. [CrossRef]
168. Chu, T.C.; Ranson, W.F.; Sutton, M.A. Applications of digital-image-correlation techniques to experimental mechanics. *Exp. Mech.* **1985**, *25*, 232–244. [CrossRef]
169. LeBlanc, B.; Niezrecki, C.; Avitabile, P.; Chen, J.; Sherwood, J.; Hughes, S. Full-field inspection of a wind turbine blade using three-dimensional digital image correlation. In *Industrial and Commercial Applications of Smart Structures Technologies 2011*; SPIE: Bellingham, WA, USA, 2011; Volume 7979, pp. 204–215.
170. Wu, R.; Zhang, D.; Yu, Q.; Jiang, Y.; Arola, D. Health monitoring of wind turbine blades in operation using three-dimensional digital image correlation. *Mech. Syst. Signal Process.* **2019**, *130*, 470–483. [CrossRef]
171. Baqersad, J.; Niezrecki, C.; Avitabile, P. Full-field dynamic strain prediction on a wind turbine using displacements of optical targets measured by stereophotogrammetry. *Mech. Syst. Signal Process.* **2015**, *62*, 284–295. [CrossRef]
172. Khadka, A.; Dong, Y.; Baqersad, J. Structural health monitoring of wind turbines using a digital image correlation system on a UAV. In *Rotating Machinery, Optical Methods & Scanning LDV Methods, Volume 6: Proceedings of the 37th IMAC, A Conference and Exposition on Structural Dynamics 2019*; Springer International Publishing: Cham, Switzerland, 2019; pp. 85–91.
173. Curt, J.; Capaldo, M.; Hild, F.; Roux, S. Modal analysis of a wind turbine tower by digital image correlation. *J. Phys. Conf. Ser.* **2020**, *1618*, 022002. [CrossRef]
174. Wadhwa, N.; Rubinstein, M.; Durand, F.; Freeman, W.T. Phase-based video motion processing. *ACM Trans. Graph. (ToG)* **2013**, *32*, 1–10. [CrossRef]
175. Chen, J.G.; Wadhwa, N.; Cha, Y.J.; Durand, F.; Freeman, W.T.; Buyukozturk, O. Modal identification of simple structures with high-speed video using motion magnification. *J. Sound Vib.* **2015**, *345*, 58–71. [CrossRef]
176. Yang, Y.; Dorn, C.; Mancini, T.; Talken, Z.; Kenyon, G.; Farrar, C.; Mascareñas, D. Blind identification of full-field vibration modes from video measurements with phase-based video motion magnification. *Mech. Syst. Signal Process.* **2017**, *85*, 567–590. [CrossRef]
177. Marks, R.; Gillam, C.; Clarke, A.; Pullin, R. Barely visible impact damage detection in a composite turbine blade using 3D scanning laser vibrometery. *Proc. Inst. Mech. Eng. Part C J. Mech. Eng. Sci.* **2016**, *231*, 2969–2983. [CrossRef]
178. Schäfer, B.E.; Picchi, D.; Engelhardt, T.; Abel, D. Multicopter unmanned aerial vehicle for automated inspection of wind turbines. In *2016 24th Mediterranean Conference on Control and Automation (MED)*; IEEE: Piscataway, NJ, USA, 2016; pp. 244–249.
179. Hung, Y.Y. Applications of digital shearography for testing of composite structures. *Compos. Part B Eng.* **1999**, *30*, 765–773. [CrossRef]
180. Sutherland, H.; Beattie, A.; Hansche, B.; Musial, W.; Allread, J.; Johnson, J.; Summers, M. *The Application of Non-Destructive Techniques to the Testing of a Wind Turbine Blade*; No. SAND-93-1380; Sandia National Laboratories (SNL-NM): Albuquerque, NM, USA, 1994.
181. Amenabar, I.; Mendikute, A.; López-Arraiza, A.; Lizaranzu, M.; Aurrekoetxea, J. Comparison and analysis of non-destructive testing techniques suitable for delamination inspection in wind turbine blades. *Compos. Part B Eng.* **2011**, *42*, 1298–1305. [CrossRef]
182. Márquez, F.P.G.; Chacón, A.M.P. A review of non-destructive testing on wind turbines blades. *Renew. Energy* **2020**, *161*, 998–1010. [CrossRef]

183. Li, Z.; Tokhi, M.O.; Marks, R.; Zheng, H.; Zhao, Z. Dynamic wind turbine blade inspection using micro-polarisation spatial phase shift digital shearography. *Appl. Sci.* **2021**, *11*, 10700. [CrossRef]
184. Li, Z.; Tokhi, M.O.; Zhao, Z.; Gao, J.; Zheng, H. A compact laser shearography system integrated with robotic climber for on-site inspection of wind turbine blades. In *CLAWAR 2020: 23rd International Conference on Climbing and Walking Robots and the Support Technologies for Mobile Machines*; CLAWAR Association: London, UK, 2020.
185. Maldague, X.; Marinetti, S. Pulse phase infrared thermography. *J. Appl. Phys.* **1996**, *79*, 2694–2698. [CrossRef]
186. Zeng, Z.; Tao, N.; Feng, L.C.; Li, Y.S.; Zhang, C.L. Relative thermal contrast analysis in the inspection of wind turbine blades using pulsed thermography. *Adv. Mater. Res.* **2011**, *301*, 591–596. [CrossRef]
187. bin Zhao, S.; Zhang, C.L.; Wu, N.M.; Duan, Y.X.; Li, H. Infrared thermal wave nondestructive testing for rotor blades in wind turbine generators non-destructive evaluation and damage monitoring. In *International Symposium on Photoelectronic Detection and Imaging 2009: Advances in Infrared Imaging and Applications*; SPIE: Bellingham, WA, USA, 2009; Volume 7383, pp. 540–547.
188. Tao, N.; Zeng, Z.; Feng, L.; Li, X.; Li, Y.; Zhang, C. The application of pulsed thermography in the inspection of wind turbine blades. In *International Symposium on Photoelectronic Detection and Imaging 2011: Advances in Infrared Imaging and Applications*; SPIE: Bellingham, WA, USA, 2011; Volume 8193, pp. 345–352.
189. Avdelidis, N.P.; Ibarra-Castanedo, C.; Maldague, X.P.V. Infrared thermography inspection of glass reinforced plastic (GRP) wind turbine blades and the concept of an automated scanning device. In *Thermosense: Thermal Infrared Applications XXXV*; SPIE: Bellingham, WA, USA, 2013; Volume 8705, pp. 124–129.
190. Yi, Q.; Tian, G.Y.; Malekmohammadi, H.; Zhu, J.; Laureti, S.; Ricci, M. New features for delamination depth evaluation in carbon fiber reinforced plastic materials using eddy current pulse-compression thermography. *NDT E Int.* **2019**, *102*, 264–273. [CrossRef]
191. Ren, W.; Liu, J.; Tian, G.Y.; Gao, B.; Cheng, L.; Yang, H. Quantitative non-destructive evaluation method for impact damage using eddy current pulsed thermography. *Compos. Part B Eng.* **2013**, *54*, 169–179. [CrossRef]
192. He, Y.; Tian, G.; Pan, M.; Chen, D. Impact evaluation in carbon fiber reinforced plastic (CFRP) laminates using eddy current pulsed thermography. *Compos. Struct.* **2014**, *109*, 1–7. [CrossRef]
193. Cheng, L.; Gao, B.; Tian, G.Y.; Woo, W.L.; Berthiau, G. Impact damage detection and identification using eddy current pulsed thermography through integration of PCA and ICA. *IEEE Sens. J.* **2014**, *14*, 1655–1663. [CrossRef]
194. Tian, G.Y.; Sophian, A. Reduction of lift-off effects for pulsed eddy current NDT. *NDT E Int.* **2005**, *38*, 319–324. [CrossRef]
195. Pan, M.; He, Y.; Tian, G.; Chen, D.; Luo, F. PEC frequency band selection for locating defects in two-layer aircraft structures with air gap variations. *IEEE Trans. Instrum. Meas.* **2013**, *62*, 2849–2856. [CrossRef]
196. Ishikawa, M.; Shiiya, Y.; Kogo, Y.; Hatta, H.; Habuka, Y.; Fukui, R.; Utsunomiya, S. Inspection of CFRP laminates using phase-transformed induction heating thermography. In Proceedings of the 11th European Conference of Non-Destructive Testing, Prague, Czech Republic, 6–10 October 2014; pp. 6–10.
197. Yang, R.; He, Y. Eddy current pulsed phase thermography considering volumetric induction heating for delamination evaluation in carbon fiber reinforced polymers. *Appl. Phys. Lett.* **2015**, *106*, 234103. [CrossRef]
198. Manohar, A.; Lanza di Scalea, F. Detection of defects in wind turbine composite blades using statistically enhanced lock-in thermography. *Struct. Health Monit.* **2013**, *12*, 566–574. [CrossRef]
199. Galietti, U.; Palumbo, D.; Calia, G.; Pellegrini, M. Non destructive evaluation of composite materials with new thermal methods. In Proceedings of the 15th European Conference on Composite Materials: Composites at Venice, ECCM, Venice, Italy, 24–28 June 2012; pp. 24–28.
200. Salazar, A.; Mendioroz, A.; Apiñaniz, E.; Oleaga, A.; Venegas, P.; Sáez-Ocáriz, I. Characterization of delaminations by lock-in vibrothermography. *J. Phys. Conf. Ser.* **2010**, *214*, 012079. [CrossRef]
201. Shepard, S.M.; Ahmed, T.; Lhota, J.R. Experimental considerations in vibrothermography. In *Thermosense XXVI*; SPIE: Bellingham, WA, USA, 2004; Volume 5405, pp. 332–335.
202. Ley, O.; Butera, M.; Godinez, V.; Chung, S. Assessing impact damage on composites using line scanning thermography. *AM&P Tech. Artic.* **2012**, *170*, 20–25. [CrossRef]
203. Ley, O.; Butera, M.; Godinez, V. Inspection of composite structures using line scanning thermography. In *Thermosense: Thermal Infrared Applications XXXIV*; SPIE: Bellingham, WA, USA, 2012; Volume 8354, pp. 28–33.
204. Zhang, H.; Gao, B.; Tian, G.Y.; Woo, W.L.; Bai, L. Metal defects sizing and detection under thick coating using microwave NDT. *NDT E Int.* **2013**, *60*, 52–61. [CrossRef]
205. Pieraccini, M.; Parrini, F.; Fratini, M.; Atzeni, C.; Spinelli, P. In-service testing of wind turbine towers using a microwave sensor. *Renew. Energy* **2008**, *33*, 13–21. [CrossRef]
206. White, J.; Zimdars, D. Time domain terahertz non destructive evaluation of water intrusion in composites and corrosion under insulation. In *2007 Conference on Lasers and Electro-Optics (CLEO)*; IEEE: Piscataway, NJ, USA, 2007; pp. 1–2.
207. Zhong, S. Progress in terahertz nondestructive testing: A review. *Front. Mech. Eng.* **2019**, *14*, 273–281.
208. García-Martín, J.; Gómez-Gil, J.; Vázquez-Sánchez, E. Non-destructive techniques based on eddy current testing. *Sensors* **2011**, *11*, 2525–2565. [CrossRef] [PubMed]

209. Gao, P.; Wang, C.; Li, Y.; Cong, Z. Electromagnetic and eddy current NDT in weld inspection: A review. *Insight-Non-Destr. Test. Cond. Monit.* **2015**, *57*, 337–345. [CrossRef]
210. He, Y.; Pan, M.; Luo, F.; Tian, G. Pulsed eddy current imaging and frequency spectrum analysis for hidden defect nondestructive testing and evaluation. *NDT E Int.* **2011**, *44*, 344–352. [CrossRef]
211. He, Y.; Tian, G.; Zhang, H.; Alamin, M.; Simm, A.; Jackson, P. Steel corrosion characterization using pulsed eddy current systems. *IEEE Sens. J.* **2012**, *12*, 2113–2120. [CrossRef]
212. He, Y.; Tian, G.; Pan, M.; Chen, D. Non-destructive testing of low-energy impact in CFRP laminates and interior defects in honeycomb sandwich using scanning pulsed eddy current. *Compos. Part B Eng.* **2014**, *59*, 196–203. [CrossRef]
213. Li, Z.; Meng, Z. A review of the radio frequency non-destructive testing for carbon-fibre composites. *Meas. Sci. Rev.* **2016**, *16*, 68–76. [CrossRef]
214. Heuer, H.; Schulze, M.; Pooch, M.; Gäbler, S.; Nocke, A.; Bardl, G.; Cherif, C.; Klein, M.; Kupke, R.; Vetter, R.; et al. Review on quality assurance along the CFRP value chain-non-destructive testing of fabrics, preforms and CFRP by HF radio wave techniques. *Compos. Part B Eng.* **2015**, *77*, 494–501. [CrossRef]
215. IoT Device Detects Wind Turbine Faults in the Field. engineering.com, 1 September 2020. Available online: https://www.engineering.com/iot-device-detects-wind-turbine-faults-in-the-field/ (accessed on 14 August 2025).
216. Civera, M.; Surace, C. Non-destructive techniques for the condition and structural health monitoring of wind turbines: A literature review of the last 20 years. *Sensors* **2022**, *22*, 1627. [CrossRef] [PubMed]
217. Yang, W.; Tavner, P.J.; Crabtree, C.J.; Wilkinson, M. Cost-effective condition monitoring for wind turbines. *IEEE Trans. Ind. Electron.* **2009**, *57*, 263–271. [CrossRef]
218. Yang, W.; Tavner, P.J.; Crabtree, C.J.; Feng, Y.; Qiu, Y. Wind turbine condition monitoring: Technical and commercial challenges. *Wind Energy* **2014**, *17*, 673–693.
219. Lian, J.; Cai, O.; Dong, X.; Jiang, Q.; Zhao, Y. Health monitoring and safety evaluation of the offshore wind turbine structure: A review and discussion of future development. *Sustainability* **2019**, *11*, 494. [CrossRef]
220. Mishnaevsky, L., Jr.; Hasager, C.B.; Bak, C.; Tilg, A.M.; Bech, J.I.; Rad, S.D.; Fæster, S. Leading edge erosion of wind turbine blades: Understanding, prevention and protection. *Renew. Energy* **2021**, *169*, 953–969. [CrossRef]
221. Johansen, N.F.J. Test Methods for Evaluating Rain Erosion Performance of Wind Turbine Blade Leading Edge Protection Systems. Ph.D. Thesis, Technical University of Denmark, Copenhagen, Denmark, 2020.
222. Eisenberg, D.; Laustsen, S.; Stege, J. *Leading Edge Protection Lifetime Prediction Model Creation and Validation*; PO-078g; Wind Europe: Brussels, Belgium, 2016.
223. Amirzadeh, B.; Louhghalam, A.; Raessi, M.; Tootkaboni, M. A computational framework for the analysis of rain-induced erosion in wind turbine blades, part I: Stochastic rain texture model and drop impact simulations. *J. Wind Eng. Ind. Aerodyn.* **2017**, *163*, 33–43. [CrossRef]
224. He, K.; Hoa, S.V.; Ganesan, R. The study of tapered laminated composite structures: A review. *Compos. Sci. Technol.* **2000**, *60*, 2643–2657. [CrossRef]
225. Mandell, J.F.; Samborsky, D.D.; Combs, D.W.; Scott, M.E.; Cairns, D.S. *Fatigue of Composite Material Beam Elements Representative of Wind Turbine Blade Substructure*; No. NREL/SR-500-24379; National Renewable Energy Laboratory (NREL): Golden, CO, USA, 1998.
226. Cairns, D.S.; Mandell, J.F.; Scott, M.E.; Maccagnano, J.Z. Design and manufacturing considerations for ply drops in composite structures. *Compos. Part B Eng.* **1999**, *30*, 523–534. [CrossRef]
227. Shim, D.J. Role of Delamination and Interlaminar Fatigue in the Failure of Laminates with Ply Drop-Offs. Doctoral Dissertation, Massachusetts Institute of Technology, Cambridge, MA, USA, 2002.
228. Samborsky, D.D.; Wilson, T.J.; Agastra, P.; Mandell, J.F. Delamination at thick ply drops in carbon and glass fiber laminates under fatigue loading. *J. Sol. Energy Eng.* **2008**, *130*, 031001. [CrossRef]
229. Jensen, F.M.; Falzon, B.G.; Ankersen, J.; Stang, H. Structural testing and numerical simulation of a 34 m composite wind turbine blade. *Compos. Struct.* **2006**, *76*, 52–61. [CrossRef]
230. Brazier, L.G. On the flexure of thin cylindrical shells and other "thin" sections. *Proc. R. Soc. Lond. Ser. A Contain. Pap. A Math. Phys. Character* **1927**, *116*, 104–114. [CrossRef]
231. Kühlmeier, L. Buckling of Wind Turbine Rotor Blades: Analysis, Design and Experimental Validation. Ph.D. Thesis, Department of Mechanical Engineering, Aalborg University, Aalborg, Denmark, 2007.
232. Overgaard, L.C.; Lund, E.; Thomsen, O.T. Structural collapse of a wind turbine blade. Part A: Static test and equivalent single layered models. *Compos. Part A Appl. Sci. Manuf.* **2010**, *41*, 257–270. [CrossRef]
233. Overgaard, L.C.T.; Lund, E. Structural collapse of a wind turbine blade. Part B: Progressive interlaminar failure models. *Compos. Part A Appl. Sci. Manuf.* **2010**, *41*, 271–283. [CrossRef]
234. Branner, K.; Berring, P. Compressive strength of thick composite panels. In Proceedings of the Risø International Symposium on Materials Science, Roskilde, Denmark, 5–9 September 2011.
235. He, X. A review of finite element analysis of adhesively bonded joints. *Int. J. Adhes. Adhes.* **2011**, *31*, 248–264. [CrossRef]

236. Abdel Wahab, M.M. Fatigue in adhesively bonded joints: A review. *Int. Sch. Res. Not.* **2012**, *2012*, 746308. [CrossRef]
237. Sayer, F.; Post, N.; Van Wingerde, A.; Busmann, H.G.; Kleiner, F.; Fleischmann, W.; Gansow, M. Testing of adhesive joints in the wind industry. In Proceedings of the European Wind Energy Conference and Exhibition, Marseille, France, 16–19 March 2009; Volume 2009, pp. 288–315.
238. Sayer, F.; Antoniou, A.; van Wingerde, A. Investigation of structural bond lines in wind turbine blades by sub-component tests. *Int. J. Adhes. Adhes.* **2012**, *37*, 129–135. [CrossRef]
239. Zarouchas, D.S.; Makris, A.A.; Sayer, F.; Van Hemelrijck, D.; Van Wingerde, A.M. Investigations on the mechanical behavior of a wind rotor blade subcomponent. *Compos. Part B Eng.* **2012**, *43*, 647–654. [CrossRef]
240. Samborsky, D.; Mandell, J.; Sears, A.; Kils, O. Static and fatigue testing of thick adhesive joints for wind turbine blades. In Proceedings of the 47th AIAA Aerospace Sciences Meeting including the New Horizons Forum and Aerospace Exposition, Orlando, FL, USA, 5–8 January 2009; p. 1550.
241. Zarouchas, D.; Nijssen, R. Mechanical behaviour of thick structural adhesives in wind turbine blades under multi-axial loading. *J. Adhes. Sci. Technol.* **2016**, *30*, 1413–1429. [CrossRef]
242. Eder, M.A.; Bitsche, R.D.; Nielsen, M.; Branner, K. A practical approach to fracture analysis at the trailing edge of wind turbine rotor blades. *Wind Energy* **2014**, *17*, 483–497.
243. Haselbach, P.U.; Eder, M.A.; Belloni, F. A comprehensive investigation of trailing edge damage in a wind turbine rotor blade. *Wind Energy* **2016**, *19*, 1871–1888. [CrossRef]
244. Lahuerta, F.; De Ruiter, M.J.; Espinosa, L.; Koorn, N.; Smissaert, D. Assessment of wind turbine blade trailing edge failure with sub-component tests. In Proceedings of the 21st International Conference on Composite Materials, Xi'an, China, 20–25 August 2017; Volume 5.
245. Branner, K.; Berring, P.; Haselbach, P.; Chen, X.; Antoniou, A.; Rosemeier, M. *Report on Validation and Improvement of Blade Design Tools*; Work Package 7.1: Efficient Blade Structure Deliverable Number 71.3, Technical Report, IRPWInd, Grant Agreement No 609795; Risø: Roskilde, Denmark, 2018.
246. Jørgensen, J.B.; Sørensen, B.F.; Kildegaard, C. Tunneling cracks in full scale wind turbine blade joints. *Eng. Fract. Mech.* **2018**, *189*, 361–376. [CrossRef]
247. Chen, X.; Berring, P.; Madsen, S.H.; Branner, K.; Semenov, S. Understanding progressive failure mechanisms of a wind turbine blade trailing edge section through subcomponent tests and nonlinear FE analysis. *Compos. Struct.* **2019**, *214*, 422–438. [CrossRef]
248. Eder, M.A.; Bitsche, R.D. Fracture analysis of adhesive joints in wind turbine blades. *Wind Energy* **2015**, *18*, 1007–1022.
249. Eder, M.A.; Bitsche, R.D.; Belloni, F. Effects of geometric non-linearity on energy release rates in a realistic wind turbine blade cross section. *Compos. Struct.* **2015**, *132*, 1075–1084. [CrossRef]
250. Lee, H.G.; Kang, M.G.; Park, J. Fatigue failure of a composite wind turbine blade at its root end. *Compos. Struct.* **2015**, *133*, 878–885. [CrossRef]
251. Hosseini-Toudeshky, H.; Jahanmardi, M.; Goodarzi, M.S. Progressive debonding analysis of composite blade root joint of wind turbines under fatigue loading. *Compos. Struct.* **2015**, *120*, 417–427. [CrossRef]
252. Jelf, P.M.; Fleck, N.A. Compression failure mechanisms in unidirectional composites. *J. Compos. Mater.* **1992**, *26*, 2706–2726. [CrossRef]
253. Boopathi, K.; Mishnaevsky, L., Jr.; Sumantraa, B.; Premkumar, S.A.; Thamodharan, K.; Balaraman, K. Failure mechanisms of wind turbine blades in India: Climatic, regional, and seasonal variability. *Wind Energy* **2022**, *25*, 968–979.
254. Mishnaevsky, L., Jr. Root causes and mechanisms of failure of wind turbine blades: Overview. *Materials* **2022**, *15*, 2959. [CrossRef] [PubMed]
255. 5 Common Wind Turbine Blade Failures and Repair Processes. VivaBlast. Available online: https://vivablast.com/new/5-common-wind-turbine-blade-failures-and-repair-processes/ (accessed on 14 August 2025).
256. Available online: https://nawindpower.com/wp-content/uploads/2016/01/12970_the_elgin_review_1.jpg (accessed on 14 August 2025).
257. Ramakrishnan, M.; Rajan, G.; Semenova, Y.; Farrell, G. Overview of fiber optic sensor technologies for strain/temperature sensing applications in composite materials. *Sensors* **2016**, *16*, 99. [CrossRef] [PubMed]
258. Chen, Y.; Griffith, D.T. Experimental and numerical full-field displacement and strain characterization of wind turbine blade using a 3D Scanning Laser Doppler Vibrometer. *Opt. Laser Technol.* **2023**, *158*, 108869. [CrossRef]
259. Ding, S.; Yang, C.; Zhang, S. Acoustic-signal-based damage detection of wind turbine blades—A review. *Sensors* **2023**, *23*, 4987. [CrossRef] [PubMed]
260. Tang, J.; Soua, S.; Mares, C.; Gan, T.H. A pattern recognition approach to acoustic emission data originating from fatigue of wind turbine blades. *Sensors* **2017**, *17*, 2507. [CrossRef] [PubMed]
261. Bouzid, O.M.; Tian, G.Y.; Cumanan, K.; Moore, D. Structural health monitoring of wind turbine blades: Acoustic source localization using wireless sensor networks. *J. Sens.* **2015**, *2015*, 139695. [CrossRef]

262. Tsopelas, N.K.; Papasalouros, D.G.; Anastasopoulos, A.A.; Kourousis, D.A.; Dong, J.W. Acoustic emission for structural integrity assessment of wind turbine blades. In *Advances in Acoustic Emission Technology: Proceedings of the World Conference on Acoustic Emission-2013*; Springer: New York, NY, USA, 2014; pp. 369–382.
263. Wang, Y.; Liang, M.; Xiang, J. Damage detection method for wind turbine blades based on dynamics analysis and mode shape difference curvature information. *Mech. Syst. Signal Process.* **2014**, *48*, 351–367. [CrossRef]
264. Hoell, S.; Omenzetter, P. Sequential projection pursuit for optimised vibration-based damage detection in an experimental wind turbine blade. *Smart Mater. Struct.* **2018**, *27*, 025007. [CrossRef]
265. Ogaili, A.A.F.; Hamzah, M.N.; Jaber, A.A. Enhanced fault detection of wind turbine using extreme gradient boosting technique based on nonstationary vibration analysis. *J. Fail. Anal. Prev.* **2024**, *24*, 877–895. [CrossRef]
266. Fremmelev, M.A.; Ladpli, P.; Orlowitz, E.; Dervilis, N.; McGugan, M.; Branner, K. Feasibility study on a full-scale wind turbine blade monitoring campaign: Comparing performance and robustness of features extracted from medium-frequency active vibrations. *Wind Energy* **2023**, *26*, 1027–1048. [CrossRef]
267. El Mountassir, M.; Yaacoubi, S.; Dellagi, S.; Sfar, M.; Aouini, M. An ultrasonic guided waves based prognostic approach for predictive maintenance: Experimental study cases. *Mech. Syst. Signal Process.* **2023**, *190*, 110135. [CrossRef]
268. Habibi, H.; Cheng, L.; Zheng, H.; Kappatos, V.; Selcuk, C.; Gan, T.H. A dual de-icing system for wind turbine blades combining high-power ultrasonic guided waves and low-frequency forced vibrations. *Renew. Energy* **2015**, *83*, 859–870. [CrossRef]
269. Yin, C.; Zhang, Z.; Wang, Z.; Guo, H. Numerical simulation and experimental validation of ultrasonic de-icing system for wind turbine blade. *Appl. Acoust.* **2016**, *114*, 19–26. [CrossRef]
270. Liu, Q.X.; Wang, Z.H.; Long, S.G.; Cai, M.; Wang, X.; Chen, X.Y.; Bu, J.L. Research on automatic positioning system of ultrasonic testing of wind turbine blade flaws. *IOP Conf. Ser. Earth Environ. Sci.* **2017**, *93*, 012074. [CrossRef]
271. Yang, B.; Zhang, L.; Zhang, W.; Ai, Y. Non-destructive testing of wind turbine blades using an infrared thermography: A review. In *2013 International Conference on Materials for Renewable Energy and Environment*; IEEE: Piscataway, NJ, USA, 2013; Volume 1, pp. 407–410.
272. Galleguillos, C.; Zorrilla, A.; Jimenez, A.; Diaz, L.; Montiano, Á.L.; Barroso, M.; Viguria, A.; Lasagni, F. Thermographic non-destructive inspection of wind turbine blades using unmanned aerial systems. *Plast. Rubber Compos.* **2015**, *44*, 98–103. [CrossRef]
273. Sanati, H.; Wood, D.; Sun, Q. Condition monitoring of wind turbine blades using active and passive thermography. *Appl. Sci.* **2018**, *8*, 2004. [CrossRef]
274. Hwang, S.; An, Y.K.; Yang, J.; Sohn, H. Remote inspection of internal delamination in wind turbine blades using continuous line laser scanning thermography. *Int. J. Precis. Eng. Manuf.-Green Technol.* **2020**, *7*, 699–712. [CrossRef]
275. Johnson, J.T.; Hughes, S.; van Dam, J. A stereo-videogrammetry system for monitoring wind turbine blade surfaces during structural testing. *ASME Early Career Tech. J.* **2009**, *8*, 1072802.
276. Yu, J.; He, Y.; Zhang, F.; Sun, G.; Hou, Y.; Liu, H.; Li, J.; Yang, R.; Wang, H. An infrared image stitching method for wind turbine blade using UAV flight data and U-Net. *IEEE Sens. J.* **2023**, *23*, 8727–8736. [CrossRef]
277. Carnero, A.; Martín, C.; Díaz, M. Portable motorized telescope system for wind turbine blades damage detection. *Eng. Rep.* **2025**, *7*, e12618.
278. Poozesh, P.; Baqersad, J.; Niezrecki, C.; Avitabile, P.; Harvey, E.; Yarala, R. Large-area photogrammetry based testing of wind turbine blades. *Mech. Syst. Signal Process.* **2017**, *86*, 98–115. [CrossRef]
279. Jasinien, E.; Raiutis, R.; Voleiis, A.; Vladiauskas, A.; Mitchard, D.; Amos, M. NDT of wind turbine blades using adapted ultrasonic and radiographic techniques. *Insight-Non-Destr. Test. Cond. Monit.* **2009**, *51*, 477–483. [CrossRef]
280. Sattar, T.P.; Marques, V.; Anvo, R.N.Z.; Gallegos Garrido, G.; Kaur, A.P.; Routledge, P.; Markham, K. Climbing robot to perform radiography of wind blades. In *Climbing and Walking Robots Conference*; Springer International Publishing: Cham, Switzerland, 2021; pp. 165–176.
281. Mikkelsen, L.P. Visualizing composite materials for wind turbine blades using x-ray tomography. In Proceedings of the Materials for Tomorrow 2019: Visualizing Materials, Gothenburg, Sweden, 4 December 2019.
282. Chen, X. Fractographic analysis of sandwich panels in a composite wind turbine blade using optical microscopy and X-ray computed tomography. *Eng. Fail. Anal.* **2020**, *111*, 104475. [CrossRef]
283. Meinlschmidt, P.; Aderhold, J. Thermographic Inspection of Rotor Blades. In Proceedings of the 9th European Conference on Non-Destructive Testing, Berlin, Germany, 25–29 September 2006; pp. 1–9.
284. Wang, C.; Gu, Y. Research on infrared nondestructive detection of small wind turbine blades. *Results Eng.* **2022**, *15*, 100570. [CrossRef]
285. Wang, C.; Gu, Y. Research on infrared nondestructive testing and thermal effect analysis of small wind turbine blades under natural excitation. *Infrared Phys. Technol.* **2023**, *130*, 104621. [CrossRef]
286. Doroshtnasir, M.; Worzewski, T.; Krankenhagen, R.; Röllig, M. On-site inspection of potential defects in wind turbine rotor blades with thermography. *Wind Energy* **2016**, *19*, 1407–1422.

287. Krankenhagen, R. EvalTherm—Passive Thermography for the Detection of Rotor Blade Damage on Wind Turbines. Bun-desanstalt für Materialforschung und-Prüfung (BAM), 28 May 2021. Available online: https://www.bam.de/Content/EN/Projects/EvalTherm/eval-therm.html (accessed on 14 August 2025).
288. Memari, M.; Shekaramiz, M.; Masoum, M.A.; Seibi, A.C. Enhanced Non-Destructive Testing of Small Wind Turbine Blades Using Infrared Thermography. *Machines* **2025**, *13*, 108. [CrossRef]
289. Du, Y.; Zhou, S.; Jing, X.; Peng, Y.; Wu, H.; Kwok, N. Damage detection techniques for wind turbine blades: A review. *Mech. Syst. Signal Process.* **2020**, *141*, 106445. [CrossRef]
290. Available online: https://nawindpower.com/stereo-dic-shows-promise-for-wind-blade-inspection (accessed on 14 August 2025).
291. Pitchford, C.; Grisso, B.L.; Inman, D.J. Impedance-based structural health monitoring of wind turbine blades. In *Health Monitoring of Structural and Biological Systems 2007*; SPIE: Bellingham, WA, USA, 2007; Volume 6532, pp. 508–518.
292. Tran, T.T.; Lee, D. Understanding the behavior of l-type flange joint in wind turbine towers: Proposed mechanisms. *Eng. Fail. Anal.* **2022**, *142*, 106750. [CrossRef]
293. Jiang, Y.; Zhang, M.; Lee, C.H. A study of early stage self-loosening of bolted joints. *J. Mech. Des.* **2003**, *125*, 518–526. [CrossRef]
294. Stephen, J.T.; Marshall, M.B.; Lewis, R. Relaxation of contact pressure and self-loosening in dynamic bolted joints. *Proc. Inst. Mech. Eng. Part C J. Mech. Eng. Sci.* **2017**, *231*, 3462–3475.
295. Liu, J.; Ouyang, H.; Feng, Z.; Cai, Z.; Liu, X.; Zhu, M. Study on self-loosening of bolted joints excited by dynamic axial load. *Tribol. Int.* **2017**, *115*, 432–451. [CrossRef]
296. Yokoyama, T.; Olsson, M.; Izumi, S.; Sakai, S. Investigation into the self-loosening behavior of bolted joint subjected to rotational loading. *Eng. Fail. Anal.* **2012**, *23*, 35–43. [CrossRef]
297. Chakherlou, T.N.; Oskouei, R.H.; Vogwell, J. Experimental and numerical investigation of the effect of clamping force on the fatigue behaviour of bolted plates. *Eng. Fail. Anal.* **2008**, *15*, 563–574. [CrossRef]
298. Korin, I.; Ipiña, J.P. Experimental evaluation of fatigue life and fatigue crack growth in a tension bolt-nut threaded connection. *Int. J. Fatigue* **2011**, *33*, 166–175. [CrossRef]
299. Wei, J.; Jiao, G.; Jia, P.; Huang, T. The effect of interference fit size on the fatigue life of bolted joints in composite laminates. *Compos. Part B Eng.* **2013**, *53*, 62–68. [CrossRef]
300. Jiménez-Peña, C.; Talemi, R.H.; Rossi, B.; Debruyne, D. Investigations on the fretting fatigue failure mechanism of bolted joints in high strength steel subjected to different levels of pre-tension. *Tribol. Int.* **2017**, *108*, 128–140. [CrossRef]
301. Ahn, J.H.; You, J.M.; Huh, J.; Kim, I.T.; Jeong, Y.S. Residual clamping force of bolt connections caused by sectional damage of nuts. *J. Constr. Steel Res.* **2017**, *136*, 204–214. [CrossRef]
302. Narayanaswamy, R. The process of materials selection for pipeline systems optimization for life cycles. In *ASME India Oil and Gas Pipeline Conference*; American Society of Mechanical Engineers: New York, NY, USA, 2017; Volume 50763, p. V001T02A001.
303. Uchneat, S.; Stevenson, M.; McDougall, J. Case study: Analysis of corrosion patterns to evaluate the preaccident configuration of an ATV tie rod end connection. *J. Fail. Anal. Prev.* **2016**, *16*, 537–542. [CrossRef]
304. Kikuchi, T.; Omiya, Y.; Sawa, T. Effects of nut thinning due to corrosion on the strength characteristics and the sealing performance of bolted flange joints under internal pressure. In Proceedings of the Pressure Vessels and Piping Conference, Baltimore, MD, USA, 17–21 July 2011; Volume 44526, pp. 35–41.
305. Charlton, R.S. Threaded fasteners: Part 2-fundamentals of threaded fasteners, friction and lubrication effects, installation methods, guidelines and corrosion upgrading. In *The NACE International Annual Conference*; NACE International: Houston, TX, USA, 2012; pp. 1–16.
306. Fukuoka, T.; Nomura, M.; Kawabayashi, H. A new experimental approach for measuring friction coefficients of threaded fasteners focusing on the repetition of tightening operation and surface roughness. In *Pressure Vessels and Piping Conference*; American Society of Mechanical Engineers: New York, NY, USA, 2013; Volume 55669, p. V002T02A034.
307. Yamamoto, E.; Wada, K.; Fukuzuka, T.; Shimogori, K.; Fujiwara, K.; Tsuji, K. Lubricating films to prevent galling of stainless steel threaded parts. *Lubr. Eng.* **1984**, *40*, 588–597.
308. Scott, R.L.; Harley, P.H. Failures of Threaded Fittings and Fasteners at Nuclear Facilities. *Nucl. Saf.* **1971**, *13*, 47–53.
309. Available online: https://www.chosun.com/site/data/html_dir/2016/03/07/2016030700528.html (accessed on 14 August 2025).
310. Nguyen, T.C.; Huynh, T.C.; Yi, J.H.; Kim, J.T. Hybrid bolt-loosening detection in wind turbine tower structures by vibration and impedance responses. *Wind Struct.* **2017**, *24*, 385–403. [CrossRef]
311. Jiang, X.; Zhang, X.; Zhang, Y. Evaluation of characterization indexes and minor looseness identification of flange bolt under noise influence. *IEEE Access* **2020**, *8*, 157691–157702. [CrossRef]
312. Wang, C.; Wang, N.; Ho, S.C.; Chen, X.; Pan, M.; Song, G. Design of a novel wearable sensor device for real-time bolted joints health monitoring. *IEEE Internet Things J.* **2018**, *5*, 5307–5316. [CrossRef]

313. Le, T.C.; Luu, T.H.T.; Nguyen, H.P.; Nguyen, T.H.; Ho, D.D.; Huynh, T.C. Piezoelectric impedance-based structural health monitoring of wind turbine structures: Current status and future perspectives. *Energies* **2022**, *15*, 5459. [CrossRef]
314. Ziat, Y.; Hammi, M.; Zarhri, Z.; Ifguis, O. Surface analysis, mechanical and corrosion behavior of welded steel in 1M HCl corrosive media with epoxy/alumina coating. *Biointerface Res. Appl. Chem.* **2022**, *12*, 3559–3571.

Disclaimer/Publisher's Note: The statements, opinions and data contained in all publications are solely those of the individual author(s) and contributor(s) and not of MDPI and/or the editor(s). MDPI and/or the editor(s) disclaim responsibility for any injury to people or property resulting from any ideas, methods, instructions or products referred to in the content.